NAVAL POSTGRADUATE SCHOOL
Monterey, California

THESIS

THE TEMPORAL AND SPATIAL VARIABILITY OF
THE MARINE ATMOSPHERIC
BOUNDARY LAYER AND ITS EFFECT ON
ELECTROMAGNETIC
PROPAGATION IN AND AROUND THE
GREENLAND SEA MARGINAL ICE ZONE

by

Douglas J. Groters

June 1988

Thesis Advisor   W.J. Shaw

Approved for public release: distribution is unlimited.

REPORT DOCUMENTATION PAGE

1a Report Security Classification Unclassified			1b Restrictive Markings			
2a Security Classification Authority			3 Distribution Availability of Report			
2b Declassification Downgrading Schedule			Approved for public release; distribution is unlimited.			
4 Performing Organization Report Number(s)			5 Monitoring Organization Report Number(s)			
6a Name of Performing Organization Naval Postgraduate School		6b Office Symbol (if applicable) 35	7a Name of Monitoring Organization Naval Postgraduate School			
6c Address (city, state, and ZIP code) Monterey, CA 93943-5000			7b Address (city, state, and ZIP code) Monterey, CA 93943-5000			
8a Name of Funding Sponsoring Organization		8b Office Symbol (if applicable)	9 Procurement Instrument Identification Number			
8c Address (city, state, and ZIP code)			10 Source of Funding Numbers			
			Program Element No	Project No	Task No	Work Unit Accession No

11 Title (include security classification) THE TEMPORAL AND SPATIAL VARIABILITY OF THE MARINE ATMOSPHERIC BOUNDARY LAYER AND ITS EFFECT ON ELECTROMAGNETIC PROPAGATION IN AND AROUND THE GREENLAND SEA MARGINAL ICE ZONE

12 Personal Author(s) Douglas J. Groters

13a Type of Report Master's Thesis	13b Time Covered From To	14 Date of Report (year, month, day) June 1988	15 Page Count 122

16 Supplementary Notation The views expressed in this thesis are those of the author and do not reflect the official policy or position of the Department of Defense or the U.S. Government.

17 Cosati Codes			18 Subject Terms (continue on reverse if necessary and identify by block number)
Field	Group	Subgroup	marginal ice zone, refractivity, electromagnetic ducting, Arctic boundary layer

19 Abstract (continue on reverse if necessary and identify by block number)

The variability of the marine atmospheric boundary layer (MABL) and its effect on the electromagnetic (EM) refractive structure around the Greenland Sea marginal ice zone were examined. Rawinsonde profiles and surface observations collected from three ships during MIZEX-87 (20 March-11 April) served as the data set for the examination. A program was developed to calculate the refractivity at each vertical level of the rawinsonde profiles. The program also identified the levels at which trapping, super-refraction and subrefraction occurred.

Temporal studies showed that a higher incidence of anomalous refractive layers occurred during periods when the region was under the influence of high pressure. More than 50% of the time, trapping and super-refractive layers were attributed to the development of a capping inversion just above the MABL during these periods.

Spatial studies showed that the refractive structure varied relative to distance from the ice edge as did the depth of the MABL. An upward slope in refractive layer heights was observed from the ice toward the open water. Significant spatial inhomogeneity was observed over horizontal ranges of less than 100 km. This was attributed both to the large-scale synoptic forcing affecting the region and to variations in the surface fluxes of heat and moisture over the ice and over the water. A range-dependent ray trace model developed at the Naval Ocean Systems Center was used to show how the ray paths of EM waves vary with a changing refractive structure.

20 Distribution Availability of Abstract ☒ unclassified unlimited ☐ same as report ☐ DTIC users	21 Abstract Security Classification Unclassified	
22a Name of Responsible Individual W.J. Shaw	22b Telephone (include Area code) (408) 646-3430	22c Office Symbol 63Sr

DD FORM 1473,84 MAR

83 APR edition may be used until exhausted
All other editions are obsolete

security classification of this page

i

The Temporal and Spatial Variability of the Marine Atmospheric
Boundary Layer and Its Effect On Electromagnetic
Propagation In and Around the Greenland Sea Marginal Ice Zone

by

Douglas J. Groters
Lieutenant, United States Navy
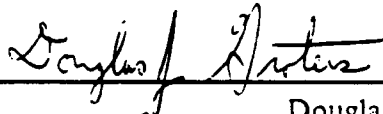B.S., United States Naval Academy, 1982

Submitted in partial fulfillment of the
requirements for the degree of

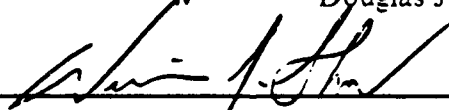MASTER OF SCIENCE IN METEOROLOGY AND OCEANOGRAPHY

from the

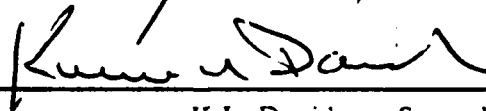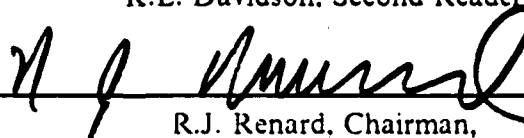NAVAL POSTGRADUATE SCHOOL
June 1988

Author: _____
Douglas J. Groters

Approved by: _____
W.J. Shaw, Thesis Advisor

_____
K.L. Davidson, Second Reader

_____
R.J. Renard, Chairman,
Department of Meteorology

_____
Gordon E. Schacher,
Dean of Science and Engineering

ii

ABSTRACT

The variability of the marine atmospheric boundary layer (MABL) and its effect on the electromagnetic (EM) refractive structure around the Greenland Sea marginal ice zone were examined. Rawinsonde profiles and surface observations collected from three ships during MIZEX-87 (20 March-11 April) served as the data set for the examination. A program was developed to calculate the refractivity at each vertical level of the rawinsonde profiles. The program also identified the levels at which trapping, super-refraction and subrefraction occurred.

Temporal studies showed that a higher incidence of anomalous refractive layers occurred during periods when the region was under the influence of high pressure. More than 50% of the time, trapping and super-refractive layers were attributed to the development of a capping inversion just above the MABL during these periods.

Spatial studies showed that the refractive structure varied relative to distance from the ice edge as did the depth of the MABL. An upward slope in refractive layer heights was observed from the ice toward the open water. Significant spatial inhomogeneity was observed over horizontal ranges of less than 100 km. This was attributed both to the large-scale synoptic forcing affecting the region and to variations in the surface fluxes of heat and moisture over the ice and over the water. A range-dependent ray trace model developed at the Naval Ocean Systems Center was used to show how the ray paths of EM waves vary with a changing refractive structure.

TABLE OF CONTENTS

LIST OF TABLES

LIST OF FIGURES

ACKNOWLEDGEMENTS

I. INTRODUCTION

A. GENERAL

The Arctic region depicted in Fig. 1 is entering a period of greatly increased economic, social, strategic and political change. The major force behind the changes taking place is resource development activity. Although the present scale of this activity is not inconsequential, it is small in comparison to its projected growth in the next two decades (Richardson, 1984). These changes, coupled with the increased use of the Arctic as a deployment area for the strategic forces of the Soviet Union, have forced the United States to develop an active and progressive Arctic research plan. The goals and objectives of this research are focused at solving scientific and technological problems related to the physical and biological components of the Arctic and the various processes that govern the behavior of these components. Increased knowledge in such areas as: the Arctic as a natural laboratory, the role of the Arctic in national defense and global/regional climate and weather are addressed in these objectives (National Science Foundation, 1987).

The United States Navy's interest in the Arctic has surged in the last several years. It has long been realized that the Arctic is an important naval operating area of the Soviet Union. The Northern Fleet is the largest of four Soviet fleets. It boasts 65% of the Soviet's nuclear ballistic missile submarine (SSBN) force and 50% of its attack and cruise missile submarines (Polmar, 1986). Recent observation of Soviet fleet operating procedures and exercises seems to suggest that at an initial onset of hostilities a large majority of the Soviet naval forces would deploy relatively near the Soviet Union (Watkins, 1986).

Advances in technology over the last ten years have resulted in ranges up to 8300 km for Soviet submarine-launched ballistic missiles. Development of submarine hull designs such as that of the Typhoon class, believed to be specifically designed for operations under ice, gives the Soviets a significant strategic advantage. They now have the option of deploying their SSBN's within Arctic waters and under the ice. This complicates the anti-submarine warfare (ASW) problem immensely and significantly reduces the vulnerability of these strategic platforms to detection by North Atlantic Treaty Organization (NATO) ASW forces (U.S. Department of Defense, 1987).

1
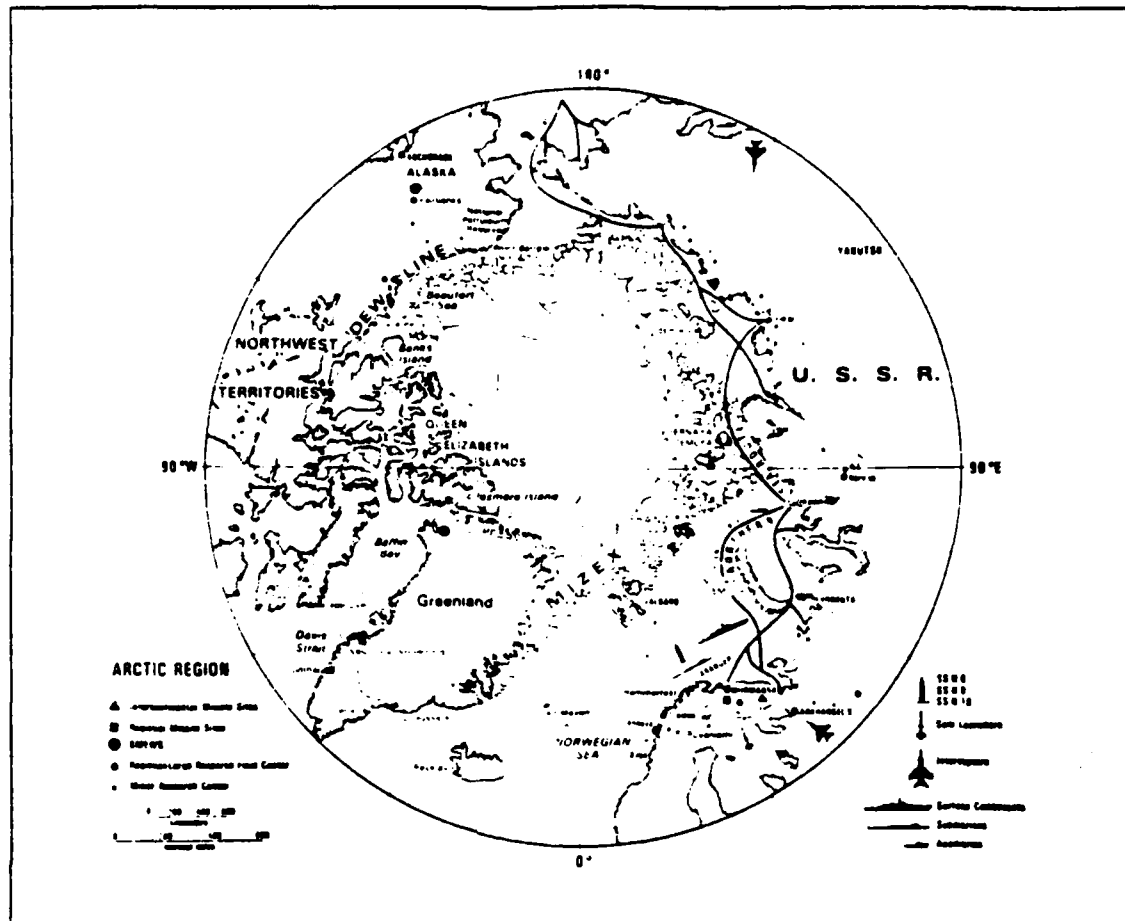
Fig. 1. Arctic Ocean and adjacent seas: heavy dotted line is the defense early warning (DEW) line; large filled in circles are ballistic missile early warning sites (BMEWS); heavy solid line shows the northern sea route; ice edge denotes average summer positions (Johnson, et al., 1984).

In the event of hostilities, it would also be in the interest of the United States to contain the Soviet fleet in the Arctic area. This requires a naval force able to effectively operate for extended periods of time in the Arctic arena at any time of the year. Fig. 2 shows the United States Navy's Arctic/Cold Weather Surface Ship Plan developed by the Vice Chief of Naval Operations for Surface Warfare (OP-03). The current and projected severe weather operating capability for naval surface ships indicates the Navy's intention of expanding its operating limits to the very edge of the marginal ice zone (MIZ) by the year 2010.
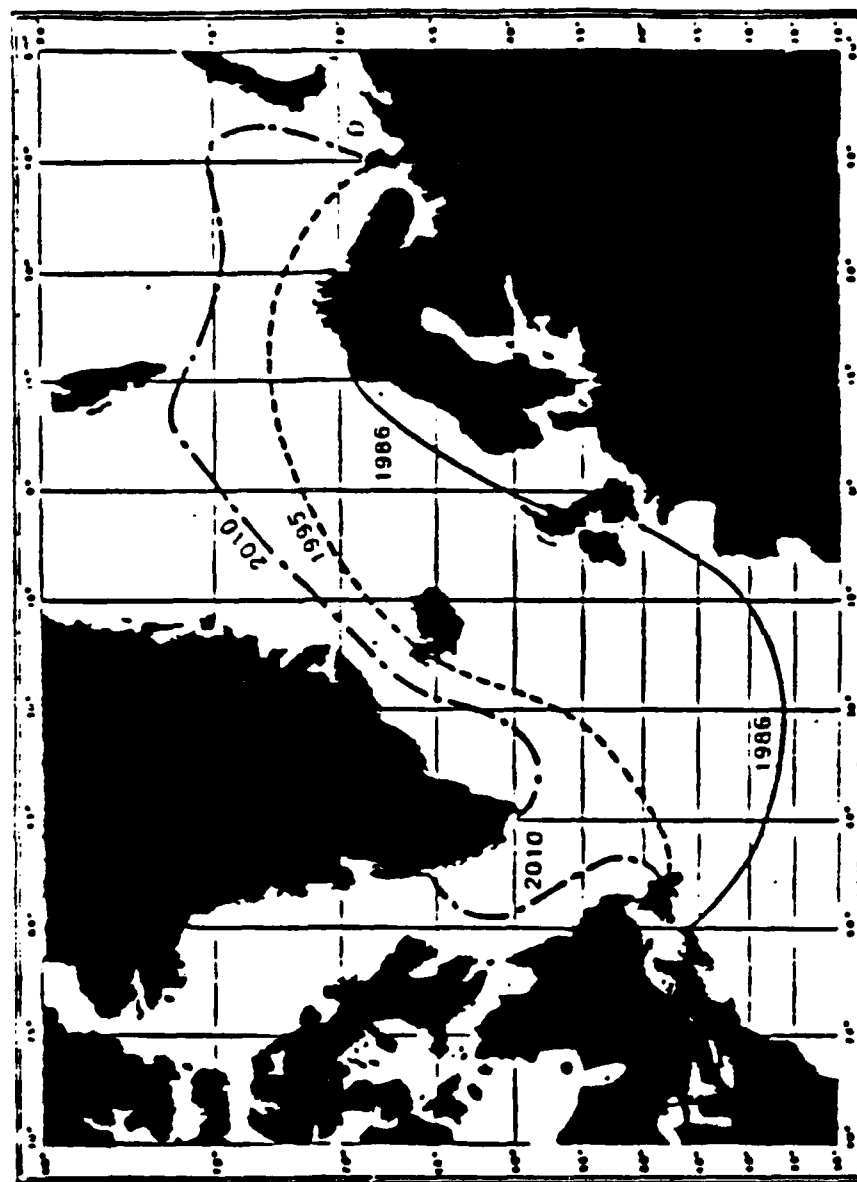
Fig. 2.   U.S. Navy's Arctic/Cold Weather Surface Ship Plan.

Our ability to operate in the seas bordering the Arctic Ocean is currently limited both by our knowledge of this area and by our ability to predict and avoid severe weather. In response to the need for a better understanding of the Arctic environment,

3

several major research efforts have been undertaken. The Marginal Ice Zone Experiment (MIZEX) series is one of these.

B. THE MARGINAL ICE ZONE EXPERIMENTS

The MIZ occurs geographically as a transition area between pack ice and the open ocean. It is an area of dynamic interaction involving the ice, the ocean and the atmosphere. The MIZ boundary is dependent on the advection of ice from the north, advection of warmer water from the south and their interaction. Such interactions occur in the form of ocean waves and swell, mesoscale eddy grinding and from *in situ* ice formation and melt. The ice edge boundary varies seasonally by hundreds of kilometers. This covering and uncovering of vast amounts of water causes significant changes in the local atmospheric boundary layer (ABL) structure. In addition, the amount of open water has a direct bearing on the amount of moisture and heat available for exchange with the atmosphere. These fluxes of moisture and heat over large areas have a significant impact in determining global climate (Johnson and Hawkins, 1987).

The MIZEX series of experiments was developed to increase our understanding of the physical and biological processes of the MIZ. The measurement program was initiated with a small test phase in June and July of 1983. The following year a full-scale experiment was conducted from 18 May to 30 July 1984. This MIZEX involved the coordinated resources of eleven different nations including seven ships, eight remote sensing/meteorological aircraft and four helicopters. Data collected during MIZEX-84 were used to study a variety of mesoscale physical processes involved in ice, ocean and atmospheric interactions (Johannessen and Horn, 1984). The operating area for MIZEX-84 is depicted in Fig. 3.

A MIZEX-87 was conducted from 20 March to 10 April 1987 to collect data during the late winter regime. Fig. 4 shows the area of operations for MIZEX-87. The operating area is in the same locale as that of MIZEX-84. The data obtained are significant in that this was the first major study of the Greenland Sea MIZ during the late winter period. Winter conditions are expected to produce substantially different dynamic balances of momentum, heat and moisture as well as different interactions between ice-ocean conditions and their remotely sensed electromagnetic radiation properties (Johnson and Hawkins, 1987). One of the primary goals of the 1987 MIZEX field programs was to provide the first data on important meteorological questions, including cyclogenesis and surface atmospheric boundary conditions in the winter MIZ (MIZEX Bulletin VIII, 1986).

4
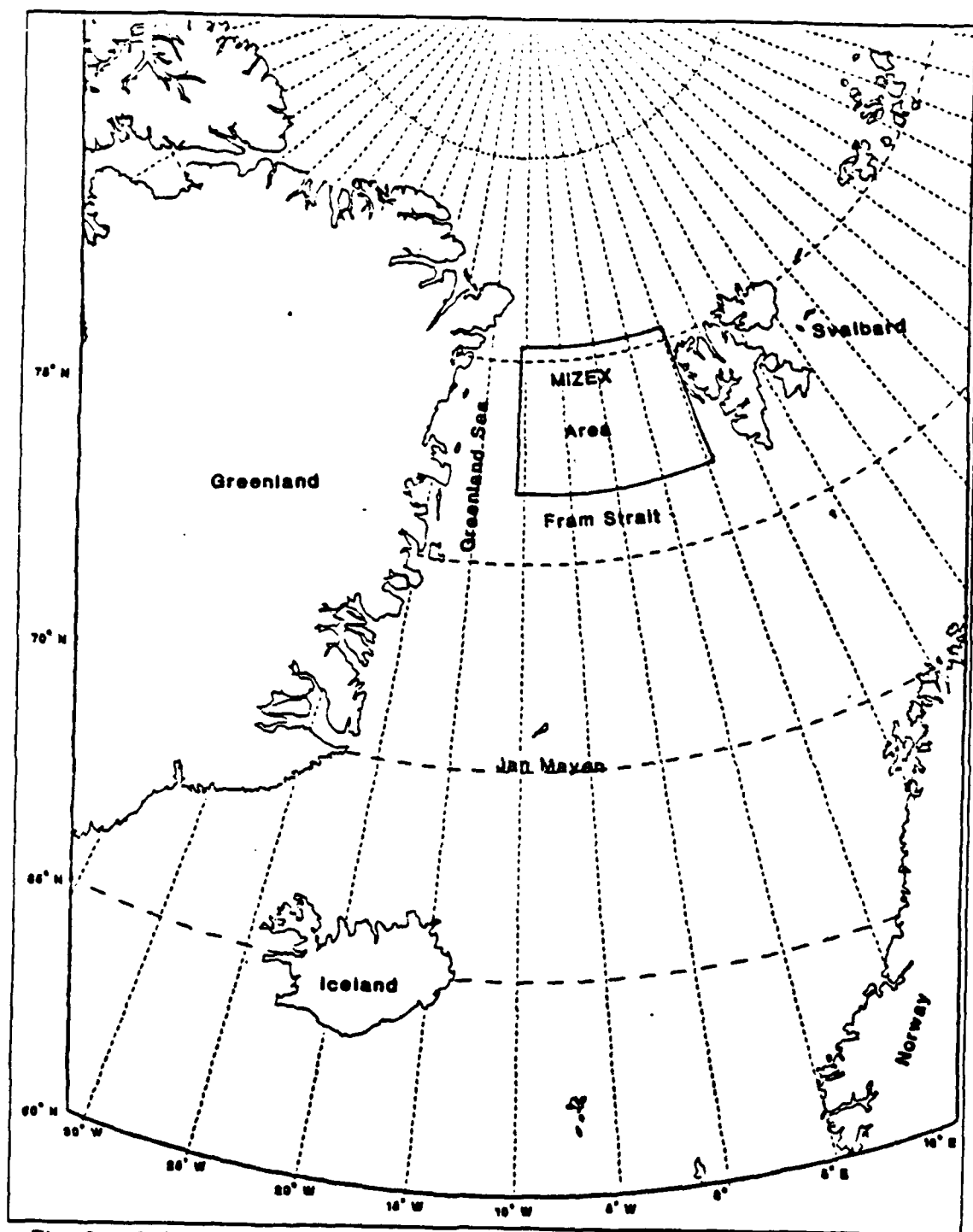
Fig. 3.   MIZEX-84 area of operations from Willis (1987).
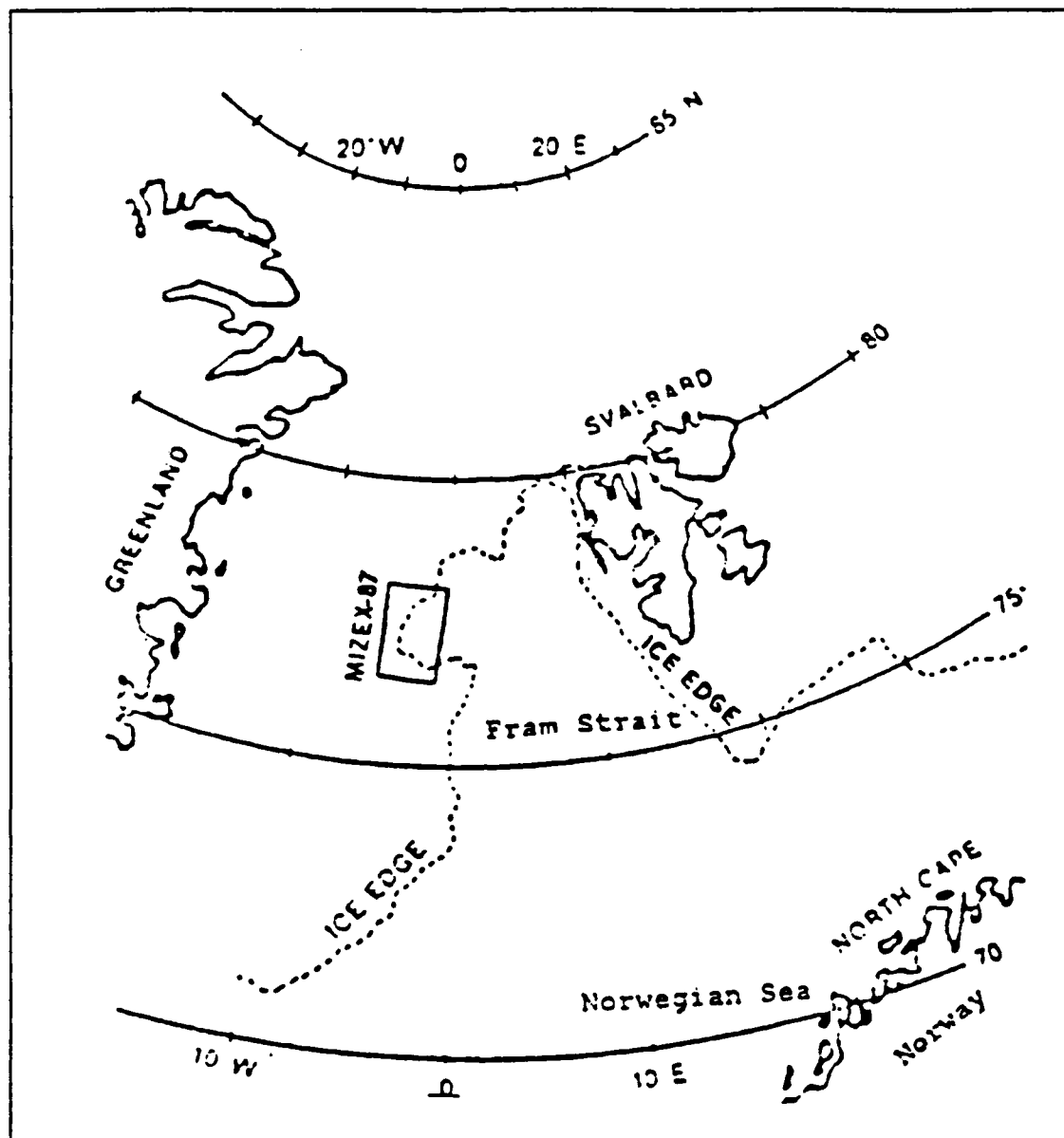
Fig. 4. MIZEX-87 area of operations (Johnson and Hawkins, 1987).

Three surface vessels were used to collect meteorological data during MIZEX-87. The Polar Circle, a Norwegian research vessel strengthened for movement in the ice, recorded three-hour surface observations, launched rawinsondes every six hours and made continuous measurements of mean wind, moisture, temperature, pressure and turbulent wind. The Polar Circle operated inside the West Fram Strait ice edge for the majority of the experiment between 74.5° to 79°N and 19°E to 6.5°W. Haakon Mosby,

another Norwegian research vessel owned by the University of Bergen, Norway, operated primarily at the ice edge or just off the ice edge and made measurements similar to those of the Polar Circle. The Haakon Mosby operated between 74.6° to 79°N and 19°E to 3.7°W. The Valdivia, a research ship from West Germany, recorded surface observations every three hours and launched rawinsondes every six hours. The Valdivia operated in the open ocean away from the ice edge during most of MIZEX-87 between 74° to 80°N and 17°E to 3°W.

A MIZEX shore forecasting center was established at Tromso, Norway. At this center reports from the three ships were received and added to routine ship and shore station reports provided by the World Meteorological Organization (WMO) reporting network to provide analyses and forecasts during the experiment. Satellite imagery from the Advanced Very High Resolution Radiometer (AVHRR) mounted on the NOAA 9 and 10 polar orbiters were used to help verify the analyses and track the observed weather systems (Schultz, 1987).

C. PURPOSE AND SCOPE OF THESIS

As the operating tempos of military forces continue to increase in the Arctic, our knowledge of the environment and how it affects platform and weapons sensors will play a key role in the deployment of these assets. The ability to predict the occurrence of various anomalies in electromagnetic (EM) propagation paths, such as radar ducts and radar holes or shadows, is a tactical necessity. This thesis follows the work done by Willis (1987) who investigated the ABL of the summer MIZ and its effects on the refractivity of electromagnetic waves within this layer. Rawinsonde data collected by four ships during MIZEX-84 were used as input into the Integrated Refractive Effects Prediction System (IREPS) to determine ducting parameters of height, thickness and strength. A spatial and temporal statistical analysis of the observed trapping layers and associated ducts was completed. A similar analysis is performed in this thesis using rawinsonde data from the three vessels that participated in MIZEX-87. The late winter ABL is discussed and compared to the conditions observed during MIZEX-84. The spatial and temporal statistical analyses are compared to those in the MIZEX-84 study by Willis. A range-dependent ray trace model is used to see the effect of a horizontally varying refractive structure on the EM wave propagation pattern coming from a transmitter. Various refractive structures are used to simulate conditions observed during MIZEX-87.

II. REFRACTIVITY IN THE ATMOSPHERE

EM energy travels in the form of waves and can be classified according to wave-length or frequency. In the context of military applications the EM spectrum is often subdivided into categories of EM and electro-optical (EO) wavelengths. The EM por-tion of the spectrum includes wavelengths greater than 1 cm but less than 10 m. The EO portion of the spectrum is defined to be wavelengths from 0.4 to 100 μm. This thesis directs its discussion only towards the EM portion of the spectrum. Further mention of EM radiation should be recognized to apply as such.

The propagation of EM radiation through the atmosphere is controlled by the ver-tical gradients of temperature, moisture and pressure. The effect of these meteorological variables on the mean refractive structure of the atmosphere is most pronounced for wavelengths ranging from 1 cm to 10 m in length. The frequencies associated with these wavelengths are classified in the radio spectrum as very high frequency (VHF; 30-300 MHz), ultra high frequency (UHF; 300-3000 MHz) and super high frequency (SHF; 3-30 GHz). In the radar spectrum these wavelengths equate to radar frequencies classified as the A-K radar bands. At longer wavelengths the ionosphere becomes the controlling influence. For wavelengths less than 1 cm but greater than 100 μm atmospheric molec-ular absorption generally makes long-distance propagation impractical.

EM radiation traveling in space at the approximate speed of 3×10^8m s^{-1} experiences an effective resistance to its propagation speed as it passes through an atmosphere with varying constituents and properties. This resistance is caused by the impinging external electric field inducing polarization of the individual molecules in the medium. This polarization produces an opposing electrical field which has the effect of reducing the propagation speed. The opposing field is caused by orientation of the molecules with a dipole moment anti-parallel to the field or by distortion of the electron shell structure.

The dielectric constant, ϵ, is used to describe the interaction of EM radiation with a medium. The amount of interaction, and therefore the strength of the opposing field, is dependent both on the type of medium and on the frequency of the radiation. The relationship is given by (2.1), where c equals the velocity in a vacuum and v equals the velocity in the medium.

$$v = c/\epsilon^{1/2} \qquad (2.1)$$

8

The index of refraction, n, is defined by (2.2) as the ratio of the velocity of an EM wave in a vacuum to its velocity in another medium and is equivalent to the square root of the dielectric constant.

$$n = c/v = \epsilon^{1/2} \qquad (2.2)$$

If an EM wave travels through a region of varying n it will be refracted towards the region of higher n or towards slower wave speeds. This is a simple application of Snell's Law defined in (2.3) and illustrated in Fig. 5.

$$n_1 \sin \theta_1 = n_2 \sin \theta_2 \qquad (2.3)$$

Generally, a denser material has a greater value of n. The density of the atmosphere usually decreases with height and thus EM waves are bent back towards the earth's surface.

The index of refraction in the atmosphere is a function of the value of pressure, temperature and water vapor pressure. The refractivity, N, defined in (2.4), is often used to represent refractive effects more conveniently.

$$N = (n - 1) \times 10^6 \qquad (2.4)$$

An equation to calculate the refractivity is given by Battan (1973) in (2.5) where P is pressure in millibars, T is temperature in Kelvin and e is water vapor pressure in millibars. This value of refractivity is simply a summation of the calculation of refractivity for dry air and for water vapor.

$$N = 77.6P/T - 5.6e/T + 3.75 \times 10^5 e/T^2 \qquad (2.5)$$

Battan indicated that carbon dioxide also contributes to N but that its contribution is negligible at less than 0.1% of the total value. The refractivity of dry air is essentially the same over the full scale of the EM spectrum. With the addition of water vapor to the atmosphere, the refractivity develops a frequency dependence. This is due to the dipole nature of the water molecule and its differing response to varying frequencies of radio waves. The greatest effect is seen in the lower frequency EM waves identified earlier and results in a greater value of n than for higher frequency optical waves.

When determining levels of EM transmission anomalies, the measure of the vertical gradient of refractivity is used. To account for the earth's curvature, a modified measure
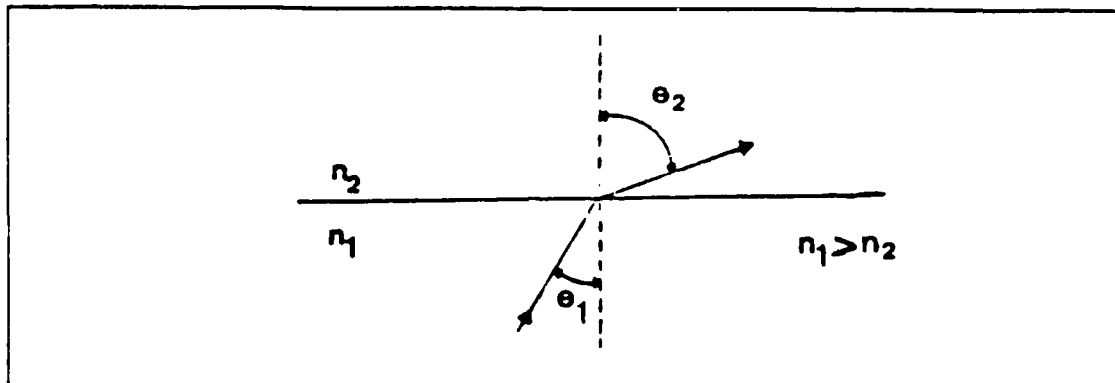
Fig. 5.   Graphical representation of Snell's Law.

of refractivity M, is defined by Battan (1973) in (2.6) where N_z is the value of N at a given height, Z, in kilometers.

$$M = N_z + 157Z \qquad (2.6)$$

This modification aids one in the identification of trapping layers and the associated ducts.

A trapping layer is a vertical section of atmosphere where M decreases with height. EM ducting is a direct result of the presence of trapping layers. An EM duct is a region in the atmosphere that tends to channel or confine EM waves. EM waves travelling in a duct incur lower spreading losses than in a normal atmosphere. This results in a signal strength that is greater at increased ranges and can lead to greatly increased radar or communications ranges. By knowing where levels of ducting exist, military tacticians can use such knowledge to plan aircraft attacks and surveillance routes. It can also be used to determine when counterdetection ranges of aircraft and surface radars are counterproductive to their useage. Finally, by knowing where enhanced and degraded ranges occur, one can better estimate initial detection ranges of hostile platforms traveling in or passing through these levels.

Fig. 6 identifies three types of ducting situations. A surface based duct caused by a surface trapping layer is depicted in profile (a). Profile (b) is an example of a surface based duct that occurs as a result of an elevated trapping layer. Finally profile (c) shows an example of an elevated duct caused by an elevated trapping layer. The thickness of the duct is determined by taking the height at the top of the trapping layer and subtracting from it the height at which an identical value of M is reached when drawing a
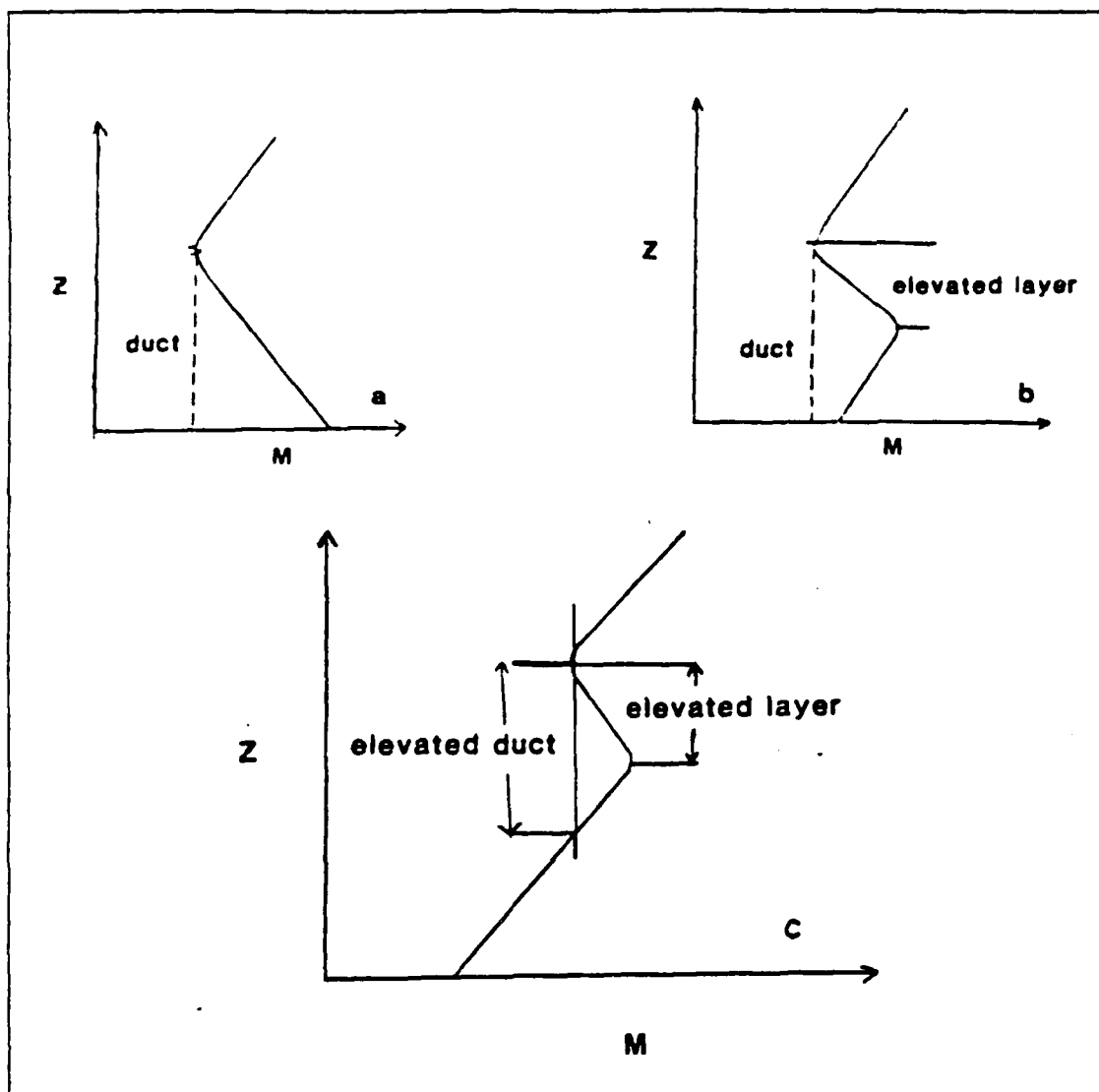
Fig. 6. Three types of ducting situations after Dotson (1987): profile (a) is a surface based duct caused by a surface trapping layer; profile (b) is a surface based duct caused by an elevated layer; profile (c) is an elevated duct caused by an elevated layer.

vertical line down from the top of the trapping layer. This is best seen in Fig. 6c. If a transmitter is located within a duct the emitted waves will be concave upward with respect to the earth's curvature as they travel through that portion of the duct with a positive M gradient. When the waves encounter the trapping layer they will be concave downward and curve back toward the earth. This ray theory concept is illustrated in Fig. 7.

11
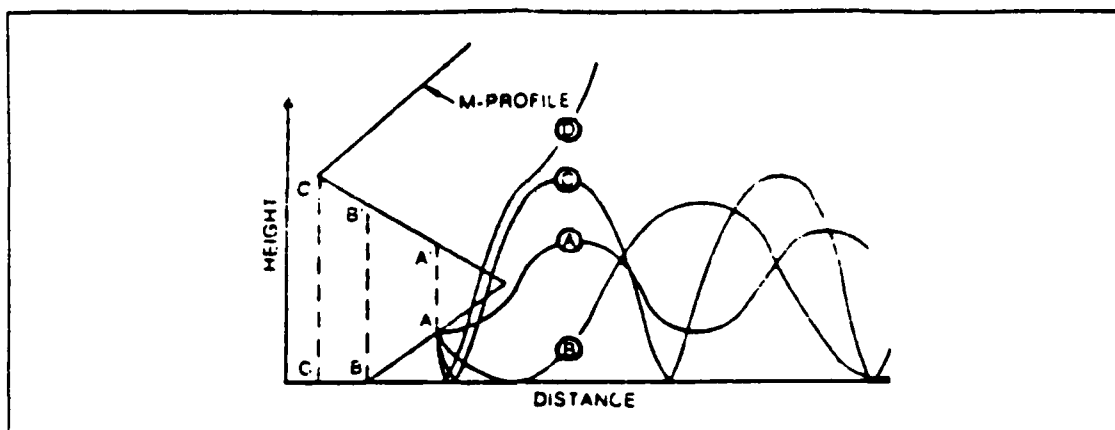
Fig. 7.   Possible ray paths in a ducting situation after Kerr (1951).

The Navy's Integrated Refractive Effects Prediction System (IREPS) is a shipboard environmental data processing and display system used to predict the effects of refraction on EM signals. The values of N and M gradients used by IREPS to define where trapping layers occur are listed in Table 1 taken from Naval Ocean Systems Center (1981). When the vertical gradient of M is equal to 0 per km, an EM wave will be refracted downward with a curvature equaling that of the earth's surface (Battan, 1973). If the M gradient has a negative value, the curvature will be greater than that of the earth resulting in a ducting situation. The M gradient value of 0 per km is defined as the threshold value for trapping of an EM wave.

Other anomalies of importance in atmospheric EM wave propagation are levels of super-refraction and subrefraction. The values of N and M gradients used by IREPS to determine levels of super-refraction and subrefraction are shown in Table 1. Super-refraction is defined to be where M gradients vary from 0 to 79 per km. In a super-refractive region the EM waves are bent towards the earth but not to the extent observed in a trapping layer. Radar propagation ranges are somewhat greater than normal in this region. In a subrefractive layer the EM waves bend away from the earth's surface. The M gradient is greater than 157 per km. A subrefractive layer causes reduced radar ranges to occur. The values listed in Table 1 are also used in this study to determine levels of trapping, super-refraction and subrefraction. The ray geometry associated with the various conditions of refraction is depicted in Fig. 8.

12
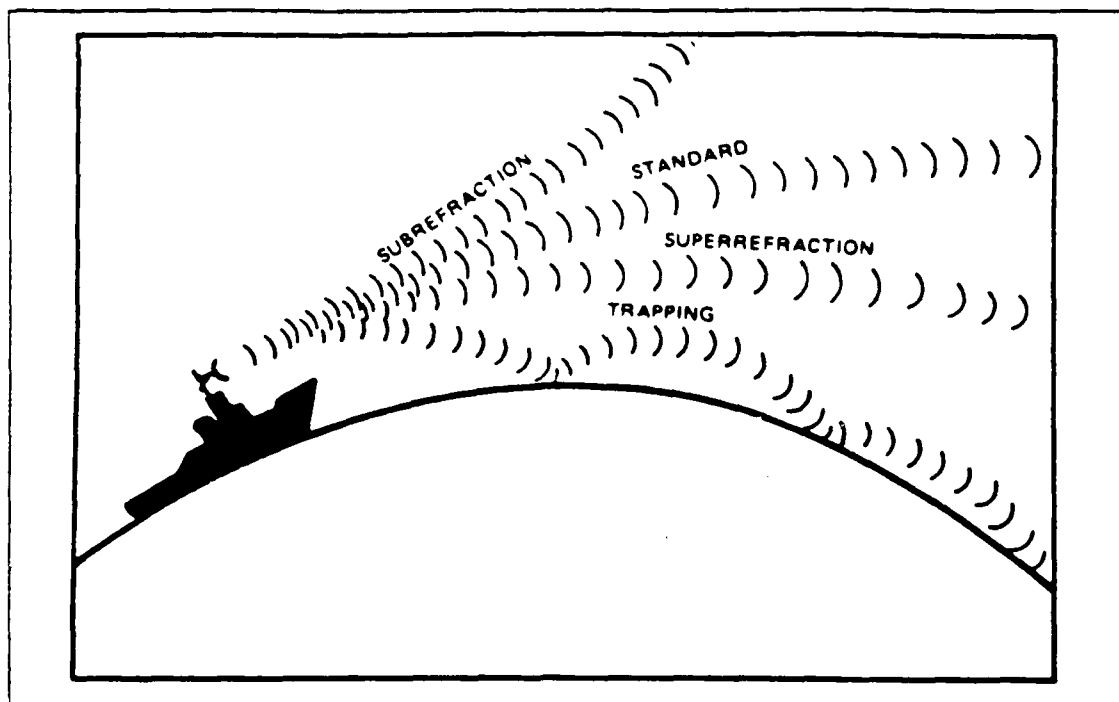
Fig. 8. Ray geometry for various refraction conditions (Naval Ocean Systems Center, 1981).

TABLE 1
IREPS CLASSIFICATION OF REFRACTION CONDITIONS

IREPS Classification	dN dZ km⁻¹	dM dZ km⁻¹	Range
Subrefraction	> 0	> 157	Reduced
Normal	0 to 79	79 to 157	Normal
Super-refraction	-79 to -157	0 to 79	Increased
Trapping	< -157	< 0	Greatly Increased

III. THE MARINE ATMOSPHERIC BOUNDARY LAYER IN THE ARCTIC

A. GENERAL

A thorough understanding of the physical mechanisms influencing the depth of the atmospheric boundary layer (ABL) is essential in the study of atmospheric refractivity. Large mean gradients of temperature and moisture often occur at the boundaries of the ABL. As discussed in chapter two, these vertical gradients cause EM waves to refract according to the sign and strength of the refractivity gradient. This attenuation in the expected path can result in greatly increased or decreased wave propagation.

The ABL is described by Dutton and Panofsky (1984) as a region of the atmosphere that varies in thickness from tens of meters in a stably stratified atmosphere to several thousand meters in an unstable case. All exchanges of momentum, moisture and thermal energy between the earth's surface and the atmosphere take place within this layer. The ABL's lower boundary is the surface of the earth or the ocean, and the flow within this layer is typically turbulent.

Turbulence may be described as being either mechanically or convectively produced. The amount of turbulence observed in the ABL is a function of the surface roughness, the vertical gradient of the near-surface wind and the sensible and latent heat flux originating from the ground and the atmosphere. Turbulence is produced mechanically from the flow of air over a rough surface by energy extracted from the gradient of the mean wind. A higher surface wind speed and a stronger vertical gradient of speed coupled with a rougher surface increases the amount of shear production of turbulent kinetic energy (TKE). This occurs to some degree regardless of the thermodynamic stability of the ABL. Sensible heating at the earth's surface or the release of latent heat during cloud formation results in the convective production of turbulence. This causes the ABL to tend towards greater instability and increases both the level of available TKE and the mixing throughout the layer. As the amount of available TKE increases, the ABL is expected to increase in thickness (Wyngaard, 1973).

The unstably stratified or convective ABL is subdivided into three distinct regions as depicted in Fig. 9. The lowest of these, the surface layer, ranges in height from a few meters to several tens of meters depending on the strength and direction of the thermal energy flux. Within this layer large vertical gradients of wind speed, temperature and
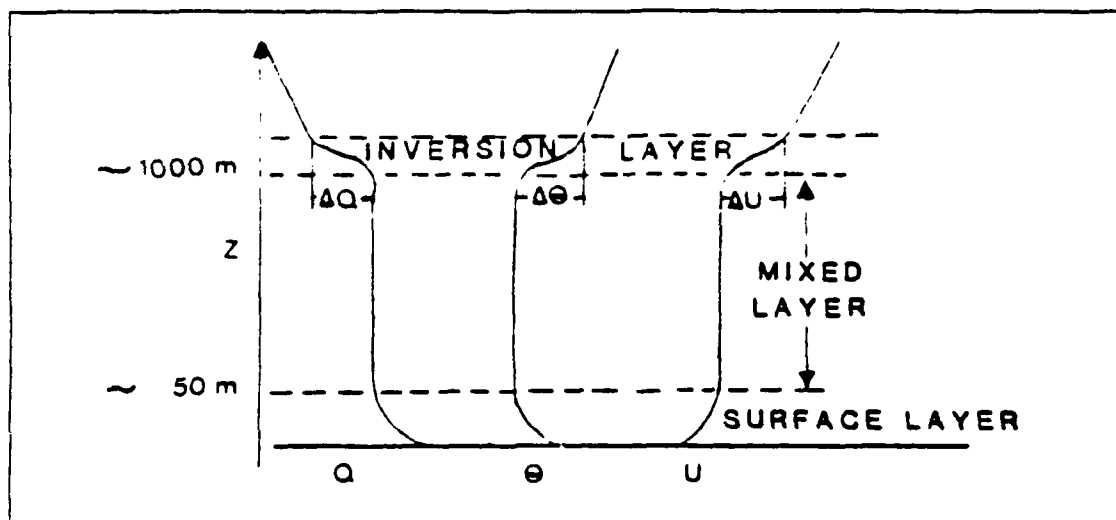
Fig. 9.   The convective atmospheric boundary layer: mean vertical profiles of potential temperature (θ), wind speed (U), and specific humidity (Q) are superimposed.

moisture occur. The strong vertical wind shear and the convection due to warmer surface temperatures produces the turbulence that transports moisture, heat and momentum up into the mixed layer. The mixed layer, directly above the surface layer, is relatively homogeneous in nature and composes the majority of the ABL. This layer approaches homogeneity as the turbulence produced within the boundary layer causes the erosion of local gradients that form within the mixed layer. The upper 50-100 meters of the convective ABL is depicted as a capping inversion layer. Within this layer the TKE available for mixing is consumed by a strong, increasing vertical temperature gradient. This gradient effectively prevents the exchange of physical properties with the free atmosphere above (Wyngaard, 1973).

A stable ABL is almost exclusively due to cooling at the surface and subsequent development of a positive vertical temperature gradient. Larger scale convectively generated turbulence is suppressed in this situation, with very little mixing occurring above the surface layer. This results in a significant decrease in the exchange of momentum, heat and moisture between the earth's surface and the atmosphere.

The marine atmospheric boundary layer (MABL) differs from the ABL over land in several ways. The ocean surface experiences a much smaller diurnal temperature variation than that of the land. This causes the height of the MABL to vary relatively less diurnally. The ABL over land often experiences significant fluctuations in height due to

15

radiative heating and cooling. The humidity structure in the MABL is often much more pronounced than that over the land. The lower liquid boundary provides a ready source of moisture to the MABL. This results in geater vertical variations of moisture over the MABL surface layer and capping inversion (Dotson, 1987). The stability of the MABL is very nearly neutral over most of the world's oceans. As air flows over the ocean for a long period of time its properties move toward equilibrium with the ocean surface. In this near-neutral state, variations in stability can have a significant effect on the surface fluxes of moisture, heat and momentum. Thus even small variations in the sea surface temperature can cause the MABL structure to change (Businger and Shaw, 1984).

B. MARCH/APRIL SYNOPTIC CLIMATOLOGY AND OBSERVED CONDITIONS

1. Unique Features

Changing synoptic conditions can significantly affect the temperature, momentum and moisture distributions in the MABL and thus alter the level of mixing in and the height of the boundary layer. Several features that are unique to the Arctic region influence the synoptic weather patterns. These features are identified in Sater *et al.* (1971) as distinctive daylight and darkness regimes, the circumpolar vortex, surface snow and ice cover, and the flatness of the Arctic region.

Distinctive regions of daylight and darkness are characteristic of the Arctic due to the tilt of the earth's axis and the lower elevation of the sun. In the winter a perpetual darkness occurs and results in large radiational loss at the earth's surface. During the summer, in conditions of nearly constant daylight, a net radiational loss is still present but not to the degree seen in the winter. These radiational losses cause cooling at the surface and development of a surface temperature inversion especially in the central Arctic. The months of March and April are a transition period between the two extremes. The shift from total darkness to total daylight occurs over only a few weeks time. During MIZEX-87 the hours of daylight lengthened at the rate of 25 minutes per day from 9 hours of daylight in mid-March to 21 hours by mid-April (Schultz, 1987).

The circumpolar vortex is the name associated with a large scale cold core low pressure region centered around the North Pole, and the belt of upper-level westerly winds that surround the low at its outer edge (Petterssen *et al.*, 1956). Fig. 10 is a 12-year mean of the 700 mb height field in decameters. The intensity of the circumpolar vortex is often associated with the packing of the 960 and 990 dm lines at this level. The surface cyclones and anticyclones that travel through the Greenland Sea region are

16
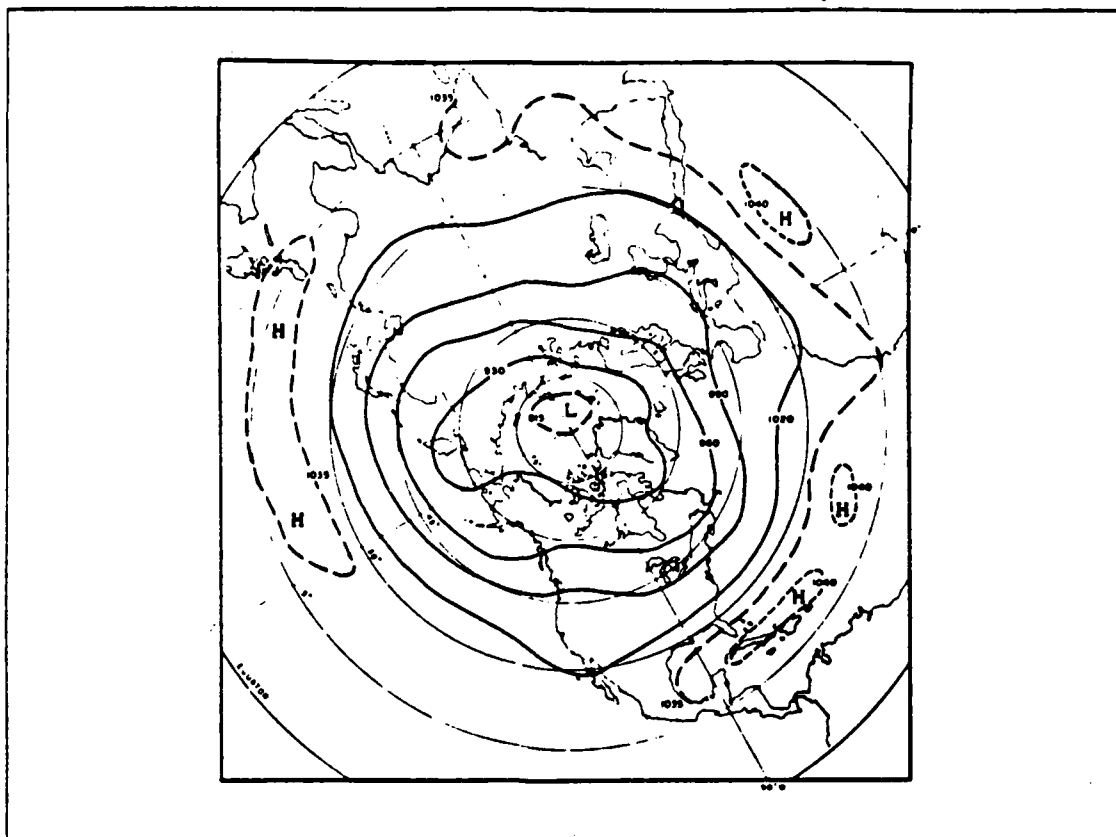
Fig. 10. Climatological 700mb heights in April from Sater *et al.*, (1971).

embedded in and steered by this upper level flow. Changes in the position and the strength of the vortex can radically affect regional conditions (Sater *et al.*, 1971). The March, April climatology shows the vortex moving from its most southern position in the winter, when the packing and the strength of the vortex is the greatest, to its most northern position in the summer, when the vortex is weakest.

The snow and ice cover so prevalent in the Arctic affects the meteorology of the area in several ways. The high surface albedo properties of snow and ice cause a much higher percentage of the incoming solar radiation to be reflected. This causes lower temperatures to be maintained over the ice compared to the ocean. The colder temperatures reduce the moisture capacity of the air to such an extent that a large portion of the Arctic is often referred to as a desert (Sater *et al.*, 1971). The ice cover also effectively blocks upward heat flux from the warmer ocean waters beneath it. This has a significant impact on the stability of the ABL over the ice. These areas tend towards

17

greater stability and lower ABL thicknesses. The presence of an ice-ocean boundary creates areas of significant horizontal temperature gradients. These gradients have been closely correlated to instances of cyclogenesis, especially during conditions of off-ice wind flow (Petterssen *et al.*, 1956). This factor is of great interest when considering the synoptic patterns in and around the MIZ.

The flatness of the Arctic region promotes relatively unlimited flow of air into the region. Cyclones that are often generated along the polar front in midlatitudes are able to travel freely into the Arctic basin. Because of the low temperatures and lack of available moisture, cyclones frequently stagnate and fill in this region. Frequent cyclonic activity is encountered in the Greenland Sea MIZ as cyclones from the midlatitudes are steered by the circumpolar vortex up into this region.

2. Spring Climatology

The region in which MIZEX-87 was conducted is under the influence of several different climatological surface pressure features. Fig. 11 shows the 12-year climatological mean sea-level pressures for April. The synoptic pattern around the MIZEX area is characterized by a weak and variable surface high over northern Greenland and a belt of low pressure extending from the southern tip of Greenland, through Iceland and up through the Norwegian Sea to the northern tip of Norway. The belt of low pressure corresponds to cyclones moving through this region that are strongly influenced by upper-level steering. The wind fields in the MIZEX area are generally easterly due to the presence of the migratory lows to the south (Sater *et al.*, 1971).

The climatological movement of cyclones is more clearly shown in Fig. 12. The primary and secondary cyclone tracks indicate that, in April, cyclones move through the Greenland Sea area in a northeastward direction. The primary storm track originates off the east coast of Iceland and moves up to a region off the northern coast of Norway. The secondary track follows the southeast coast of Greenland northward and then cuts across the Greenland Sea, passing just south of the Svalbard Islands and into the same sink region as the primary track.

3. Meteorological Conditions Observed in MIZEX-87

The synoptic and mesoscale meteorological features observed during MIZEX-87 have been examined and separated into five distinct periods by Schultz (1987). During period one, from 20-23 March, the MIZEX area was under the influence of a high pressure system centered over the Fram Strait. Period two was from 24-27 March.
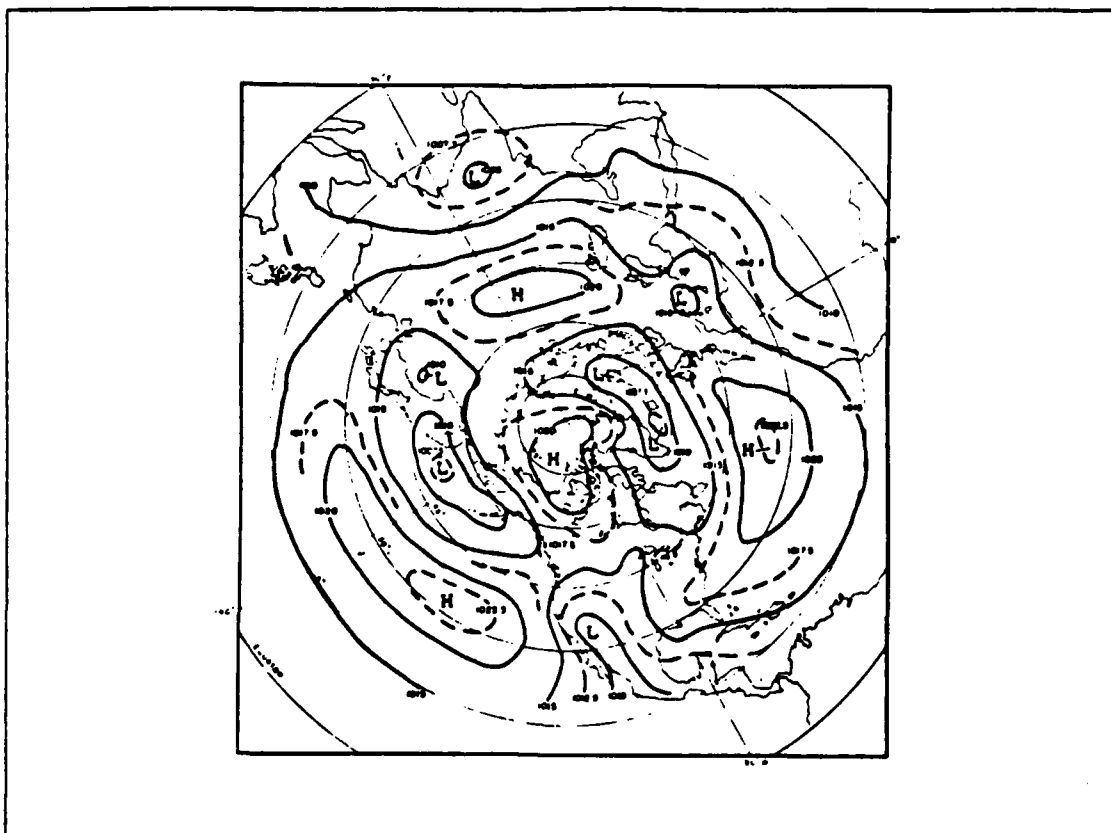
Fig. 11.   Climatological sea-level pressures for April from Sater *et al.*, (1971).

During this time the area was influenced by a mesoscale boundary layer front that formed just west of the Svalbard Islands. The Fram Strait high weakened during this period and surface pressures fell. The third period, from 28 March to 31 March was influenced by a small scale low that persisted until the last two days and then began to fill. The fourth period was from 1-3 April. During this period the Fram Strait region was under the influence of a small high pressure system. A synoptic scale low moving northeast passed to the south of the MIZEX area but did not significantly influence the local conditions. The final period, from 4 to 10 April, saw the area under the influence of two separate synoptic-scale lows. These lows formed about 50 km off the east coast of Greenland at about 71°N and 15°W. The first low moved across the Greenland Sea, following the secondary storm track depicted in Fig. 10 and stalled about 100 km southwest of the Svalbard Islands on 5 April. The second low caught up and merged with the first low on 8 April creating a larger, more intense system that significantly

19
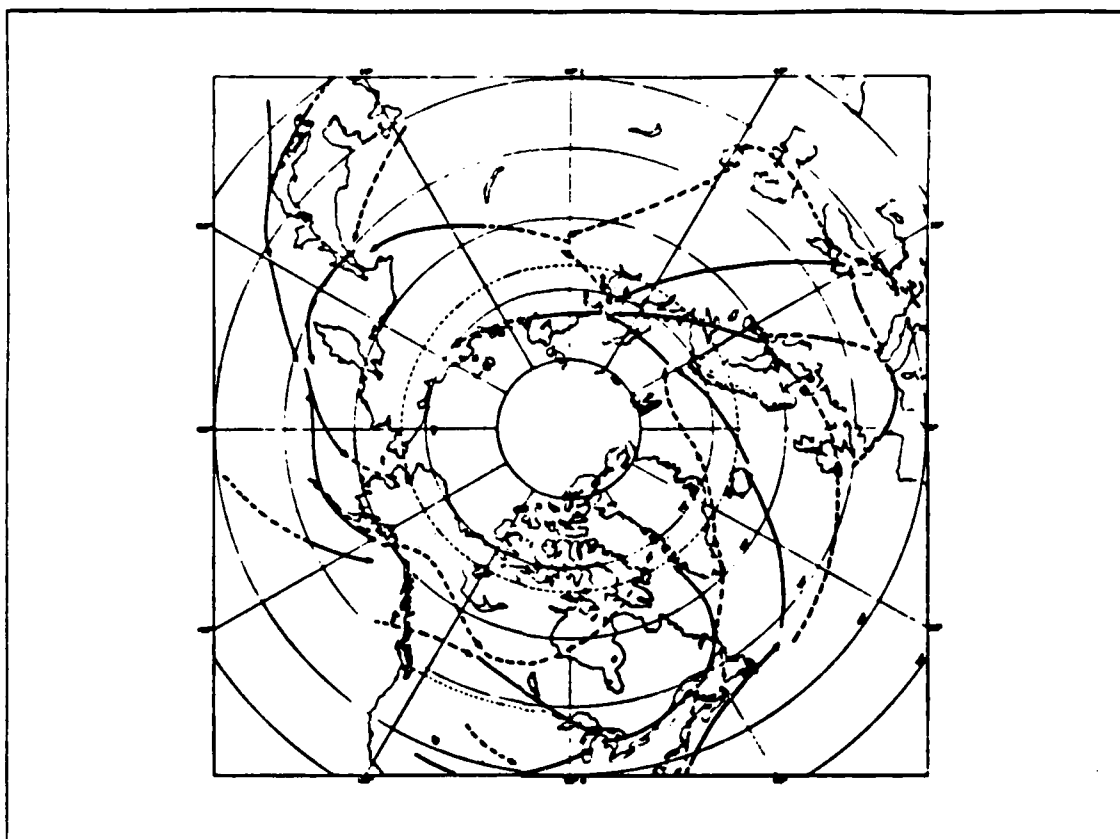
Fig. 12. Climatological tracks of cyclones in April from Sater *et al.*, (1971): Primary tracks indicated by solid lines. Secondary tracks indicated by dashed lines.

affected the boundary layer structure of the region. These five periods will be examined in greater detail in chapter five to determine how the observed meteorological features altered the refractive structure of the atmosphere.

The observed synoptic and mesoscale features were consistent with the climatology of the MIZEX area discussed earlier. The region was dominated by high pressure except during the movement of synoptic lows along the secondary cyclone track. The occurrence of the boundary-layer front is also a common feature of this region. Winds tended to be generally from the north during MIZEX-87. This differs from the climatological easterly winds proposed by Sater *et al.* (1971) suggesting a lessened influence by the transiting low pressure systems on the wind direction during this period.

C. MIZEX-87 BOUNDARY LAYER STRUCTURE

The structure of the ABL during MIZEX-87 varied considerably both spatially and temporally. Variations in the height of the ABL have been correlated by Guest et al. (1988) with respect to the synoptic situation, wind speed and direction relative to the ice edge, and horizontal location with respect to the ice edge. In the absence of turbulence measurements, the level of mixing in the boundary layer was determined by visual inspection of the rawinsonde data. Levels where the potential temperature was nearly constant with height were considered to be well-mixed. This is strictly true only when no liquid water drops are present. The potential dewpoint temperature and specific humidity were used to identify cloud layers and well-mixed regions respectively. Two humidity variables were used in determining cloud layers and mixed layers because no single humidity variable can easily show their location (Guest and Davidson, 1988).

Investigation of the rawinsonde data revealed that the boundary layer normally presented a well-mixed appearance with a pronounced capping inversion when the area was under the influence of high pressure. Fig. 13a shows a plot of potential temperature, potential dewpoint temperature and specific humidity for a rawinsonde launch from the Valdivia taken at 0608 UTC on 23 March. During this time the Valdivia was located just south of a high centered over the Fram Strait. The boundary layer is well-mixed up to 650 m, where a capping inversion separates it from the free atmosphere above. During periods of lower pressure and frontal activity as in periods 2 and 5, the boundary layer increased in thickness to heights which often exceeded 1500 m. Fig. 13b is an example of this situation taken from the Haakon Mosby at 1147 UTC on 6 April. The layer is well mixed up to 1600 m and the inversion is nonexistent or very weak at best. Lindsay et al. (1986) presented similar results in demonstrating that the inversion tends to descend in response to warming conditions in the free atmosphere associated with higher pressure and rises during periods of cooling and greater instability brought on by low pressure systems.

Correlation of the observed surface wind speed with the boundary layer height is depicted in Fig. 14. The median height of the top of the mixed layer generally increases as wind speed increases in a somewhat linear fashion from a median value of 500 m at 1.5 m s^{-1} to a median value of 1075 m at 13.5 m s^{-1}. As discussed earlier, increases in the surface wind speed aid in the generation of TKE available for mixing of the boundary layer. However, higher wind speeds were experienced during periods of lower pressure, and this almost certainly causes some contamination of the correlation.

21
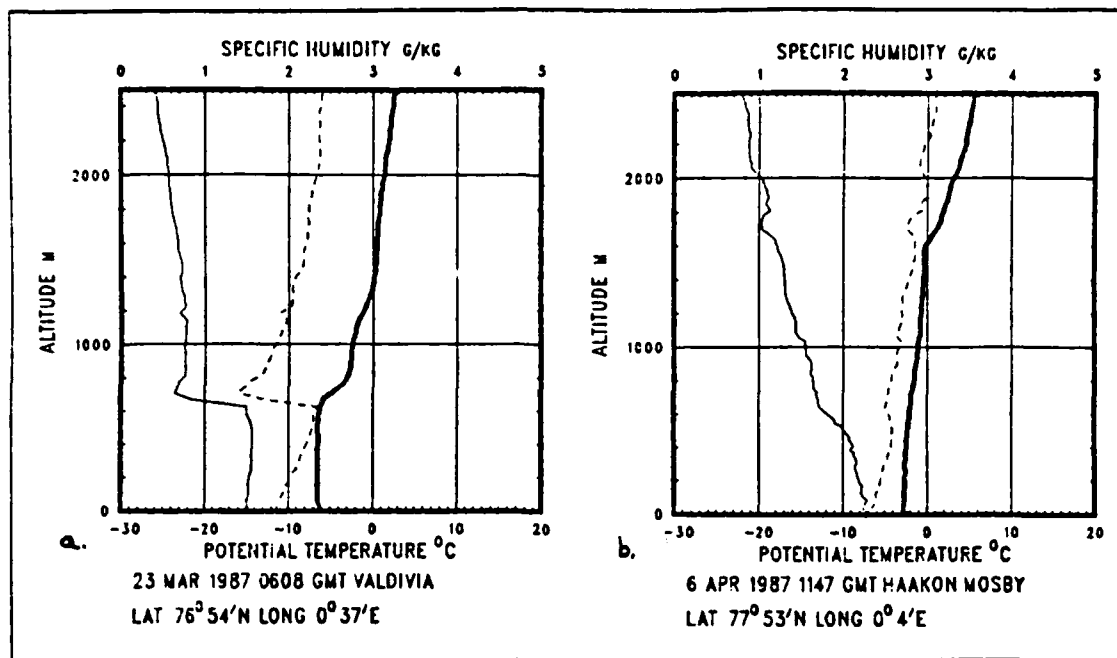
Fig. 13. Vertical profiles from two different pressure regimes: potential temperature (bold solid line); potential dew-point temperature (dashed line); specific humidity (solid line).

Wind direction and horizontal position with respect to the ice edge also appears to show some correlation with the height of the MABL. Fig. 15 from Guest *et al.* (1988) shows that on-ice winds produced deeper well mixed layers than off-ice winds. The on-ice winds however, had much more individual scatter in the layer heights than did the off-ice winds. This scatter is not shown in Fig. 15. Guest reported that the on-ice winds often produced multiple inversion layers as the offshore air flowing onto the colder ice surface produced new boundary layers. These new boundary layers were associated with lower inversion heights, however the median change is not nearly as drastic as that observed in the off-ice flow.

The off-ice flow shows median mixed layer heights to be below 200 m over the ice and then to increase rapidly as the air moves out into the open ocean. This increase can be attributed to the increase in heat flux from the ice to the open ocean resulting in a less stable more turbulent boundary layer over the ocean. Fairall and Markson (1987) determined that the heat flux near the ice edge was close to zero and that the heat flux over the ocean was 30 W m^{-2}. The increased heat flux over the ocean results in an increase in the energy available for mixing in the layer and entrainment of the free atmosphere.

22
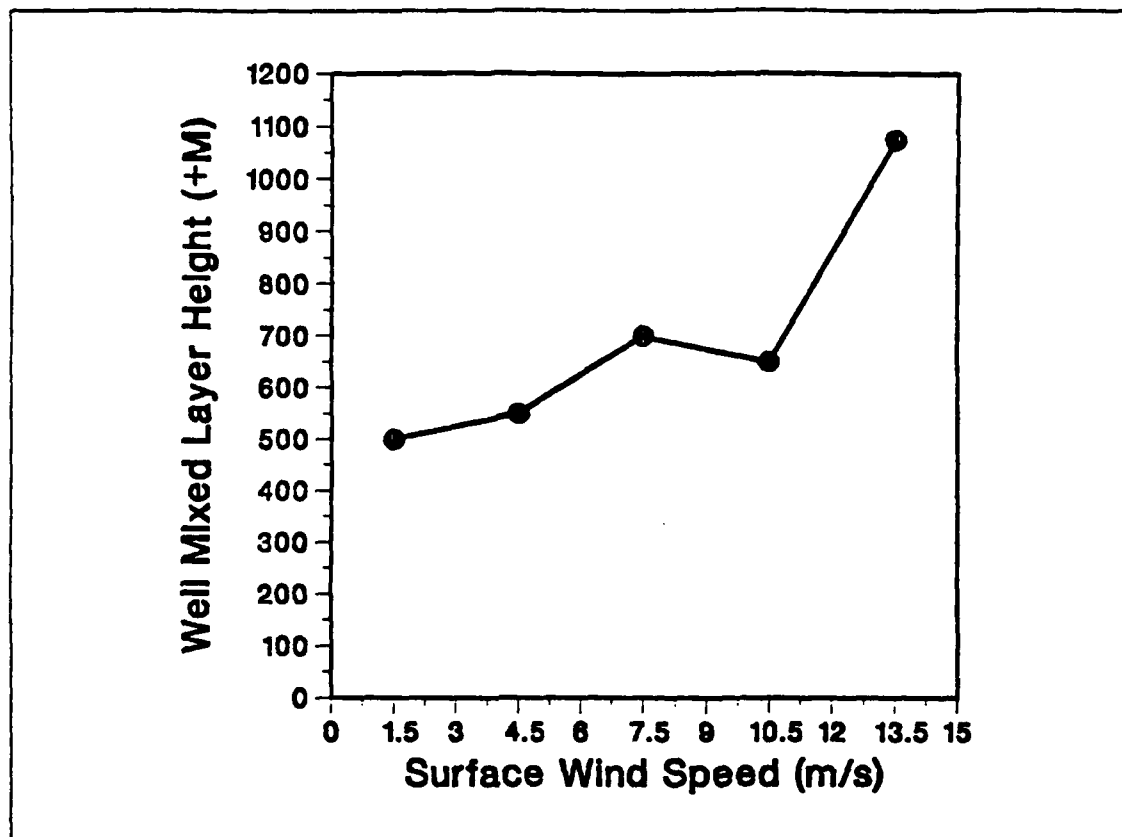
Fig. 14.   Variation of median mixed layer height with surface wind speed.

This entrainment will cause the inversion height to increase while decreasing the inversion strength.

Winds parallel to the ice edge with the ice to the right of the wind flow showed a rather mixed pattern in the median mixed layer heights. Guest *et al.* (1988) suggests that the zig-zag type pattern may be a result of varying surface roughnesses normal to the wind vector or across the ice edge. This varying roughness can induce vertical motions due to frictional convergence or divergence and thus cause variations in the level of mixing.

D.   COMPARISON OF MIZEX-84 AND MIZEX-87 MABL STRUCTURE

Several differences were noted in the boundary layer structure between the MIZEX-84 summer case and the late winter, early spring MIZEX-87 data. Fig. 16 from Guest *et al.* (1988) shows the median well mixed layer heights for both MIZEX-84 and MIZEX-87 as a function of horizontal position. Both data sets displayed a similar
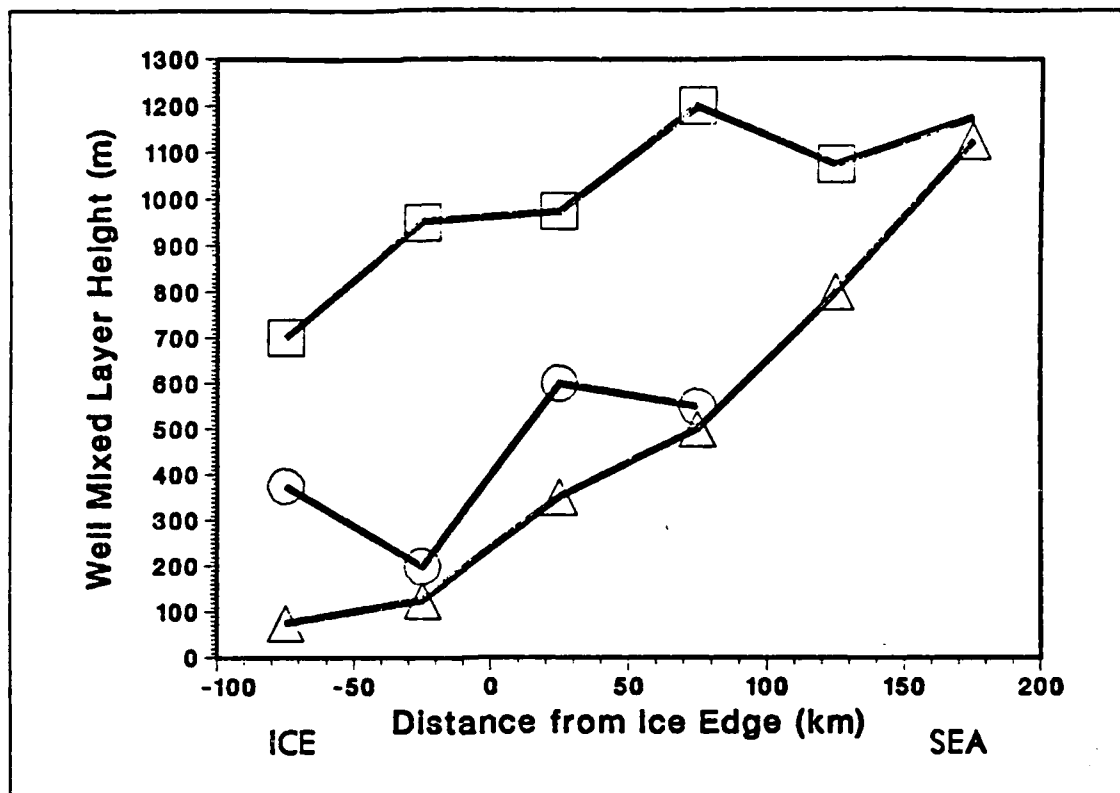
Fig. 15.   Median mixed layer heights from Guest *et al.*, (1988):   off-ice, on-ice and parallel winds are indicated by triangles, squares and circles, respectively.

pattern, however the mixed layer depth was consistently higher for the springtime case. It was also noted that the strength of the inversion layer was typically stronger during the summer MIZEX.   In addition, the air above the inversions was warmer over ice-covered areas as opposed to open ocean areas. This suggested a greater degree of subsidence over the ice. This variation in upper air temperatures was not evident during MIZEX-87, and the boundary layer appeared to be much less stable. Overland (1985) determined that the winter boundary layer in the MIZ was generally shallower with sharper inversions. The summer regime was marked by a deeper boundary layer with weaker capping inversions. The data presented by Guest *et al.* (1988) do not seem to follow this trend. There are several possible reasons for the height differences observed during the two MIZEX's.   One possible reason is that the cyclone tracks during MIZEX-87 were farther north than those in MIZEX-84, which may have reduced the divergence in the area. Another cause suggested is that during the summer the warm air associated with the nearby land masses may have been advected into the atmosphere

24
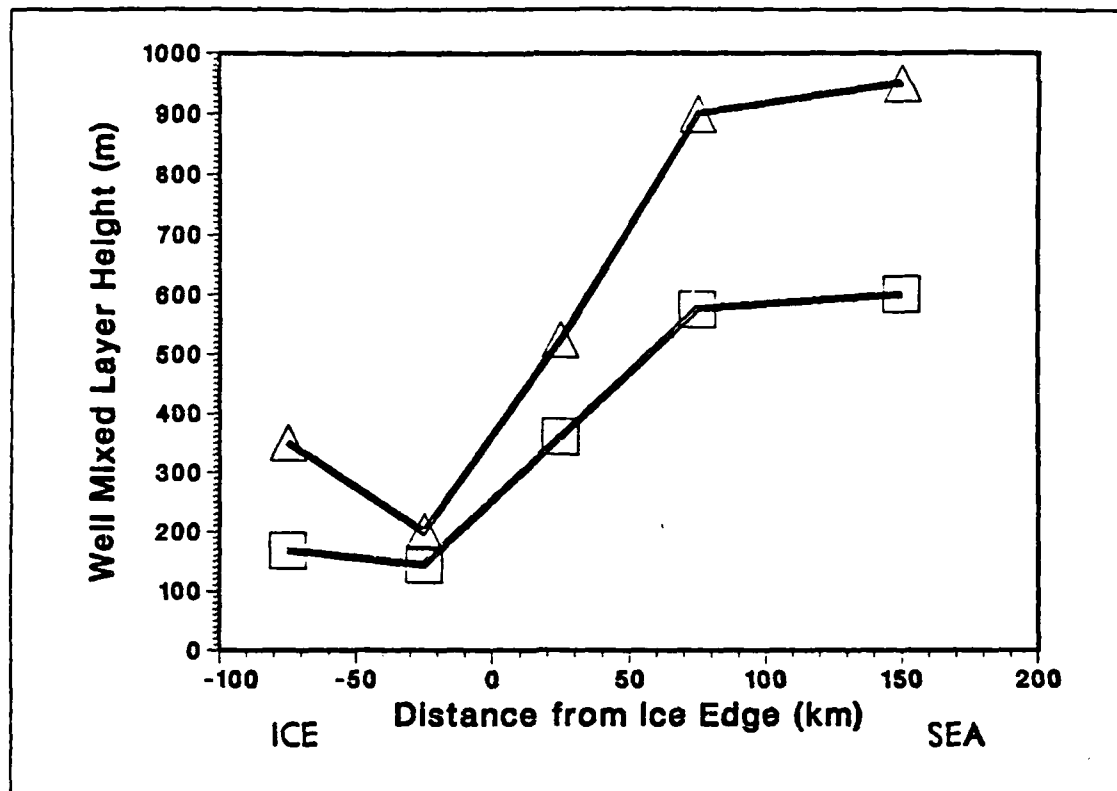
Fig. 16.   Comparison of mixed layer heights from Guest *et al.*, (1988):   MIZEX-84
is indicated by squares, MIZEX-87 is indicated by triangles.

over the inversions above the ice by an ice breeze circulation causing stronger inversions. This supply of air is not present over the cooler continents during the March·April time frame (Guest *et al.*, 1988).   Another possible cause in the height differences may be due to more periods of onshore flow during MIZEX-87 as compared to MIZEX-84. Onshore flow resulted in higher median mixed layer heights, and this could explain part of the difference.   One other possibility is that the colder air temperatures experienced during MIZEX-87 would have created greater surface-to-air heat fluxes in the MIZEX-87 boundary layer.   Greater heat fluxes would influence the turbulence driving the mixing in the layer and would yield higher inversion layers.

IV. DATA ACQUISITION AND PROCESSING

A. DATA ACQUISITION AND SOURCES OF ERROR

The data used to analyze the refractive conditions observed during MIZEX-87 were obtained from the three surface ships operating in and around the MIZ and from the Norwegian Meteorological Institute based in Tromso, Norway. The research vessels Polar Circle, Haakon Mosby and Valdivia launched rawinsondes at approximately 6-hour intervals and collected meteorological data using ship-mounted instruments. Visual surface observations were also made on each ship every three hours.

1. Polar Circle

The Polar Circle collected data from 22 March through 11 April 1987. The ship was equipped with a meteorological instrument station mounted on a platform located 16 m above sea level and just forward of the low mast. The station failed to give accurate measurements for wind speeds above 9 m s^{-1}. During these episodes wind speed was measured by a sonic anemometer located next to the meteorological station. For wind speeds less than 9 m s^{-1} the two instruments showed excellent agreement with maximum speed differences of only 0.3 m s^{-1}. The instrument accuracy of the winds at these slower speeds should be less than or equal to this difference. Distortion of the winds by the ship's structure were estimated to be less than 5% due to the instruments being located away from any blocking structures. An exception to this is for winds coming directly from astern when errors may have been as great as 20%. Measurements of wind direction were subject to errors in the magnetic compass of the meteorological station due to magnetic anomalies caused by the ship or by the local geology. This resulted in extreme directional errors in the winds for short periods of time. For a majority of the time the wind direction measurements from the meteorological station on Polar Circle were estimated to be accurate to within 20 degrees. The surface temperatures were estimated to be accurate to within 0.2°C and the relative humidity to within 5% of the stated value. The above data were sampled continuously onboard the Polar Circle at a sampling rate of 12 seconds. Surface atmospheric measurements presented in this thesis represent 10-minute averages of these data. Pressure was recorded using automatic pressure sensors. These sensors are not as accurate as other instruments but provided increased data coverage. Errors in pressure readings were not greater than 2 mb (Guest and Davidson, 1988).

26

2. Haakon Mosby

The Haakon Mosby measured the same parameters as the Polar Circle using the same instrumentation as the Polar Circle except for wind speed. A miniature cup anemometer was used on the Haakon Mosby for higher wind speeds. Errors in wind direction were not as extreme because the ship did not cause significant magnetic distortion. Wind directions were usually accurate to within 5°. Winds from the stern of the ship exhibited errors of up to 20% in speed and direction due to flow distortion. The other instrument accuracies are the same as those reported for the Polar Circle (Guest and Davidson, 1988).

3. Valdivia

The Valdivia measured the same parameters as the previous two ships, however, due to timing errors in the recording instruments the most reliable data were taken during the surface observations every three hours. The accuracies of the measurements were similar to those reported for the Haakon Mosby (Guest and Davidson, 1988).

4. Rawinsondes

Rawinsondes manufactured by the VIZ corporation were used on the Polar Circle and Valdivia to obtain vertical profiles of atmospheric parameters. The VIZ-Beukers W-8000 RP+ Microsonde system and its associated software were used on these two ships to obtain measurements of pressure, temperature, dew-point temperature, relative humidity, altitude, wind speed and wind direction. The sampling interval of the rawinsonde was every 10 seconds for a period of 50 minutes. This provided a maximum of 300 vertical data points per launch. The wind speed and wind direction were measured by tracking a signal from the rawinsonde using an Omega tracking system. The temperatures measured using this system were accurate to 0.2°C and the dew-point temperature was accurate to 1.0°C. Heights were calculated to be accurate to within 30 meters. The wind speeds were accurate to 1 m s^{-1} except in regions of strong wind shear where the accuracy dropped to 2 m s^{-1} (Guest and Davidson, 1988).

The Haakon Mosby used a rawinsonde system manufactured by the Vaisala Corporation. Omega tracking was used for calculation of wind speed and direction. The measured parameters were identical to those measured by the VIZ system.

A total of 169 successful launches were made from the three ships. The Polar Circle recorded 66 launches from 24 March to 11 April, 1987. Valdivia recorded 48 total launches from 19 March to 3 April, 1987. Haakon Mosby recorded 55 launches from

27

24 March to 11 April, 1987. Of these, two of the launches resulted in only partial data sets.

The vertical gradient of moisture, as noted previously, is a key variable in determining the refractivity gradient dM/dZ. Willis (1987) described a possible error in the dewpoint curves of 37% of the MIZEX 84 rawinsonde profiles examined in her study. In the suspect profiles the dewpoint temperature equaled the air temperature just below the inversion, indicating saturation and the presence of a cloud layer. At the inversion base the dewpoint normally decreases with height. This decrease is due to the drying out of the air caused by subsidence in the air above the inversion. The profiles examined by Willis did not follow this pattern. The dewpoint curve was observed to remain saturated through the inversion and decreased sharply at a variable height above the inversion. Fig. 17 from Willis (1987) shows an example of this phenomenon.

Willis offered several physical explanations as to the cause of the suspect profiles. One suggestion was the possibility that warmer and more moist air, originating over the northern boundary of the Gulf Stream, could have been lifted and advected into the Arctic region. This would require the winds to be primarily from a southerly direction which was not the case during MIZEX 84. Another explanation proposed by Ohtake *et al.* (1982) attributed the saturation above the inversion layer to the increased water vapor flux from open leads in the ice during sub-zero temperatures. This would cause the atmosphere to be supersaturated with respect to the ice. This proposal assumes that the measurements are being taken in an area predominantly covered by ice.

A second possibility addressed by Willis was that of a humidity sensor problem. It was suggested that the humidity sensor may have been lagging after encountering an area of saturation. This could have been caused by moisture accumulating on the sensor in the form of condensation or possibly frost/ice. It was noted that the dewpoint often decreased rapidly shortly after ascending through 0°C into warmer temperatures. It is possible that frost formed on the humidity sensors would be able to melt and subsequently evaporate in the drier air above the inversion. The effect of such an error in the moisture gradient would be to increase the height of the base of a trapping layer as well as lessen the strength and the thickness of the layer. Willis applied a correction to the suspect profiles to eliminate the saturated dewpoint curve along and above the inversion. Her results were reported using both the corrected and uncorrected data sets. The frequency of ducting events using the corrected data was found to be only half that measured using the original data.

28
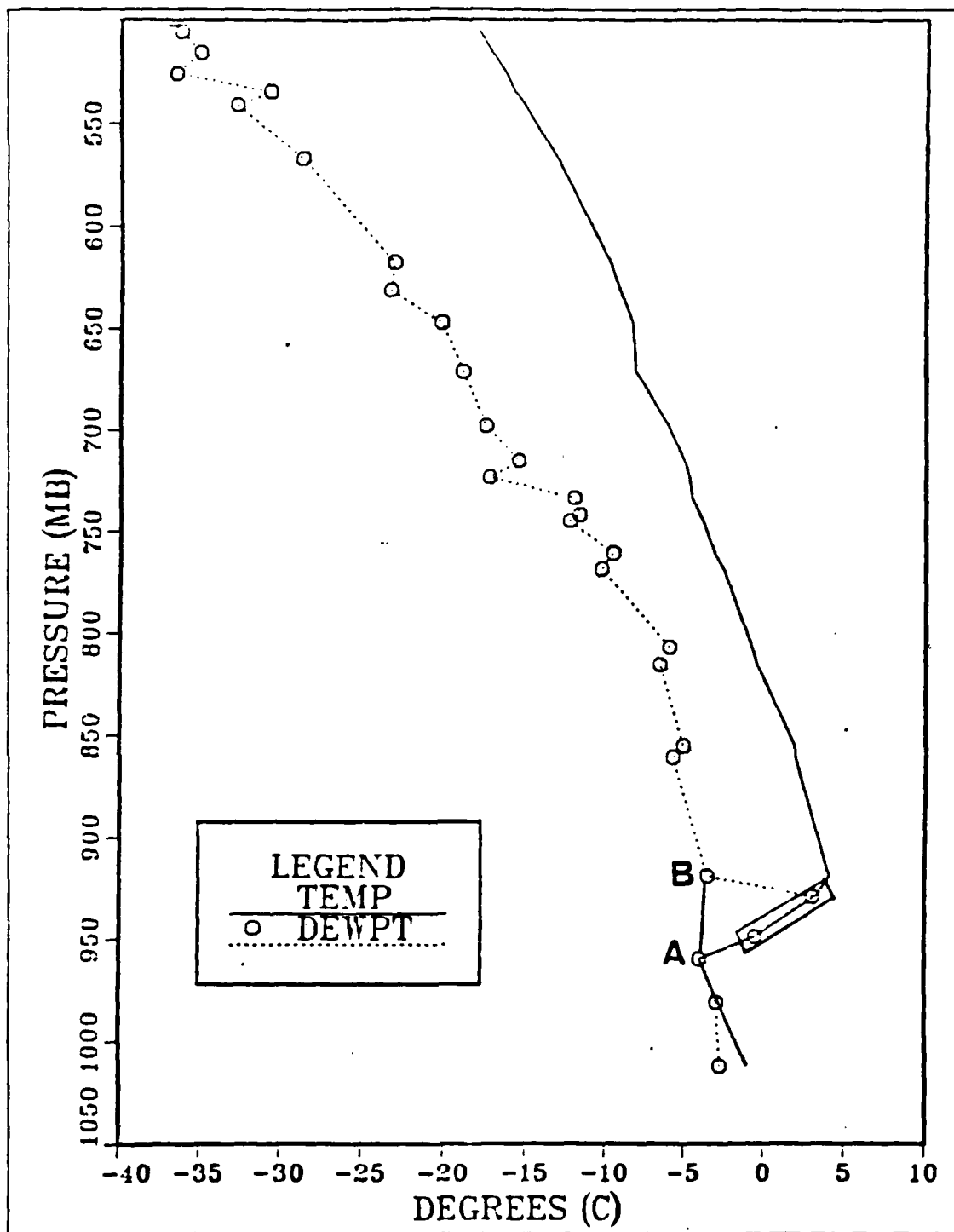
Fig. 17. Suspect Dewpoint Curve from Willis (1987).

The dewpoint problem described by Willis was observed very infrequently in the MIZEX-87 rawinsonde profiles. In 13 of 169 launches (7.7%) a situation similar to that described by Willis in the MIZEX-84 data was noted. Of the 23 incidences of ducting observed, five of them were affected by this phenomenon. Of the 13 suspect profiles, five were only near saturation as they followed the temperature curve up through the inversion. In 10 of the 13 profiles the rapid decrease in the dewpoint occurred before the temperature reached 0°C. Additionally, 10 of the 13 profiles were launched from the Polar Circle and occurred while the Polar Circle was inside the ice edge or very near to it. This fact lends support to the theory presented by Ohtake *et al.* (1982). Although an error in the humidity sensor could be a problem, it was determined that the dewpoint problem was not extensive enough in the MIZEX-87 data to warrant the correction.

Future experiments in the MIZ should address this issue specifically to determine if the phenomenon is real or due to instrument error. Willis (1987) suggested that rawinsonde profiles could be compared to the dewpoint profiles of an aircraft descending from the dry, warm air above down through the inversion. This would provide more conclusive evidence as to the authenticity of the strange dewpoint trace.

B. DATA PROCESSING

Rawinsonde data serve as the primary data source for this study. Intitial processing of the data included checking the raw data for any errors caused by loss of signal, loss of tracking, multiple readings at the same level or balloon bursts. These errors were identified automatically by the system software. A second review of each data set was then done to manually identify any errors missed by the software. An interpolation routine was used to smooth the data through the error points. In certain cases wind speeds and directions were not available due to a loss of the rawinsonde tracking signal by the Omega tracking system. This did not affect refractivity measurements. Surface data collected from shipboard instruments was plotted in time series of temperature, relative humidity, pressure, wind speed and direction.

A Fortran computer routine was prepared to calculate the refractivity N and the adjusted refractivity value M defined in chapter two. Equations 2.5 and 2.6 were used to calculate these values. The vapor pressure required in equation 2.5 was calculated using the formula in (4.1) after Buck (1981), where e is vapor pressure in mb, P is pressure in mb and TD is the dew-point temperature in K.

$$e = (1.0007 + (3.46 \times 10^{-6} \times P)) \times 6.1121 \times \exp^{(17.502 \times TD/(240.97 + TD))} \quad (4.1)$$

Values of the vertical gradients of M were determined between each level. These values were compared to the categories listed in Table 1 to determine if the atmosphere between two consecutive levels was either subrefractive, normal, super-refractive or trapping in nature. The gradient values were subsequently used to determine the strength and the thickness of individual EM ducts. The height of a duct was defined as the optimum coupling height (OCH). This is the height at which dM/dZ changes from a positive to a negative value. The height of super-refractive and subrefractive layers was defined as the height at the base of each layer.

A range-dependent raytrace program, developed by Wayne Patterson of the Naval Ocean Systems Command (NOSC), was used to see the effects of a horizontally varying refractive structure on the raypaths of EM waves (Patterson, 1987). Refractivity profiles similar to those observed in the previous case studies were input into the program at range intervals of 50 km. The height of a source transmitter was varied to see how the raypaths would be altered when the source was placed within a ducting layer as opposed to outside of one. The transmitter was given a beam width of 1.5° and an elevation angle of 0° with the horizontal. The program incorporates linear ray theory into the determination of the ray paths and is frequency independent.

V. TEMPORAL STUDIES

Incidences of EM ducting, super-refraction and subrefraction were studied to determine variations in the frequency of occurrence and changes in individual heights of the layers as a function of time. A synoptic regime case study covering the period 20 March through 10 April, 1987 was performed to see how the refractive structure was influenced by the synoptic-scale forcing during each period. A diurnal study was performed to see if the height and frequency of refractive events varied over a 24 hour period.

A. SYNOPTIC REGIME STUDY

A synoptic regime study was performed by separating the MIZEX-87 data set into a series of five periods based on the synoptic situation present during each period. These periods were defined and described in depth by Schultz (1987).

1. Description of the Synoptic Periods

Period one covered the first four days from 20-23 March, 1987. Fig. 18 shows the surface pressure pattern for 0000 UTC 20 March, 1987. A surface high of 1045 mb is situated over northeast Greenland. A surface low of 990 mb is present between Iceland and southern Norway. During the four-day period the surface high moved northeastward and then southward over the Fram Strait and began to weaken. The low pressure to the south moved towards Iceland and began to weaken. Fig. 19 shows a high of 1035 mb situated over the Fram Strait and a 1000 mb low just to the east of Iceland at 1500 UTC 23 March. The prevailing winds were easterly during this period. The Valdivia recorded wind speeds that varied from a maximum of 24 m s^{-1} on 20 March to no wind on 23 March. During this time the Valdivia was moving westward from the Svalbard Islands towards the MIZEX-87 operating area.

The second period was from 24-27 March, 1987. During this four-day period a boundary layer front developed about 100 km west of the Svalbard Islands. The boundary layer front is a mesoscale phenomenon observed to form along the ice edge boundary when cold dry air is advected from over the pack ice to the open water. The air over the water warms due to sensible heat flux from the water. Cloud formation enhances this warming with the addition of latent heat. The front develops at the boundary between this modified air and the unchanged air mass over the ice or land surface. The front moved rapidly westward across the Fram Strait on 25 March and stalled upon reaching the MIZ. Sea-level pressure in the Fram Strait dropped from 1035 mb to 1017

32

Fig. 18.   Sea-level pressure analysis, 0000 UTC 20 March 1987.
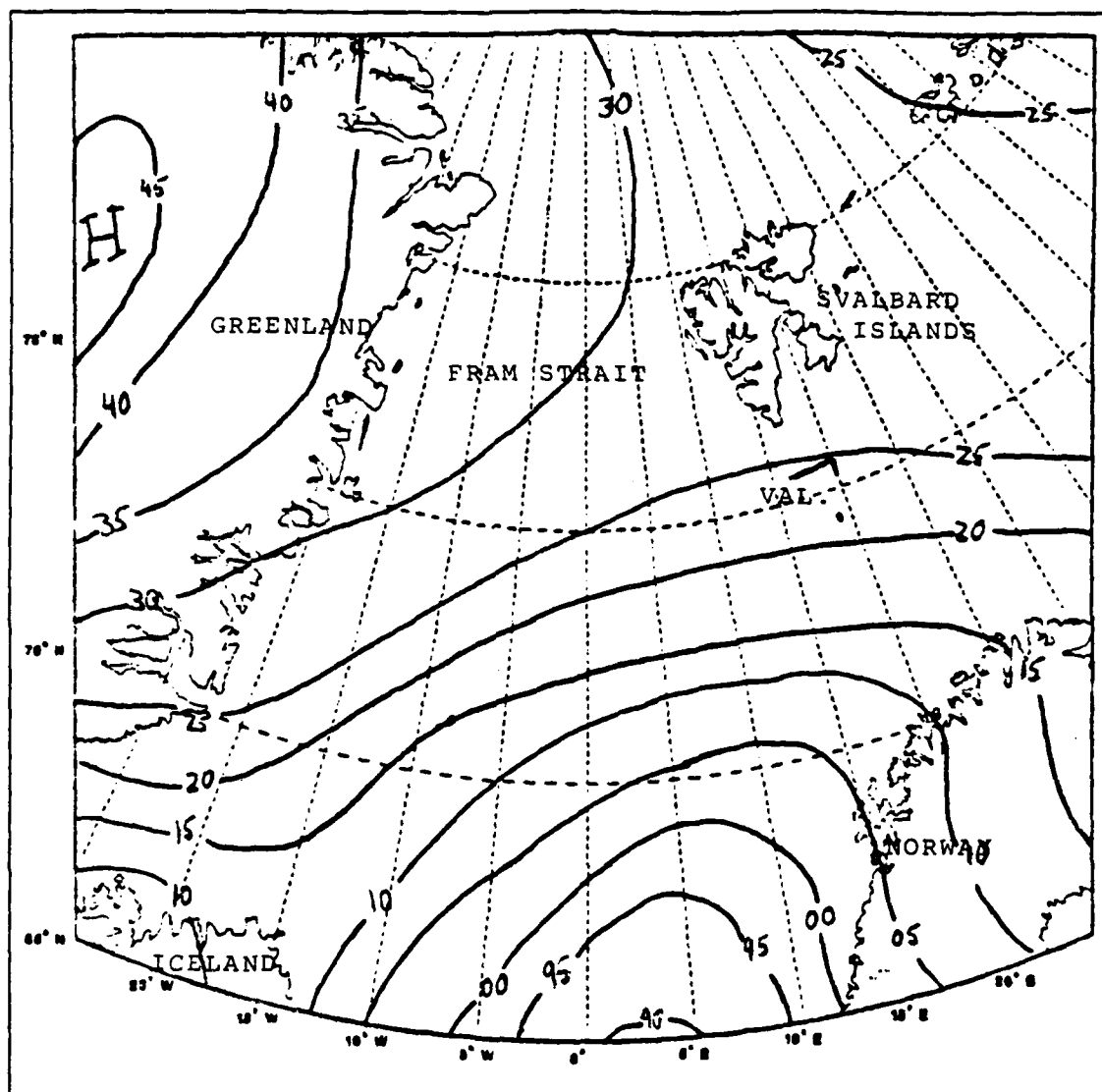
mb over the period.   An upper level high continued to persist in association with the front.   As the front passed the three vessels, wind speeds increased by about 10 m s^{-1} and wind direction shifted clockwise from northerly to southeasterly.   Fig. 20 shows that the surface low pressure area associated with the boundary layer front is centered just south of the Fram Strait on 1200 UTC 25 March.

During the third period, from 28-31 March, 1987, development of a weak surface low was observed over the Fram Strait.   The sea-level pressure pattern for 1200 UTC 28 March is depicted in Fig. 21.   The pressure in the MIZEX-87 operating area

33
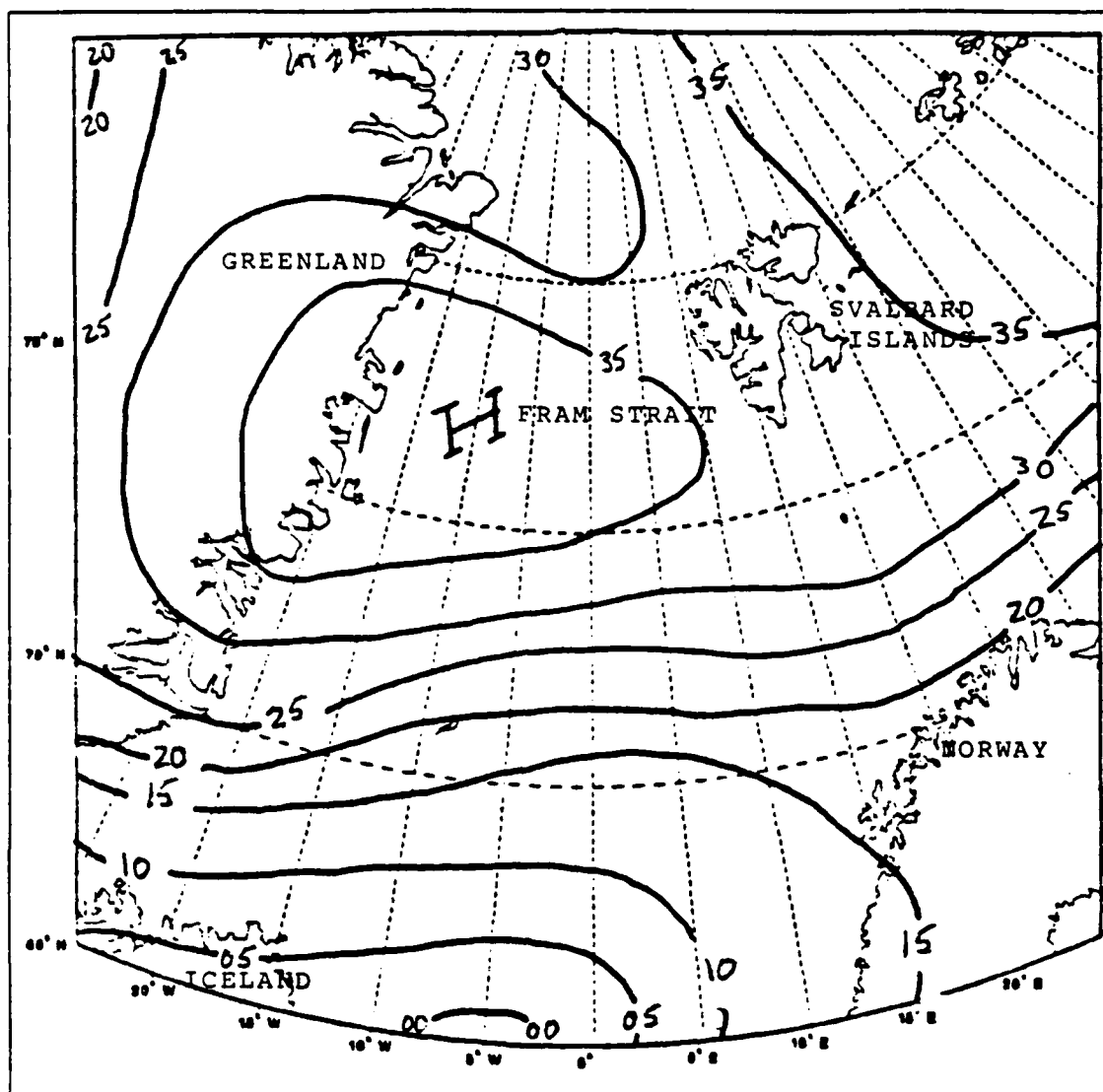
Fig. 19.   Sea-level pressure analysis, 1500 UTC 23 March 1987.

to a minimum of about 1010 mb on 29 March and then rose steadily throughout the period to 1024 mb on 31 March. During this period the upper level high continued to weaken. Winds were primarily from the north and northeast during the period and ranged from 3 to 10 m s^{-1} . By 31 March the high pressure to the north shown in Fig. 22 began to have the dominating influence on the Fram Strait region.

Period four was from 1-3 April, 1987. During this period a synoptic-scale low formed just to the east of Iceland. Fig. 23 shows an inverted trough analyzed over the Fram Strait region with high pressure to the east and west. Although the low was fairly

34
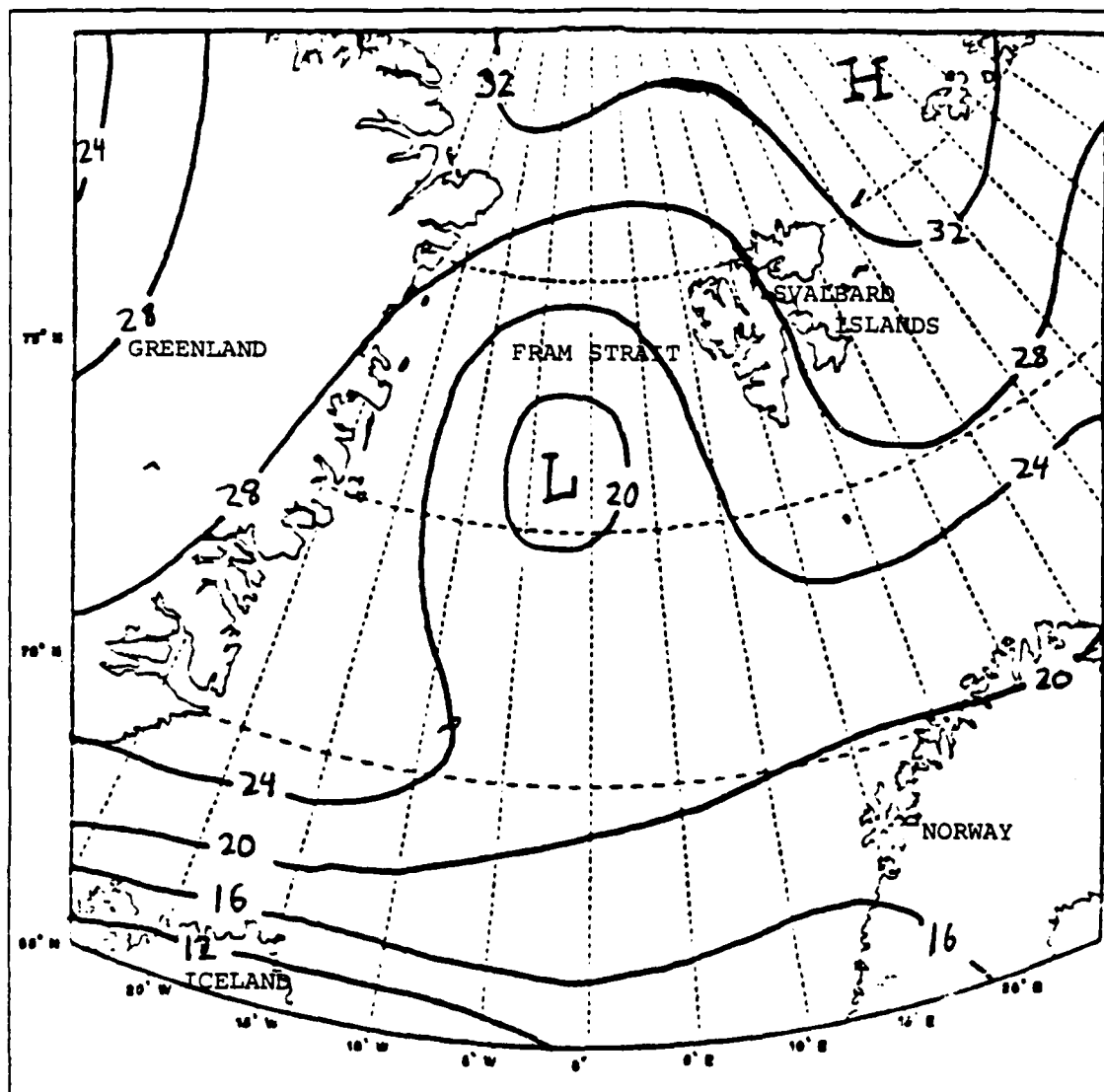
Fig. 20.   Sea-level pressure analysis, 1200 UTC 25 March 1987.

large, its effects were not significantly felt by the ships operating in the Fram Strait region. The pressure in the MIZEX-87 operating area rose from 1024 mb on 1 April to 1032 mb on 3 April as the high pressure on either side of the strait dominated the large-scale forcing. Winds during the fourth period were generally from the north. A significant shift in the wind direction occurred at 0400 UTC on 3 April from northerly to southeasterly. The wind speed was constant at about 7 m s^{-1} before the shift and became highly variable after the shift, ranging from 3 to 13 m s^{-1}. This shift in wind direction was probably due to the passing of a weak front associated with the low

35
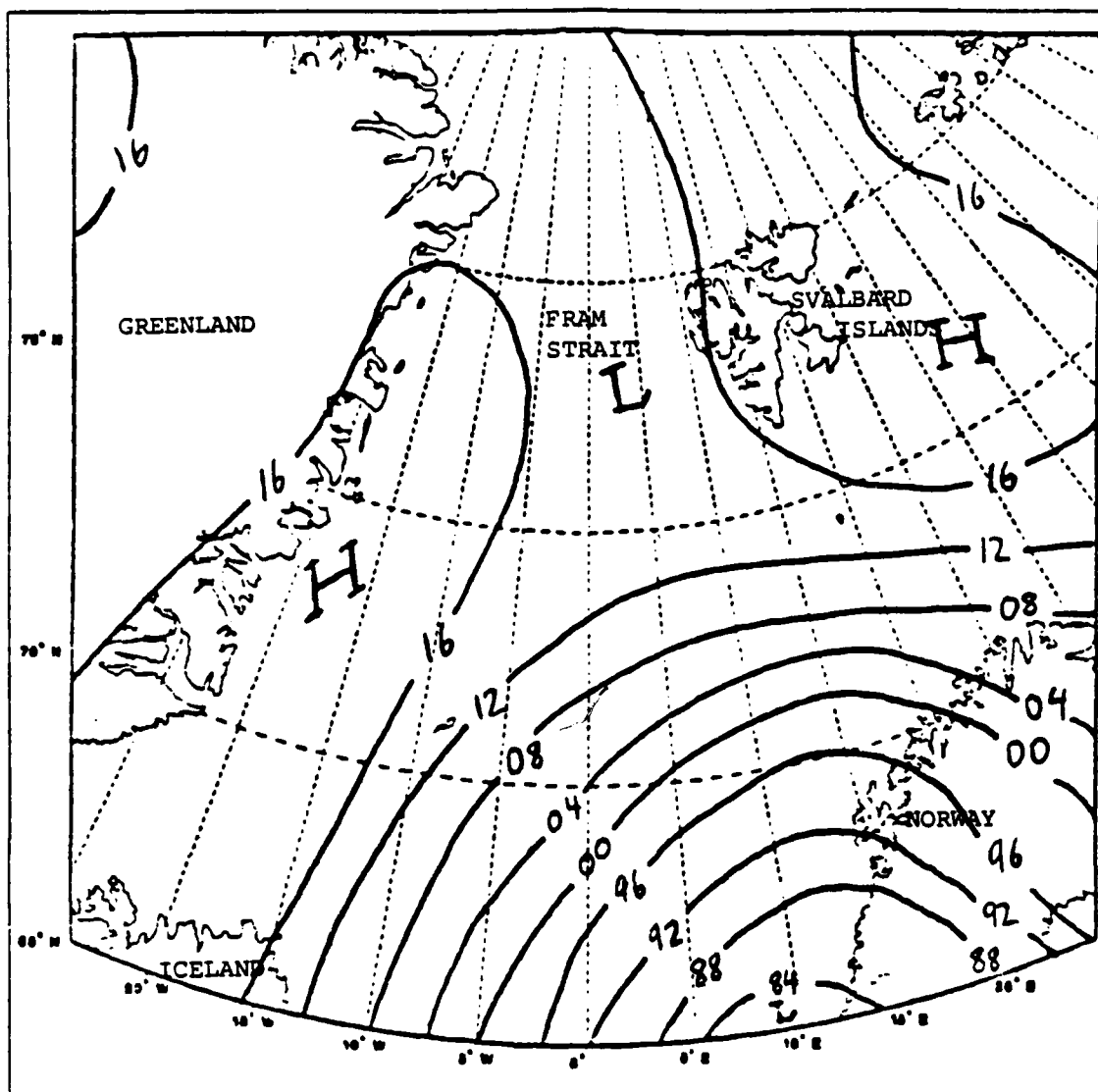
Fig. 21.   Sea-level pressure analysis, 1200 UTC 28 March 1987.

pressure center located to the south as depicted in Fig. 24. The Valdivia departed the MIZEX-87 operating area on 2 April en route to Tromso, Norway.

The fifth period included the last seven days from 4-10 April, 1987. Two more major cyclones formed about 400 km north of Iceland. On 5 April the first low moved to the northeast from a position 50 km off the east coast of Greenland to a position 150 km south of the Svalbard Islands. The final position of this low is shown in Fig. 25. The second low formed in the same area as the first low and followed its track, over-taking and merging with it on 8 April at a position 200 km southwest of the Svalbard

36
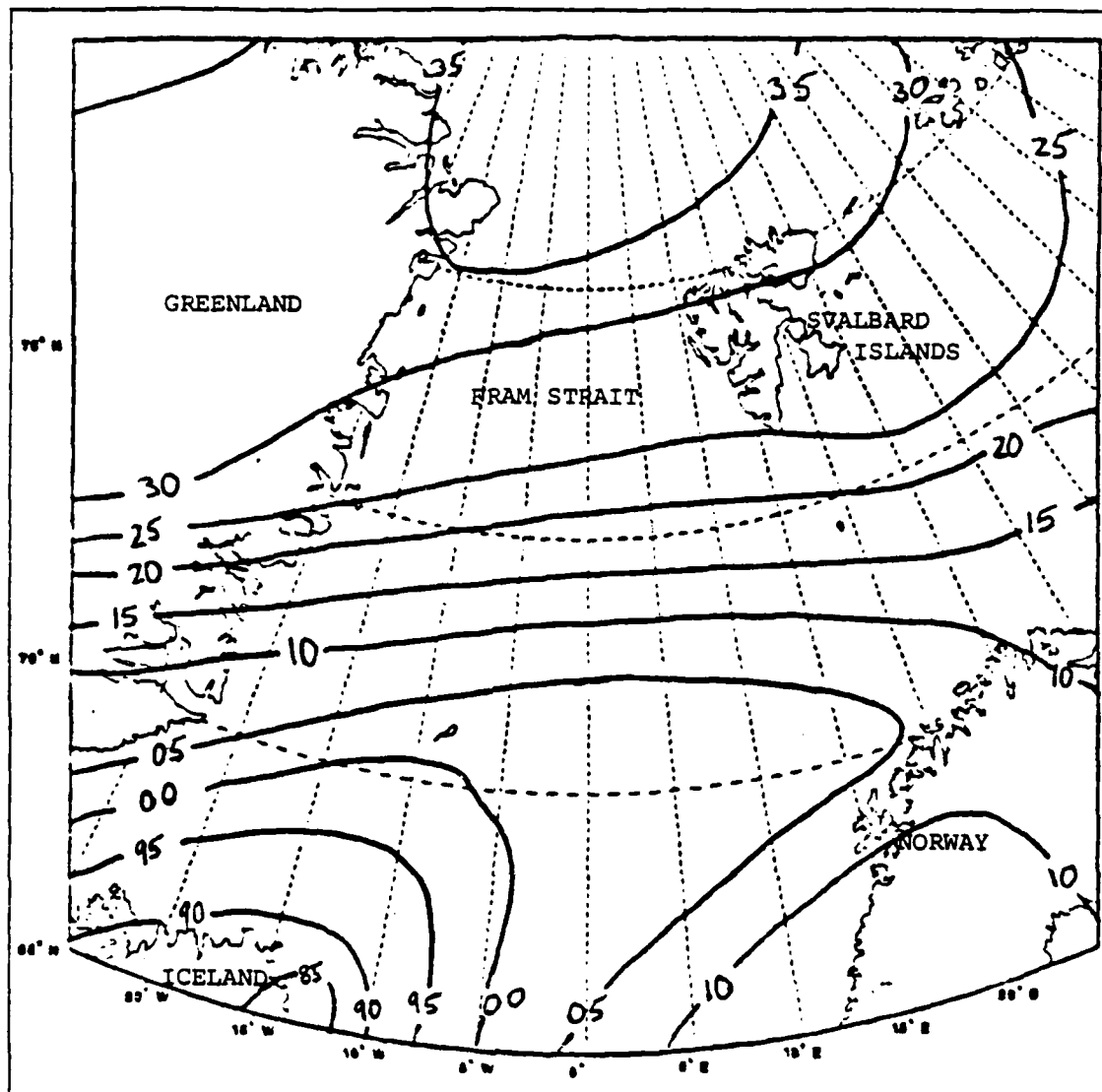
Fig. 22. Sea-level pressure analysis, 0000 UTC 31 March 1987.

Islands. The pressure in the MIZEX-87 operating area remained fairly constant around 1015 mb through 8 April. The winds were generally from the north although shifts in wind direction to the southeast were measured on 6 April along with an increase in wind speed of 5 m s⁻¹. The Polar Circle and Haakon Mosby departed the MIZ late in the evening on 8 April and on 9 April encountered a low pressure system formed from the merger of the two previous lows. The Haakon Mosby recorded a drop in pressure from 1015 mb to 1003 mb over 12 hours time. Wind speeds increased from 7 to 14 m s⁻¹ and a shift in wind direction from the north to the southeast was noted. After moving
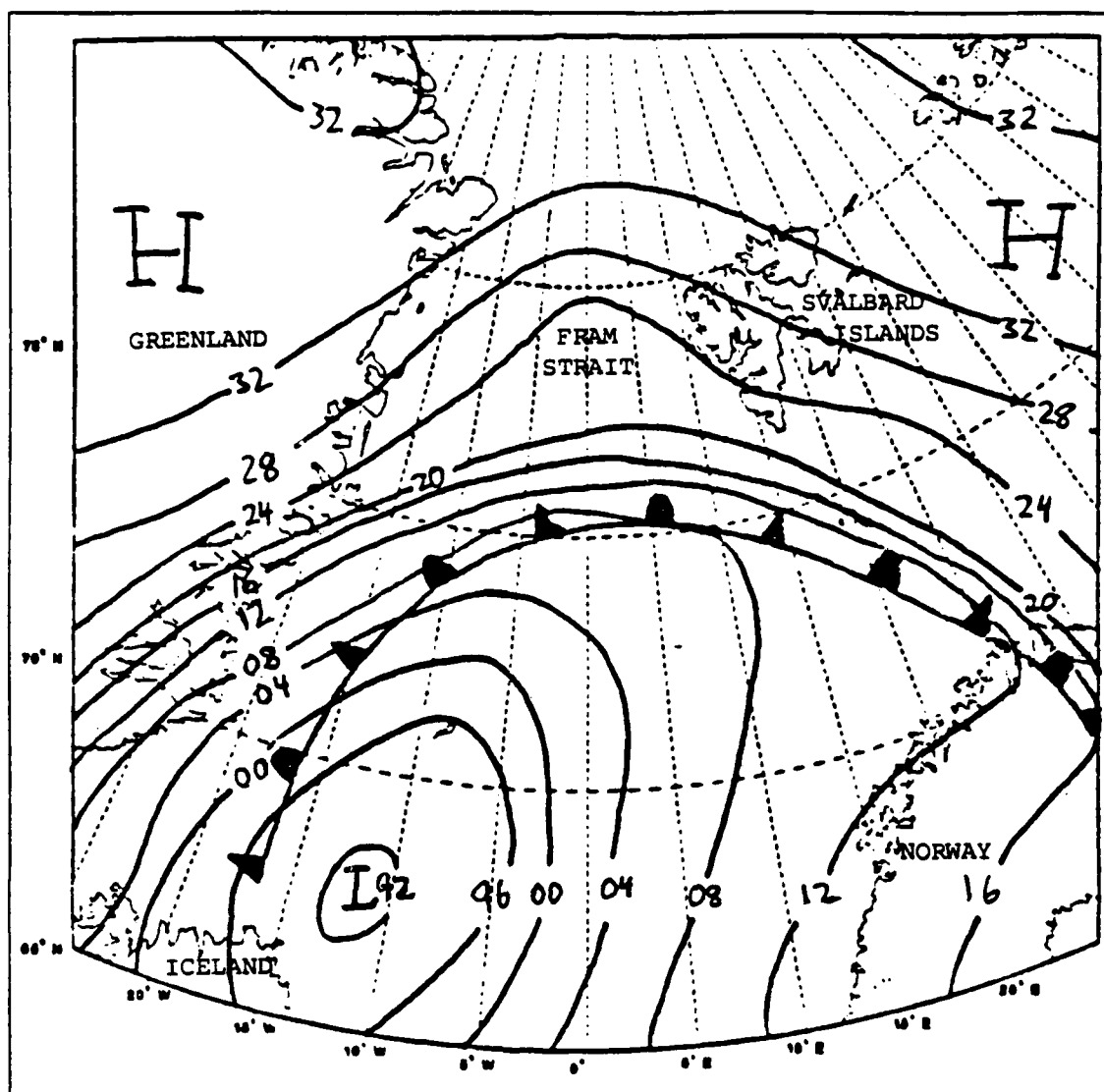
Fig. 23.   Sea-level pressure analysis, 1200 UTC 1 April 1987.

through the low, the observation on Haakon Mosby showed a pressure increase back
to 1015 mb and a shift in wind direction back to the north. The wind speed decreased
to about 6-8 m s⁻¹.

2.   Refractive Structure During Each Period

a.   *Period One (20-23 March)*

During period one the Valdivia was just arriving on station in the MIZ area.
The Polar Circle and Haakon Mosby were still en route to the area. On 20 March, the
Valdivia was moving northward towards the Svalbard Islands. Fig 18 shows the position
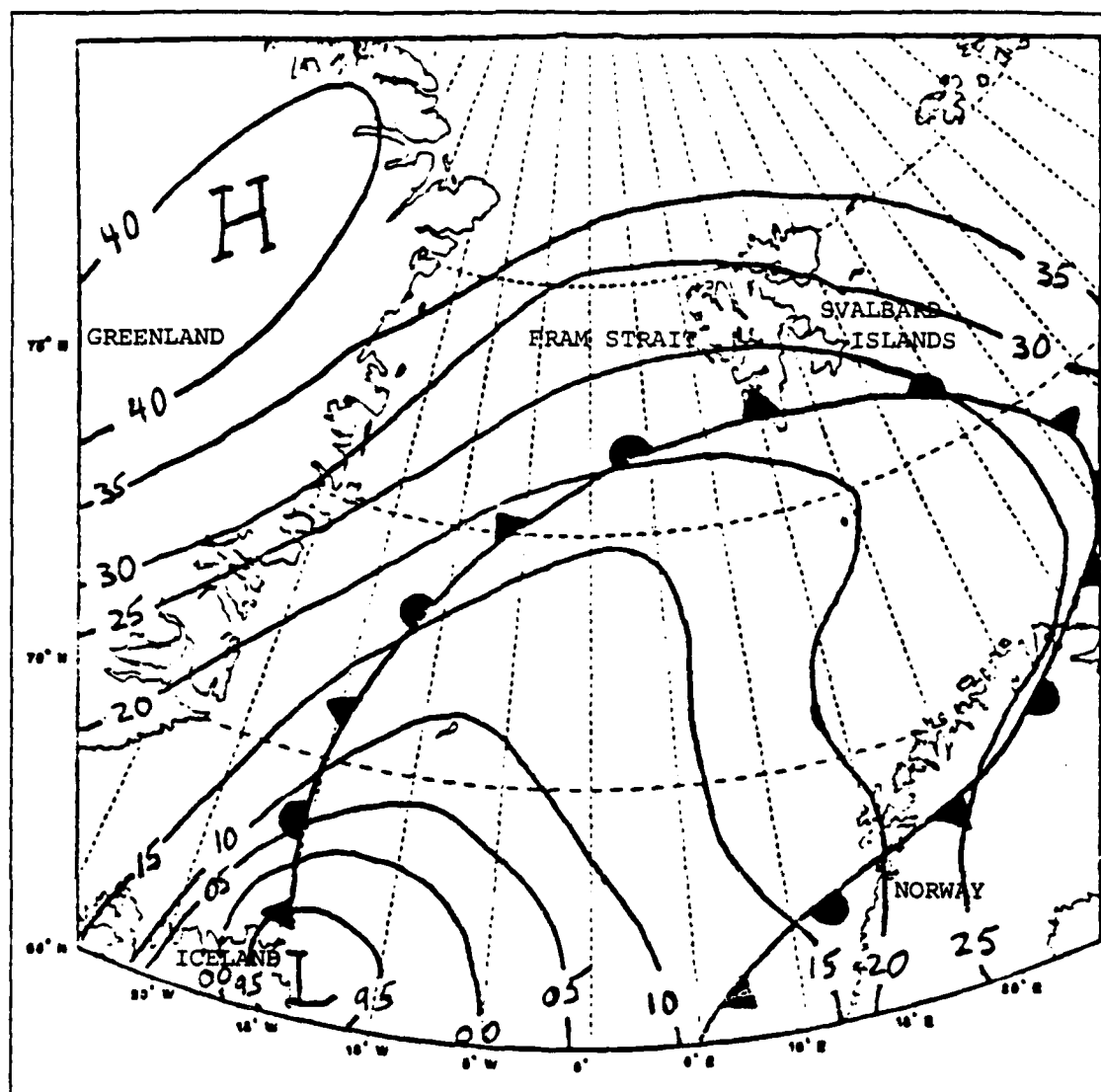
Fig. 24. Sea-level pressure analysis, 0000 UTC 2 April 1987.

of Valdivia at 0000 UTC. By 23 March the Valdivia had moved to the west, nearer to the MIZ. During this period the Valdivia recorded increasing surface pressure as it moved towards the high pressure centered over the Fram Strait. Fig. 26 shows that during this period one duct was detected by the Valdivia. This duct was detected at a height of 709 m and was caused by the boundary layer inversion forming at that level. Analysis of the rawinsonde profiles in Fig. 27 reveals that the inversion continued to strengthen and the mixed layer shallowed as the ship moved into an area of increased subsidence aloft.

39
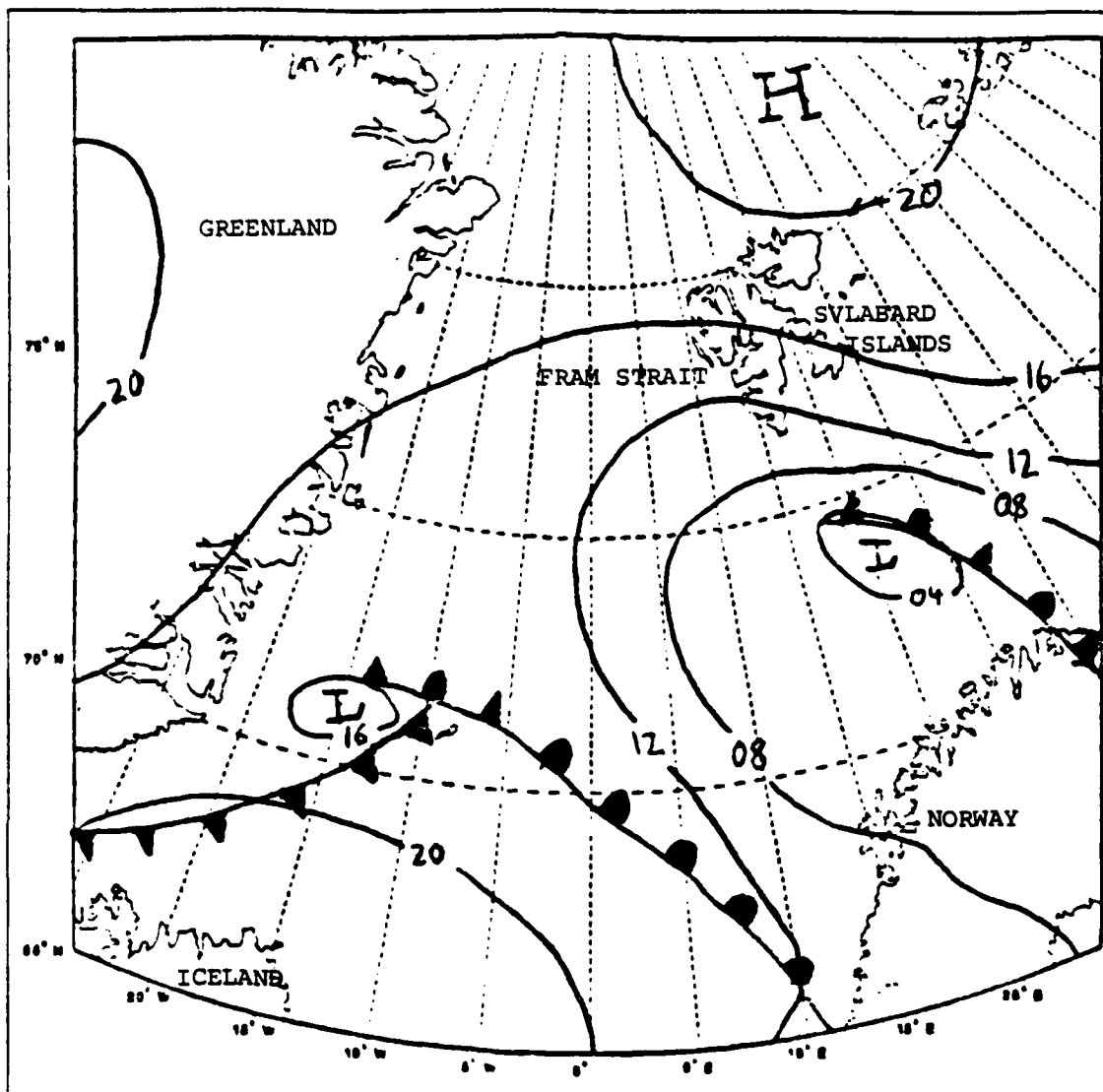
Fig. 25.   Sea-level pressure analysis, 1200 UTC 5 April 1987.

Fig. 28 shows the super-refractive layer occurrences and heights over time. Super-refractive layers were observed in seven of the nine rawinsondes launched during this period. In five of the seven cases the super-refractive layer was caused by the primary inversion. The other incidences of super-refraction occurred due to sharp drops in the dewpoint temperature with height as the rawinsonde passed into a drier layer not associated with the capping inversion .

Subrefractive layers occur primarily above the boundary layer in areas where there is either a substantial negative vertical temperature gradient or, more

importantly, a large positive moisture gradient. This often occurs where differential advection of moisture into an area above the boundary layer produces the necessary moisture gradient. If the moisture is sufficient to form a cloud, the subrefractive layer will be just below cloud base. Fig. 29 shows that, in period one, subrefractive layers were observed in three of the launches. On 21 March the subrefractive layer was associated with a thin moist layer at about 800 m. Multiple subrefractive layers were detected in the other two launches. Of these, one was detected just below a cloud layer at 115 m. Another one of the multiple subrefractive layers was based at the surface and had a thickness of 75 m. It was associated with a relatively dry surface relative humidity of 42% that increased over 75 m to 65%. The large variation in relative humidity may be due to an inaccurate value for the first data point measured. The first few data points of a rawinsonde profile are often observed to be in error and strong low-level gradients such as those above may be suspect. The final three subrefractive layers were caused by thin layers of more moist air above the well-mixed layer.

b. Period Two (24-27 March)

The refractive structure of the second period was affected significantly by the inversion that had developed over the MIZ during the previous period. Ducts were observed during eight of the 16 launch episodes. A launch episode includes all of the rawinsondes launched by the three ships at approximately six-hour intervals. All but one of the ducting incidents occurred during the first two days of the period. Fig. 26 shows the duct heights relative to time. In each case the duct was caused by the presence of a strong capping inversion over the well-mixed layer. Fig. 30 shows that the capping inversion remained relatively strong around the MIZ through 26 March. At 2300 UTC on 26 March the boundary layer front described in the synoptic overview of period two passed over the Polar Circle. The rawinsonde profile for 1125 UTC 27 March in Fig. 30 indicates that the front has destroyed the inversion and caused the temperature to be fairly well-mixed up past 2000 m. Similar trends were observed in the profiles of the other two ships as the boundary layer front advanced westward across the Fram Strait. Only one duct was recorded during the last two days of the period at an elevation of 1229 m where the inversion was beginning to reform following frontal passage.

Incidents of super-refraction closely paralleled those of ducting during the second period. A super-refractive layer was observed by at least one of the ships during 13 of the 16 launch episodes. Of the 27 super-refractive layers identified, five of them were adjacent to a trapping layer. 17 of the super-refractive layers were caused by the

Fig. 26.   Duct height relative to day and time of launch.

Fig. 27.   Rawinsonde profiles from synoptic period one.

43

Fig. 28.   Super-refractive layer heights relative to day and time of launch .

44

Fig. 29. Subrefractive layer heights relative to day and time of launch.

45

boundary layer inversion. Fig. 28 shows the scatter of the super-refractive layers during period two. Similar to the trapping layers, most super-refractive layers were detected before the boundary layer front moved through. The super-refractive layers observed at the Valdivia and Haakon Mosby about 24 hours after frontal passage indicated that the inversion layer was beginning to reform but was not strong enough to produce conditions required for the formation of trapping layers.

Very few subrefractive layers were seen during period two. Over the four-day period, Fig. 29 indicates that only four episodes produced subrefractive layers. The scarcity of subrefraction during this period is due to the high levels of moisture throughout the boundary layer. Very few significant increases in the moisture gradient were observed in the profiles. The passage of the boundary layer front increased the mixing to higher levels. Although there was little indication of upper level advection of moist layers into the region, any gradients that were forming would have been reduced by the enhanced mixing.

c. Period Three (28-31 March)

During period three the MIZEX-87 region was under the influence of a weak low pressure system. The increased instability associated with this low and a further weakening of the upper-level high pressure resulted in only one ducting episode at the very end of the period as shown in Fig. 26. This duct occurred as the pressure had steadily risen from a low of 1010 mb on 29 March to 1024 mb by 31 March. Fig. 31 shows that the boundary layer was rather deep throughout the period and lacked a well-defined capping inversion. The inversion is just begining to develop in the last profile shown in Fig. 31 at a height of 1250 m.

Numerous detections of super-refractive layers were noted in period three during 12 of the 16 launch episodes. Of the 25 layers observed in the rawinsonde profiles of the three ships, 18 were associated with a weak inversion above the boundary layer accompanied by decreases in the dewpoint. The weaker inversions were caused by a reduction in the subsidence rate due to the weakening upper-level high pressure. The remaining super-refractive layers were detected just above upper-level bands of increased moisture where the moisture gradient dropped significantly. These super-refractive layers did not occur in coincidence with a strong temperature inversion.

Subrefractive events were noted during eight of the 16 launch episodes. The subrefractive layers formed at levels where a transition to a substantially more moist layer was observed. In only three of the events was saturation apparent, indicating
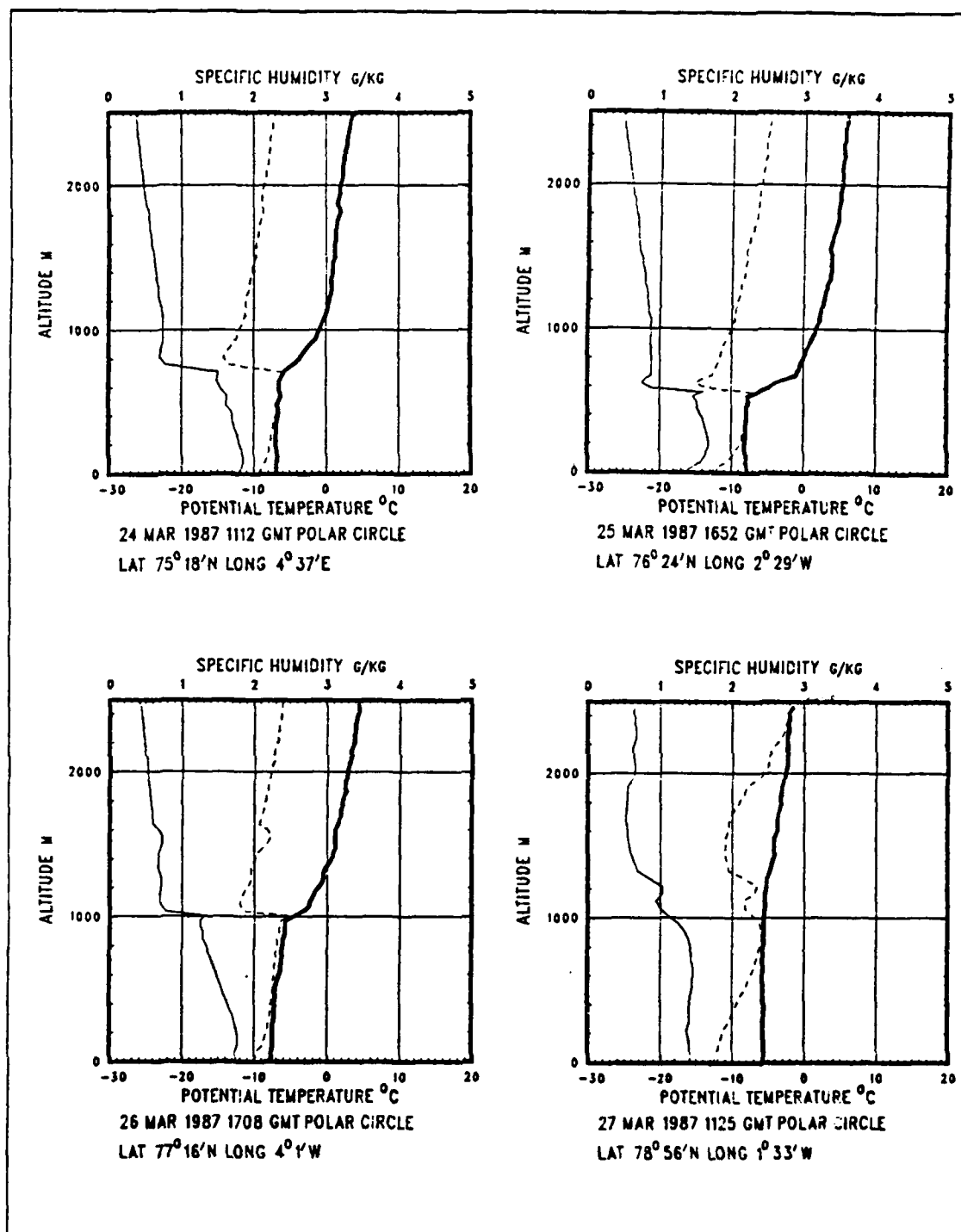
Fig. 30.   Rawinsonde profiles from synoptic period two.

cloud formation. This suggests that although cloud layers are often observed just above subrefractive layers, the presence of clouds is not a necessary requirement for subrefration to occur.

d. Period Four (1-3 April)

The fourth synoptic period exhibited a similar refractive structure to that observed during the end of period one and the beginning of period two. High pressure dominated the MIZEX area and resulted in the development of a stronger capping inversion above the well-mixed layer. The stronger inversion provided the necessary M-gradient for ducting to occur during seven of the first eight launch episodes. Fig. 32 shows that the duct heights varied between 750 and 1100 m as the inversion height fluctuated over the period. Four rawinsonde profiles in Fig. 33, from the Haakon Mosby, indicate that the inversion remained pronounced until early afternoon on 2 April. By late afternoon on the same day the inversion began to weaken and it appears that a deep layer of mid-level moisture was advected into the area. The wind shift noted in the synoptic discussion of period four signaled the passage of the front associated with the low to the south. The effects of the advected moisture and the frontal passage are evident in the final profile of Fig. 33 which shows the boundary layer nearly saturated with no evidence of an inversion.

Super-refractive events observed during the fourth period followed a pattern similar to that observed in the ducting episodes. Super-refractive events were recorded in all of the launch episodes during the first two days of the period. No events were recorded during the last day. The super-refractive layers identified in Fig. 34 were associated with a temperature inversion in 16 of the 37 reported layers. Nine more of the super-refractive layers occurred just above layers of clouds. The remaining layers occurred where the dewpoint decreased sharply over a very short distance through a series of narrow bands of increased moisture.

Subrefractive layers were detected primarily during the first two days of the period as indicated in Fig. 35. A majority of these layers were found at levels where the moisture gradient was strongly positive but did not reach a point of saturation. These subrefractive layers were found between the thin super-refractive layers mentioned above.

e. Period Five (4-10 April)

Period five was the longest (7 days) of the synoptic regimes. Refractive events of interest occurred during 4-5 April and 7-8 April. By 4 April the sea-level
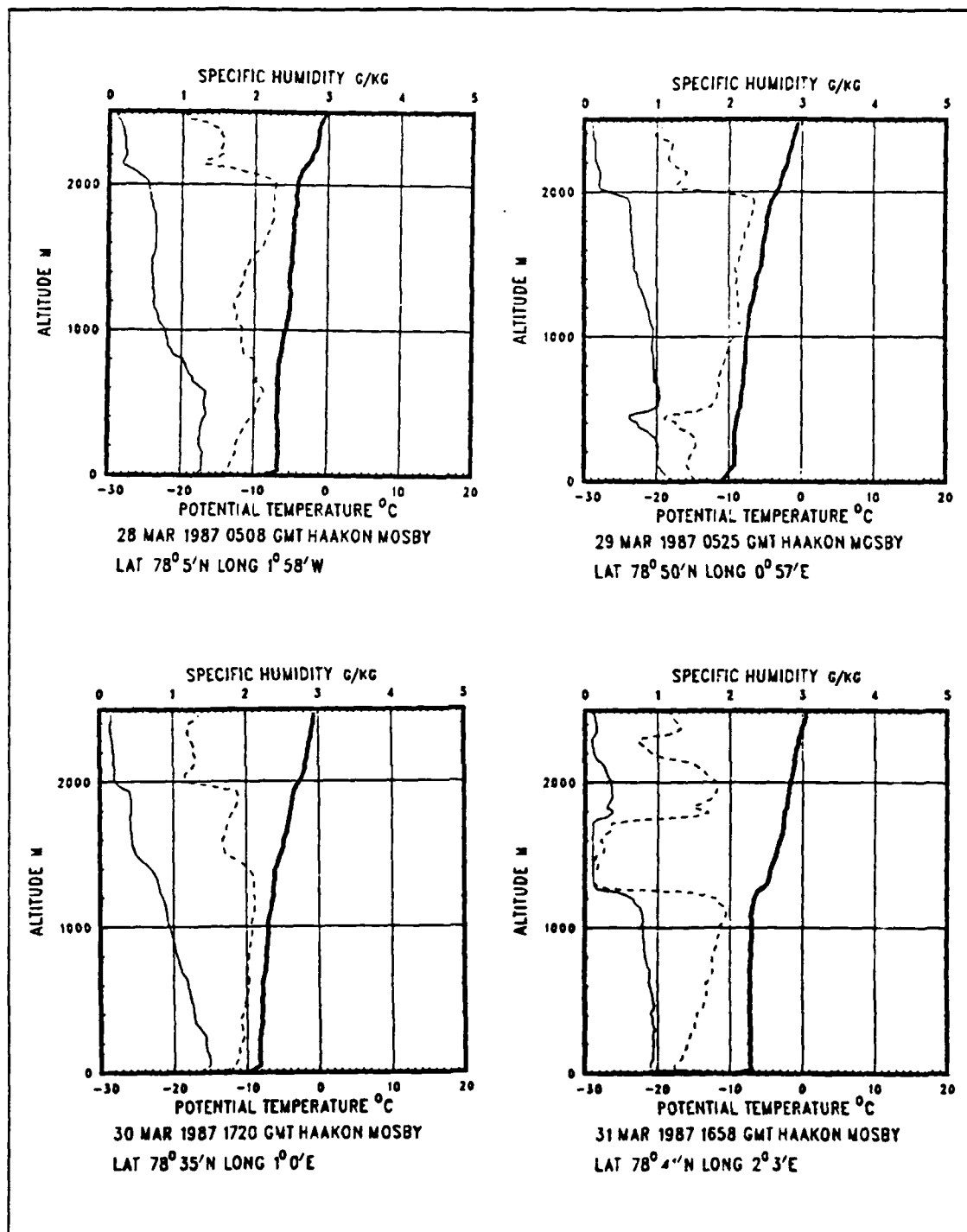
Fig. 31. Rawinsonde profiles from synoptic period three.
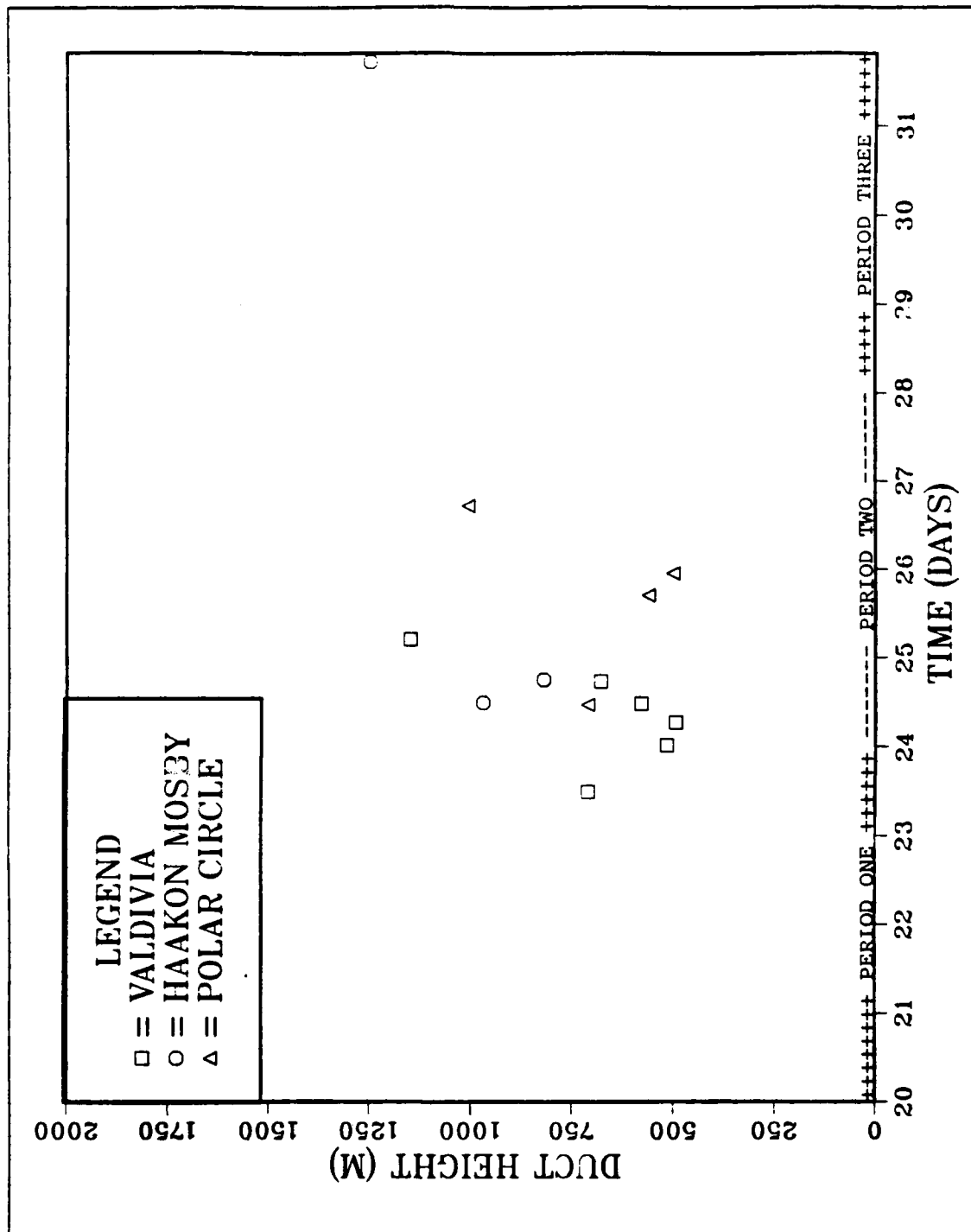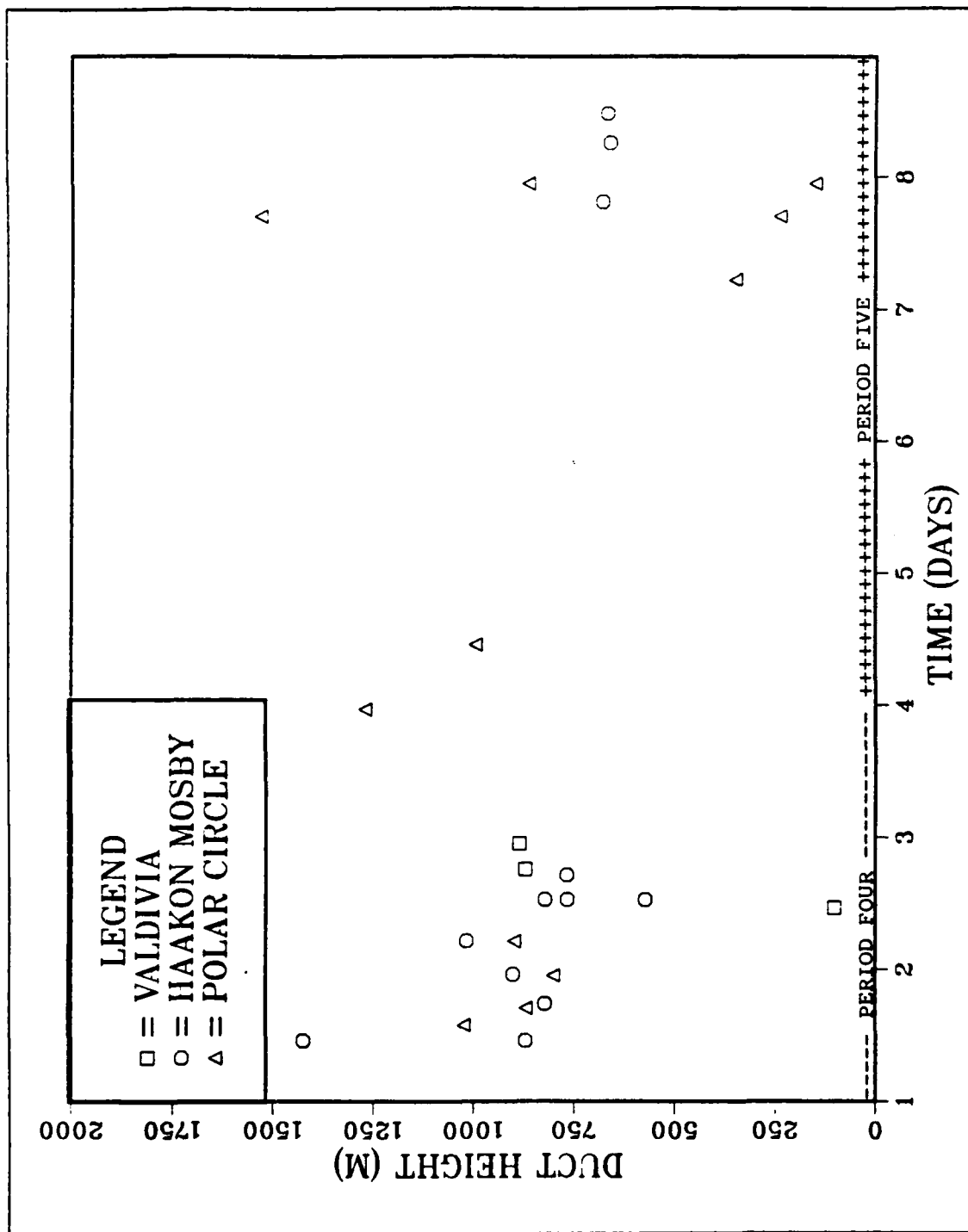
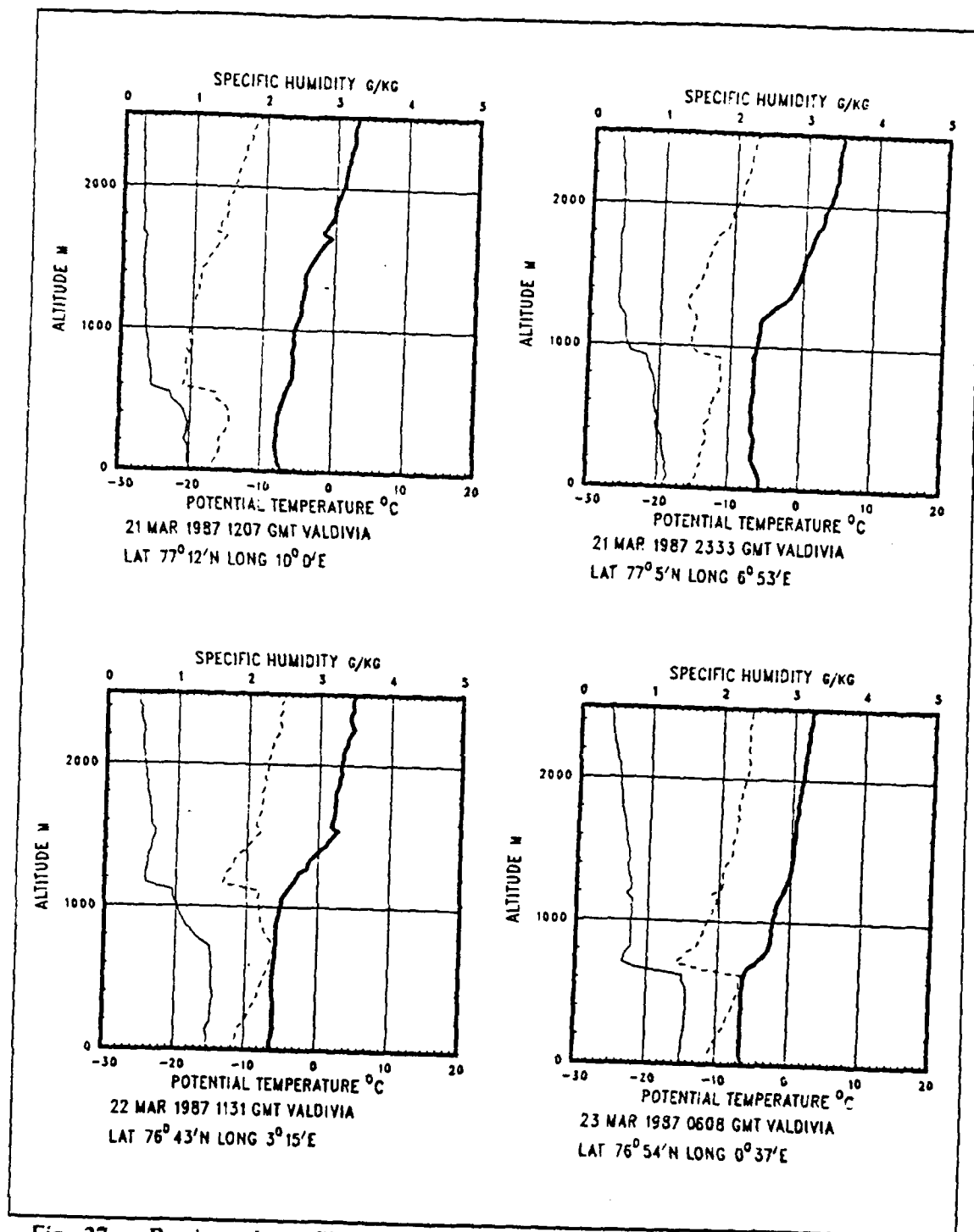Fig. 32. Duct height relative to day and time of launch.
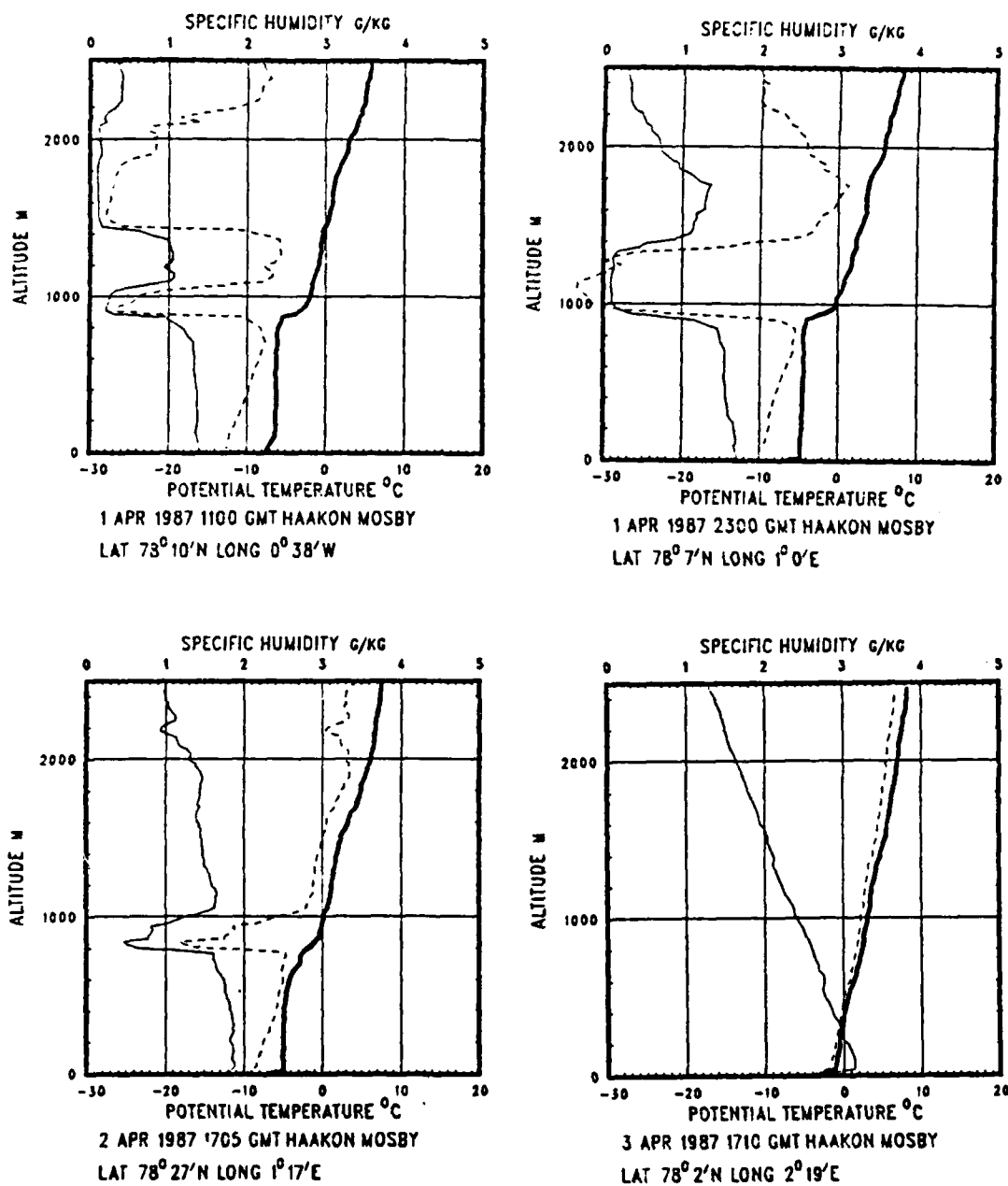
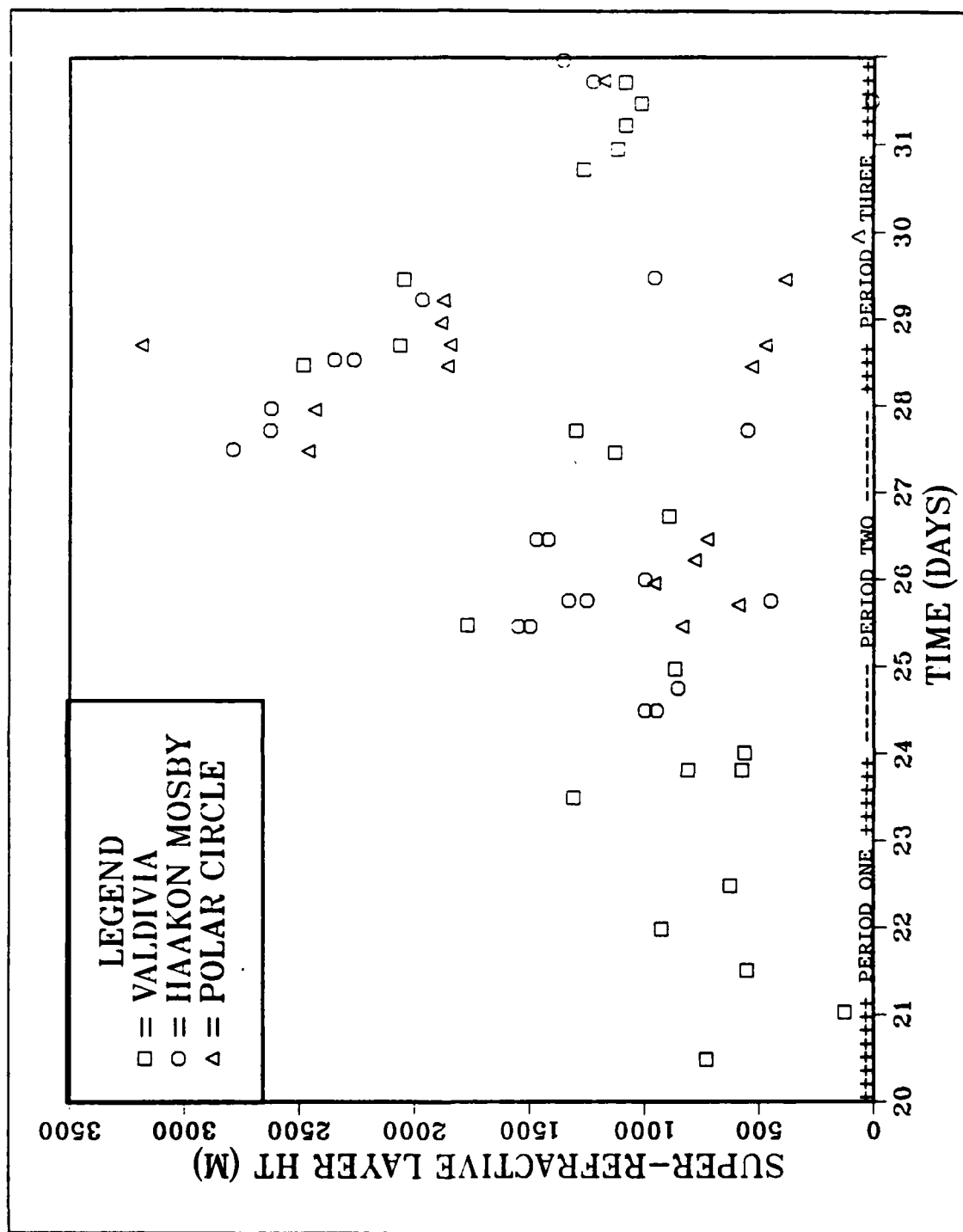Fig. 33.   Rawinsonde profiles from synoptic period four.

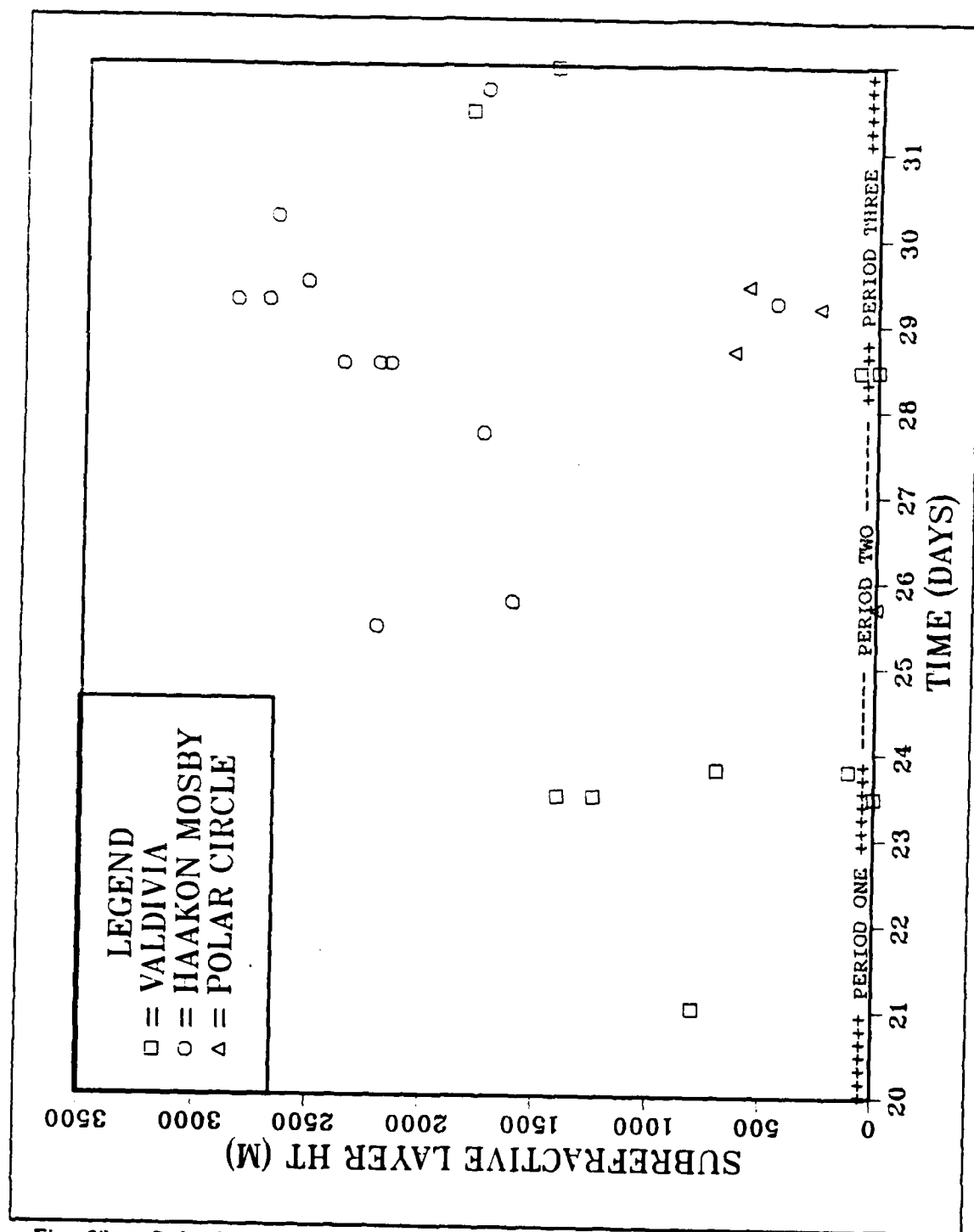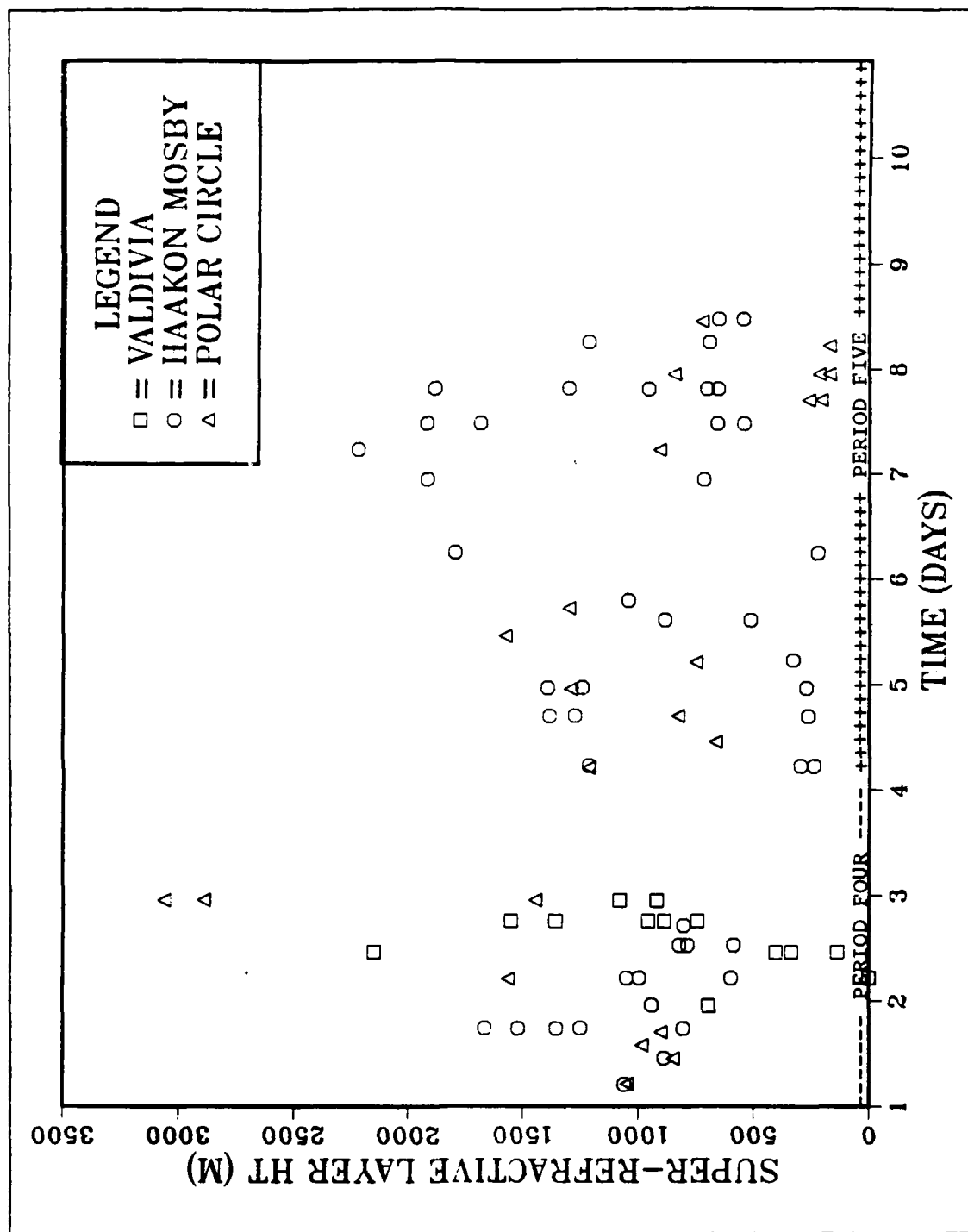Fig. 34.   Super-refractive layer height relative to day and time of launch.
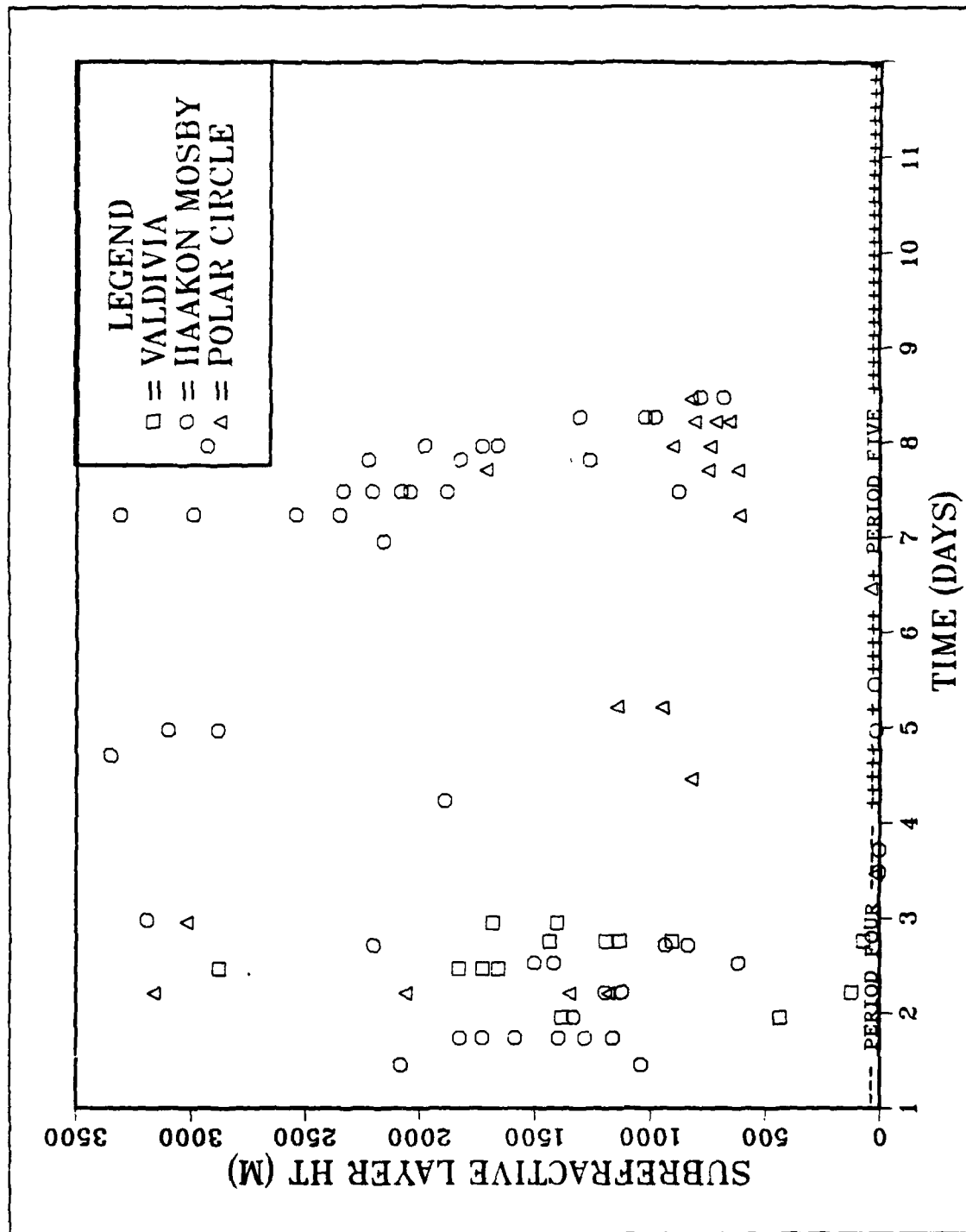
Fig. 35.   Subrefractive layer height relative to day and time of launch.
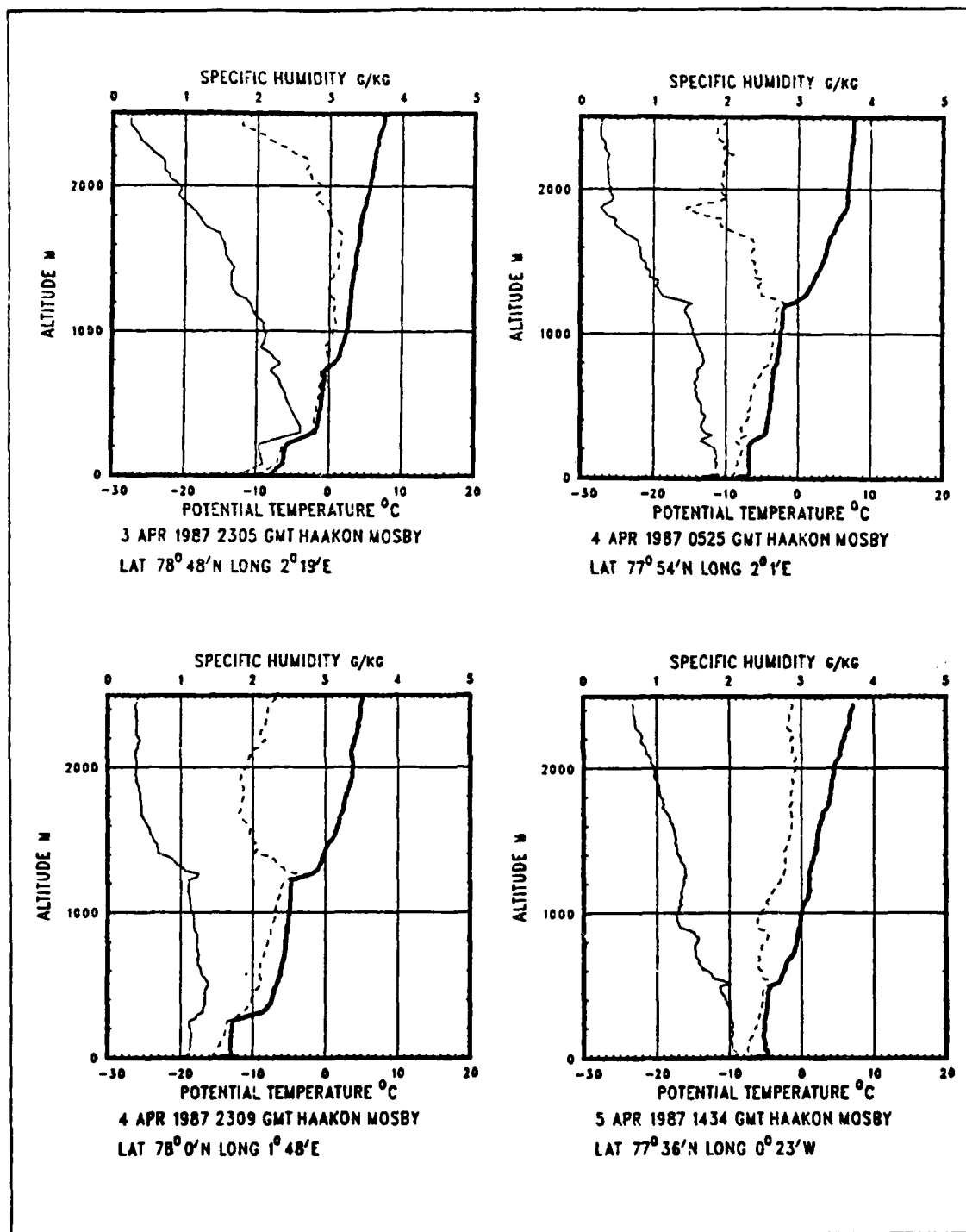
Fig. 36.   Rawinsonde profiles from synoptic period five.

54

pressure had become steady at 1015 mb following the passage of the front on the day before. Surface temperatures dropped almost 10°C on 4 April as the winds shifted to the west/northwest bringing in colder air from the Greenland land mass. The atmosphere tended towards more stable conditions and the boundary layer inversion began to re-form. Just outside the MIZ a rawinsonde profile showed two inversions in the vertical. The lower inversion formed at about 300 m. The second inversion capped a well-mixed layer at about 1200 m. Fig. 36 shows the development of the inversions during 4 April. The inversions were not strong enough to produce more than one ducting event as indicated in Fig. 32, however, a significant number of super-refractive layers were created by the two inversions. These are plotted in Fig. 34. The super-refractive layers found between 500-1000 m appeared to occur just above the tops of some deep cloud layers that descended nearly to the surface. Incidents of subrefraction were scarce during 4-5 April due to a lack of moist layers in the profiles.

During 6 April the MIZEX area experienced relatively few refractive events. This was probably due to increased convergence and thus mixing in the MABL brought on by the second low pressure system of the period as it moved across the Greenland Sea. Numerous refractive events were detected during 7-8 April. Fig. 32 shows that the Polar Circle recorded three low-level ducts and two higher ducts over the ice while the Haakon Mosby, located outside the ice boundary, recorded three ducts at about 650 m. Fig. 34 shows a large number of super-refractive layers detected on these two days during the first six launch episodes. The layers were found at nearly the same levels as the ducting. Subrefractive events during these two days were located just below cloud layers both above and below the inversion levels.

3. Trends in the Refractive Structure.

Several trends were noted as a result of the regime study. Refractive events occurred with much greater frequency during periods of increased atmospheric stability. During the periods dominated by high pressure the boundary layer capping inversion was able to develop and strengthen, providing the conditions necessary for trapping layers to occur. During frontal passages or when the MIZ was under the influence of low pressure, the vertical stability of the atmosphere was degraded. This results in increased vertical mixing and reduced subsidence in the air above the MABL and a subsequent decay of the inversion.

Many more super-refractive layers than trapping layers were observed during MIZEX-87. In addition, the bases of the super-refractive layers were higher than the

duct heights. The average duct height recorded during MIZEX-87 was 835 m. The average super-refractive layer height was 1048 m. The difference in these heights was noted during every series of launch episodes in which ducts and super-refractive layers were observed. This pattern is due to the way the inversion develops. Upper-level subsidence causes adiabatic warming and drying of the air as it descends. As it comes in contact with the well-mixed layer a temperature inversion and a negative moisture gradient begin to form. As the strength of these gradients increase, the M-gradient required for super-refraction occurs before that for trapping. As subsidence increases, the rate of descent of the air above the MABL exceeds the upward growth of the layer due to entrainment generated by mechanical and convective turbulence. This results in a depression of the inversion to a lower level and a strengthening of the inversion gradient. If the subsidence is strong enough a trapping layer will eventually develop at this lower level.

Another observation of interest was that in all cases a ducting event was associated with both a temperature inversion and a negative moisture gradient. Both of these conditions had to be present at the same level before a trapping layer would form. Super-refractive layers were frequently observed when only one of the two conditions was met. A majority of the time that condition was a sharp decrease in moisture.

Subrefractive layers were almost always seen when individual cloud layers were present above the boundary layer. However, saturation was not a requirement for subrefraction. Many instances of subrefraction were recorded when clouds were not present. During periods of increased instability the number of subrefractive layers detected dropped significantly due to increased mixing of the moisture profile. Subrefractive events were attributed primarily to sharp positive increases in the moisture gradient rather than negative vertical temperature gradients.

4. Comparison to MIZEX-84 Regime Studies

Ducting episodes were studied and described by Willis (1987) over the period 19 June - 14 July, 1984. Six different synoptic regimes were determined based on the large-scale synoptic forcing that influenced the area. Fig. 37 shows the percentage of launch episodes during each regime in which a ducting event was observed. Both corrected and uncorrected data results are given. For the uncorrected case, regimes three, four and six recorded ducting in greater than 50% of the launch episodes. These regimes were identified by Willis as being under the influence of ridging caused by high pressure systems located over Greenland and Norway. The subsidence aloft produced by this ridging caused the inversion to develop sufficiently during these regimes to provide

conditions necessary for persistent ducting to occur. Regimes one, two and five were dominated by low pressure systems moving through the Greenland Sea and resulted in a reduced number of ducting episodes. These results are consistent with the ducting observed during MIZEX- 87.

In the analysis of EM refractivity around the Greenland Sea MIZ, it is apparent that the large-scale forcing has a dominant effect on the upper boundary of the MABL and on the strength of the associated inversion. A majority of the ducts and super-refractive events observed during MIZEX-87 were associated with this inversion. The large-scale synoptic forcing must be considered as a primary factor in the development of conditions necessary for anomalous refractive events to occur.

B. DIURNAL STUDY

A study was conducted to determine if the diurnal cycle had any effect on either the heights of refractive events or on their frequency of occurrence. The diurnal cycle was driven by the large change in the number of daylight hours over the three week period. The number of daylight hours increased from 9 to 21 hours over the course of MIZEX-87. Figs. 38, 39 and 40 are plots of the heights of ducting, super-refractive and subrefractive events respectively versus the time of day the event was detected.

1. Diurnal Variations in Height

Duct heights and super-refractive layer heights would be expected to follow diurnal height changes in the MABL inversion. A thorough study of the rawinsonde profiles during each diurnal cycle was completed. No discernable diurnal patterns in the MABL height were obvious. Diurnal changes would be expected due to radiational heating and cooling at the cloud tops below the base of the inversion. Diurnal changes in the fluxes responsible for generating the mixing in the boundary layer could also cause variations in the boundary layer height. Time series of the sea-surface temperature, surface air temperature, relative humidity and surface winds were examined. Although large-scale fluctuations caused by the synoptic forcing were apparent, diurnal fluctuations were not observed in these time series. Rawinsonde profiles were examined over 24 hour periods to see if the changes in the heights followed any pattern. Diurnal variations were not observed. Movement of synoptic-scale systems through the area, as well as continuous movement of the ships could be causing any diurnal variations in the refractive layer heights to be effectively masked. The scatter observed in the heights of all three diurnal plots was significant during each launch period and no appreciable trends were evident when comparing one launch period to another.

57
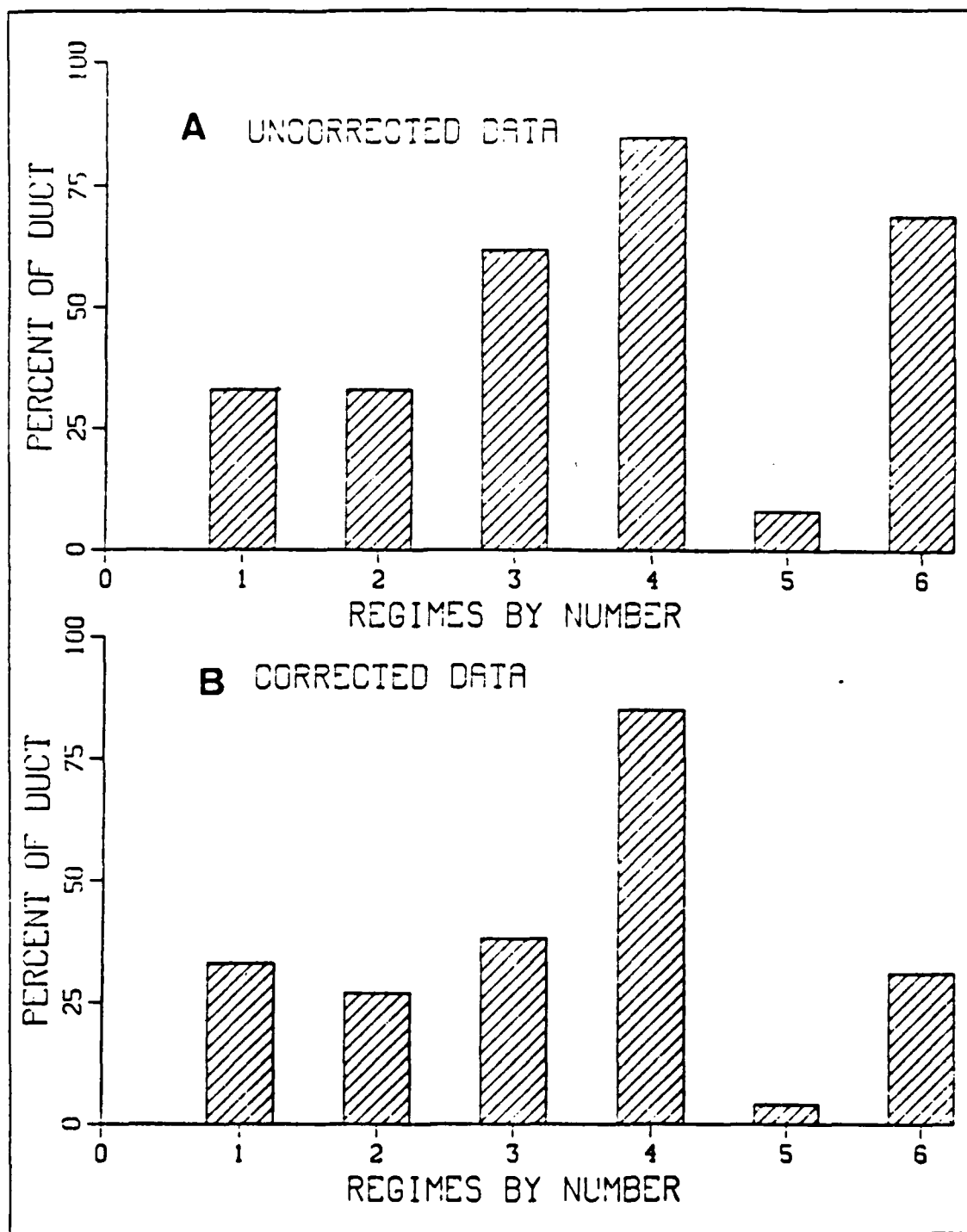
Fig. 37.   Percent of duct occurrence during each regime from Willis (1987).
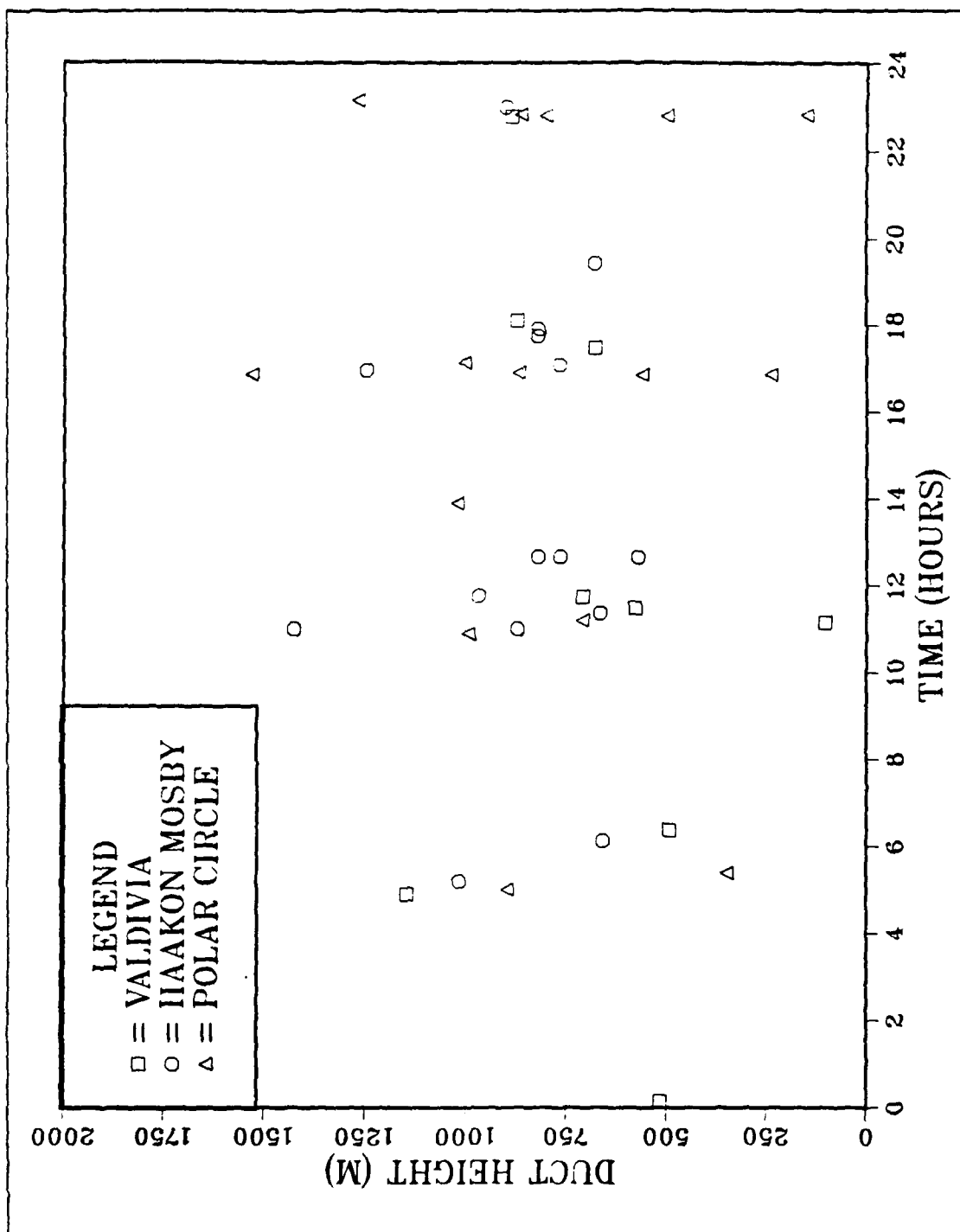
Fig. 38. Duct height relative to time of day observed.
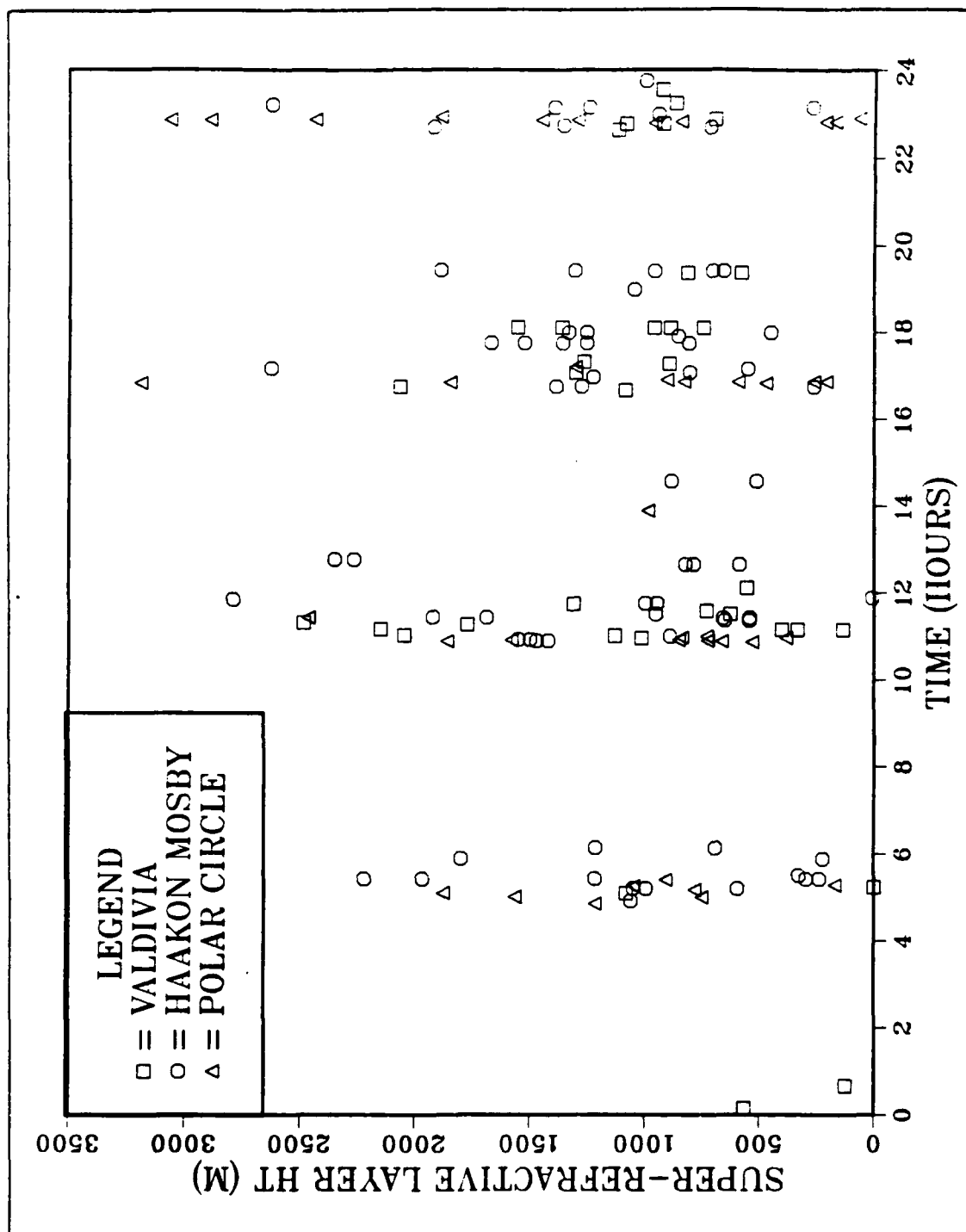
Fig. 39. Super-refractive layer height relative to time of day observed.
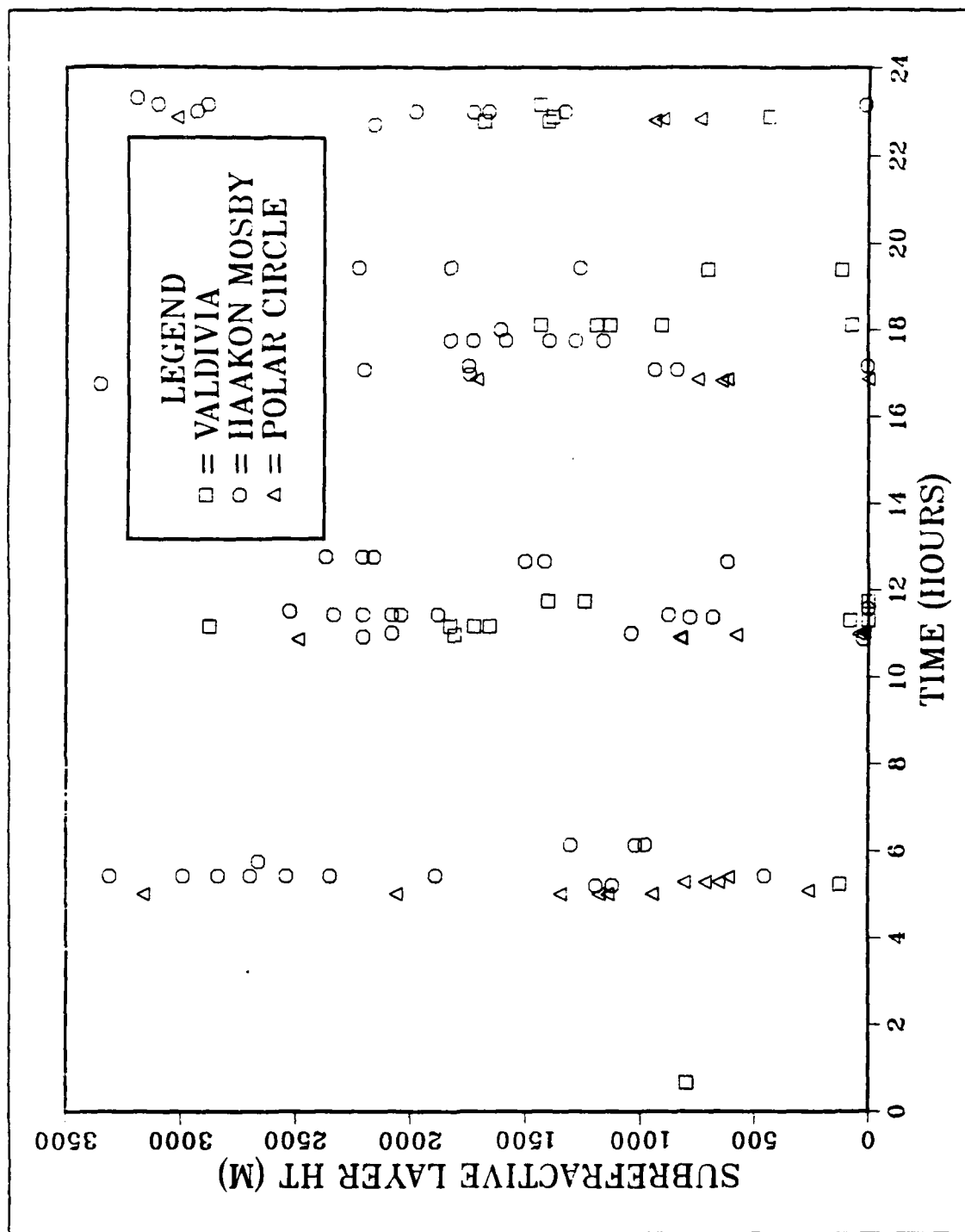
Fig. 40.   Subrefractive layer height relative to time of day observed.

61

2. Diurnal Variations in Frequency of Occurrence

Examination of the diurnal scatter plots seemed to indicate a larger occurrence of refractive events during the midday and early evening launch periods. A statistical study was completed to determine if these variations in frequency of occurrence were significant. The results of this study are presented in Table 2. The number of rawinsondes launched during each launch period varied. In order to account for this in the statistical study, a percentage of occurrence for each of the refractive effects was calculated for each period based on the total number of rawinsondes launched during that period.

Incidents of ducting were detected more frequently during the midday and early evening launch periods compared to those for early morning or late evening. This observation is significant in that the trend is opposite to that normally observed or expected. Normally conditions for ducting tend to improve during the hours of darkness due to radiational cooling at the top of clouds. This causes an increase in the temperature jump across the inversion which should lead to a greater occurrence of ducting at night. An explanation for the increased frequency of ducting during the midday and early evening hours is not readily apparent. This observation could be of significant tactical interest if it is observed in other data sets and should be investigated further.

TABLE 2 PERCENTAGE OF OCCURRENCE OF REFRACTIVE EVENTS BASED ON TOTAL LAUNCHES PER LAUNCH CYCLE			
Launch Period	Percentage of Ducts	Percentage of Super-refractive Layers	Percentage of Subrefractive Layers
Early Morning 0500-0600 UTC	16%	47%	31%
Midday 1100-1200 UTC	22%	64%	40%
Early Evening 1700-1800 UTC	28%	54%	30%
Late Evening 2300-2400 UTC	18%	52%	31%

Super-refractive layers followed a pattern similar to that of ducting although the highest percentage of super-refractive layers was 64%, observed at midday. It may be possible that the increase of ducting rates between the midday and early evening periods is related to the decrease in super-refractive rates during the same times. If the inversion strengthened during the interval between the two periods, ducting conditions could exist where previously super-refractive conditions existed. This suggestion, while plausible, was not readily apparent in the data set. Investigation of this observation was complicated by frequent changes in the large-scale forcing present over the region and by continuous movement of the ships. Further studies of this phenomenon should be made with data measured from a fixed position during a period of relatively stable large-scale forcing.

Subrefractive events showed little diurnal change in frequency of occurrence. A midday percentage of 40% was higher than the rate of the other three periods which were nearly equal at 30%. The cause of this is not obvious.

VI. SPATIAL STUDIES

Several spatial studies were conducted to investigate variations in EM refractivity over horizontal distances. In the first study, variations in EM ducting, super-refraction and subrefraction were examined based on position relative to the ice edge. The second study looks at cases where rawinsondes were launched at approximately the same time to determine how homogeneous the refractive structure of the atmosphere is over horizontal ranges. A range-dependent ray tracing program was used to show how inhomogeneity in the refractive structure affects EM wave propagation.

A. HORIZONTAL VARIABILITY RELATIVE TO THE ICE EDGE

Considerable variability in the heights of the various refractive layers was observed relative to the ice edge. Variations in duct thickness and strength were also noted. The results of these findings are summarized in Table 3. The ice edge boundary was taken to be where 50% of the surface was covered by pack ice. This boundary remained fairly constant during MIZEX-87. The average position of the ice edge is indicated by the dashed line in Fig. 4. For the purpose of this study the area within 25 km of either side of the ice boundary was considered to be within the MIZ. This boundary is for statistical purposes only as the actual width of the MIZ varies considerably depending on the season, currents and wind direction/speed.

Guest and Davidson (1988) determined that the well-mixed layer height was greater over the ocean than over the pack ice. This was described in chapter three and illustrated in Fig. 16. In chapter five the duct heights and super-refractive layer heights were associated with the capping inversion at the top of the well-mixed layer during many of the launch episodes. One would expect the duct and super-refractive layer heights to follow a pattern similar to that of the well-mixed layer relative to the ice edge. This trend was observed during the statistical study to a certain extent. To more closely examine the variations in height, thickness and strength, the data were plotted in scatter plots as a function of distance from the ice edge. Fig. 41 is a plot of duct height versus distance from the ice edge. The mean and median values of duct height were calculated over the ice, MIZ and water. The duct heights increased from a mean value of 632 m over the ice to 890 m over the water. The median values for these two areas showed a similar trend. The duct heights over the MIZ were the highest with mean/median values of 982 m and 994 m respectively. The increase in the heights over the MIZ is an

64

unexpected feature and was also observed for super-refractive and subrefractive layers. Several explanations for this observation will be discussed later in this chapter.

TABLE 3 VARIABILITY IN REFRACTIVE STRUCTURE RELATIVE TO THE ICE EDGE (values given as mean/median in meters)			
Measured Variable	Over Ice	Marginal Ice Zone	Over Water
Duct Height	632/530	982/994	890/793
Duct Thickness	42/45	46/43	54/59
Duct Strength*	1.4/1.3	1.0/0.8	2.0/1.6
Super-refractive Layer Height	620/753	1332/1217	1192/1061
Subrefractive Layer Height	624/728	1644/1782	1569/1511
* Duct strength measured in M-units			

Duct thickness is plotted relative to the ice edge in Fig. 42. The thickness of the ducts was relatively constant over the ice and varied less than 10 m for 80% of the ducts. Over the ice the average duct thickness was 42 m. In the MIZ the thickness varied greatly although the mean and median values closely resembled those measured over the ice. The duct thickness over the water was highly variable, ranging from less than 20 m to greater than 100 m. The mean and median values of 54 m and 59 m were somewhat larger than those over the ice or MIZ.

Duct strength was higher over the water than over the ice or the MIZ. Fig. 43 indicates that over the ice no ducts were detected with a strength greater than 3 M-units. Over the MIZ the ducts were even weaker. Over the water the strength of the ducts varied from values that approached zero to duct strengths as high as 7 M-units. 70% of the ducts detected over the ocean had strengths less than 3 M-units.

Super-refractive layer heights and subrefractive layer heights were also examined relative to the ice edge. Fig. 44 is a scatter plot of super-refractive layer heights versus distance from the ice edge. Super-refractive layer heights over the ice resembled those

observed for ducting. The mean super-refractive layer height over ice was 620 m which is slightly less than observed for ducting. The median super-refractive layer height of 753 m over the ice is greater than the median value of 530 m for duct heights and more clearly represents the observed situation. Over the MIZ, the super-refractive layer median height nearly doubles to 1217 m and then falls slightly over the water to a median height of 1061 m. Subrefractive layer heights, illustrated in Fig. 45, followed the same general pattern observed for super-refractive layers. A median height of 728 m over the ice increased to 1782 m over the MIZ and then decreased to a median value of 1511 m over the water.

To more graphically show the tendencies of the heights relative to the ice edge two plots were constucted. Fig. 46 shows the first plot. In this plot all incidences of ducting are shown when at least two ships launched rawinsondes within the same launch episode. If a duct was observed by more than one of the ships in a given launch episode the lines between the ducts were connected. Some evidence of an increasing slope going from right to left is apparent in this plot. The second plot, shown in Fig. 47 is similar to the first. However, in this plot super-refractive layers are added to the trapping layers. The super-refractive layers had to be associated with the same meteorological condition that produced the duct during that episode. In most cases this was the primary inversion. Fig. 47 indicates the positive slope even more clearly and supports the results observed using the mean and median values.

The spatial variation in the heights of the various refractive layers relative to the ice edge is partly a function of the strength of the surface fluxes available for the formation of TKE in the MABL. The wind flow during most of MIZEX-87 was northerly. This sets up a flow pattern that brings relatively cold, dry air off from the pack ice over the warmer ocean surface. Air that remains over the pack ice is not influenced by increased surface heat and moisture fluxes and maintains a shallower mixed layer. This is consistent with observations by the Polar Circle as it operated within the pack ice. Air flowing over the warmer ocean surface experiences an increase in both heat and moisture fluxes. This causes increased turbulence and results in a deeper well-mixed layer. The higher refractive events detected over the water were often associated with the strong temperature and moisture gradients found at the top of the well-mixed layer.

Over the MIZ higher mean and median heights were observed for all of the refraction categories discussed. Based on the above physical discussion, one would expect these heights to fall between those observed over the ice and water. There are several
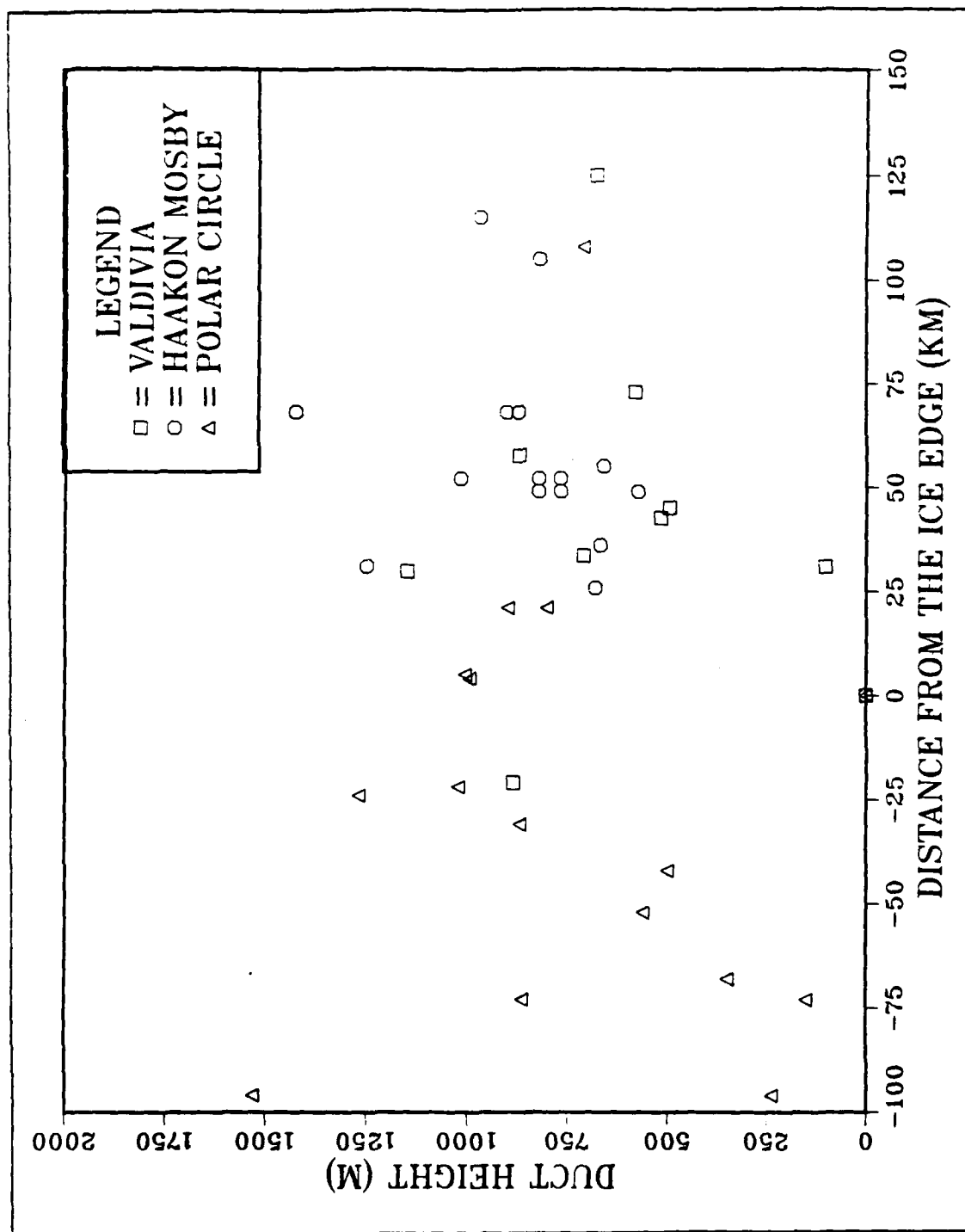
Fig. 41. Duct height relative to distance from the ice edge.
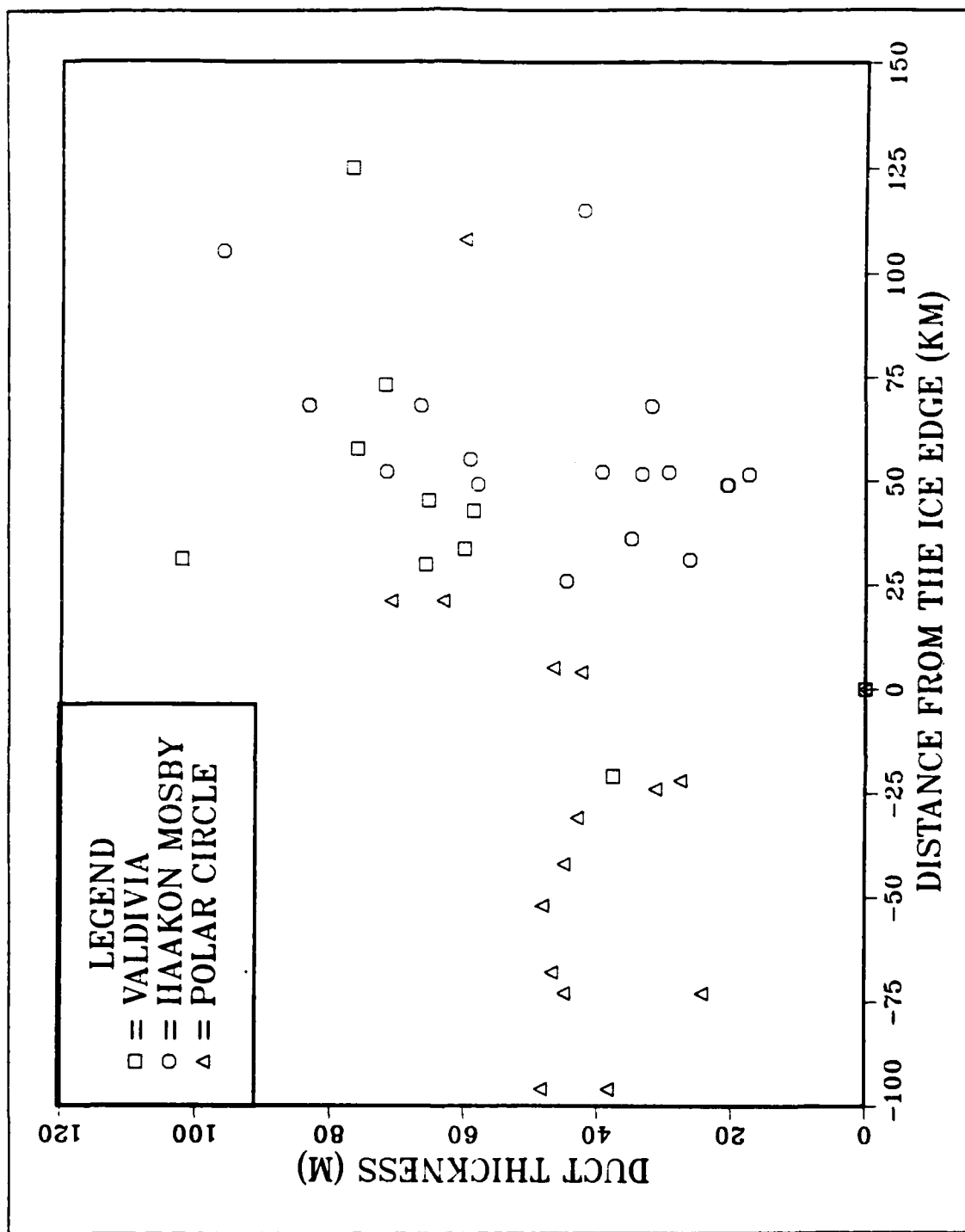
Fig. 42. Duct thickness relative to distance from the ice edge.

Fig. 43.   Duct strength relative to distance from the ice edge.

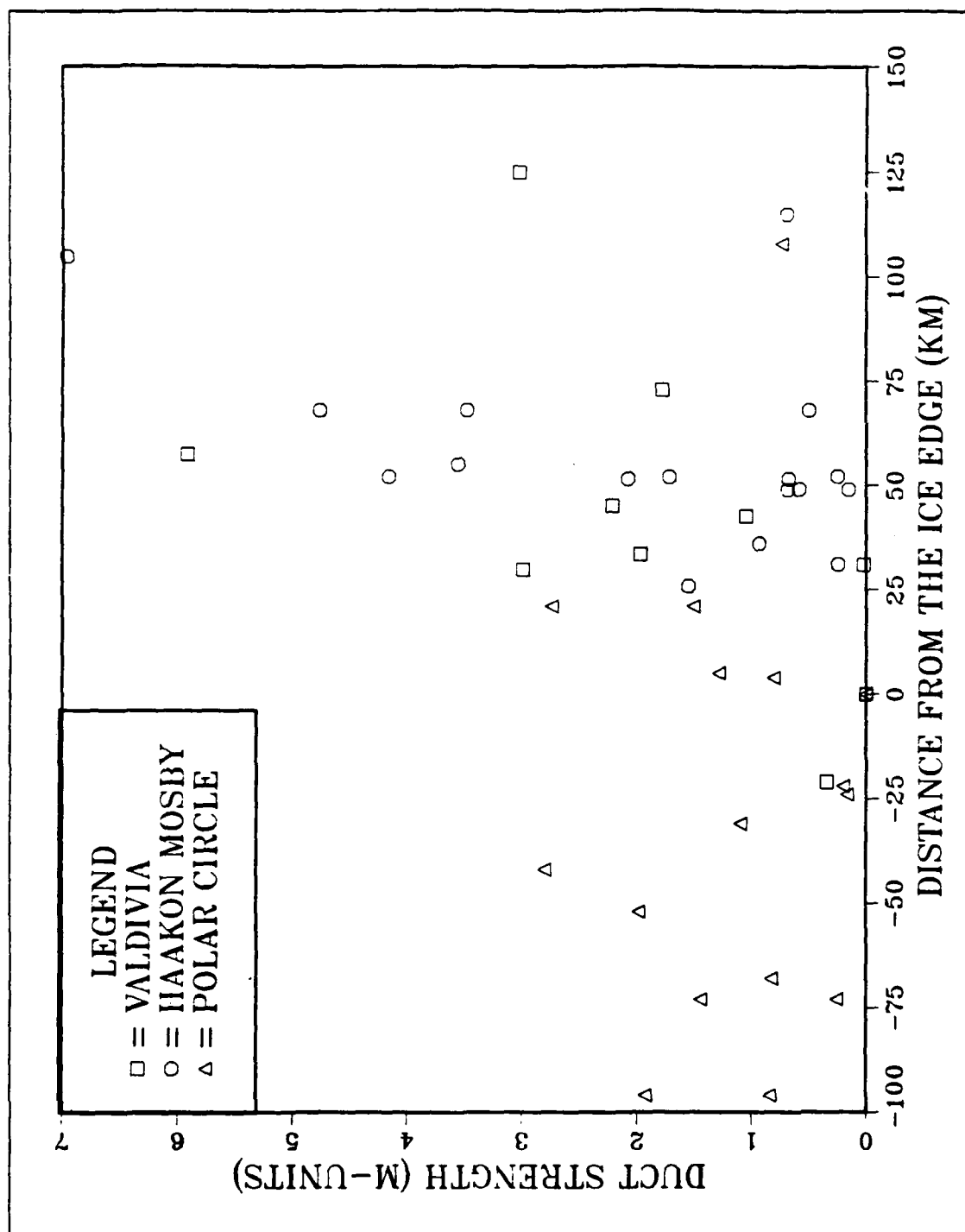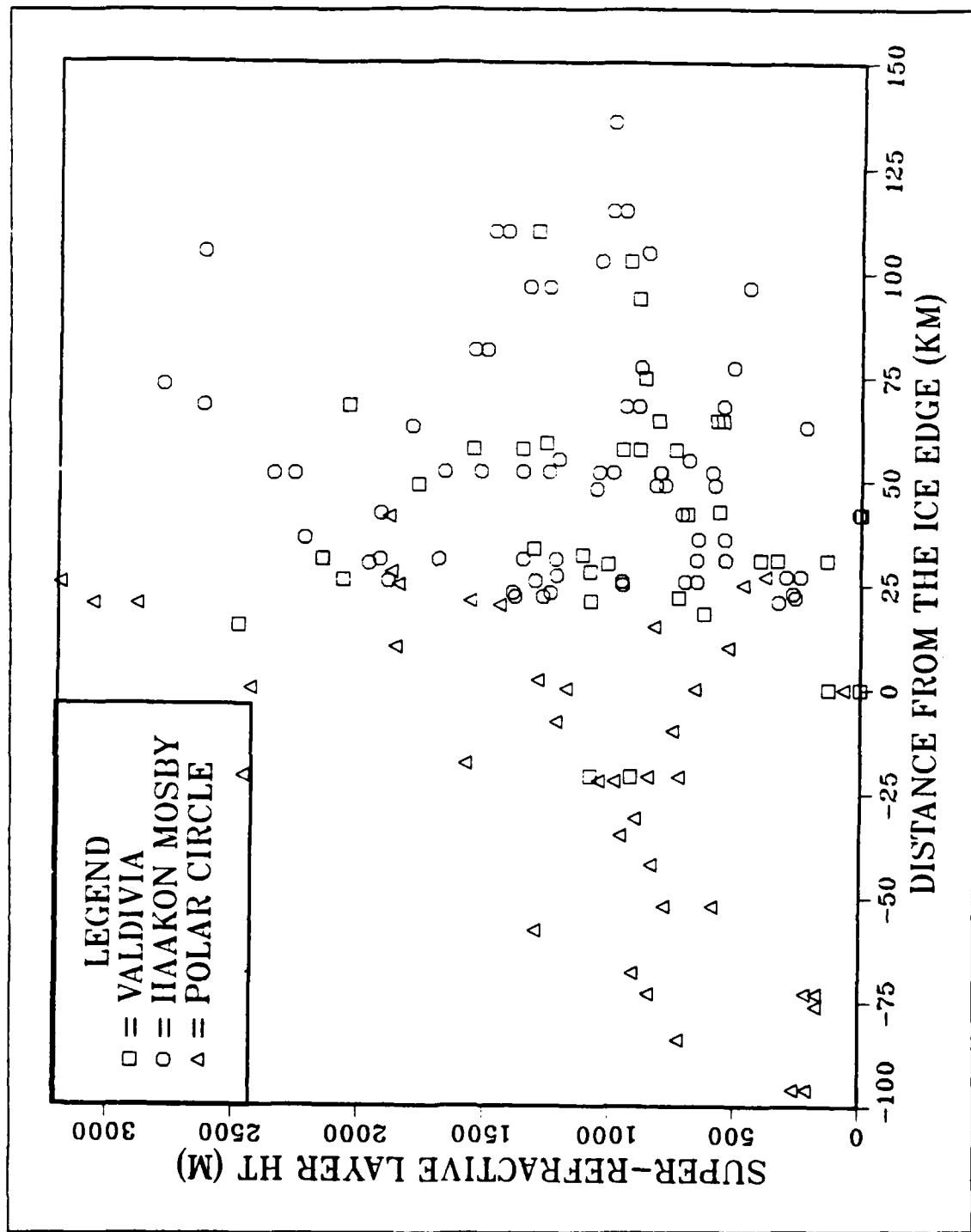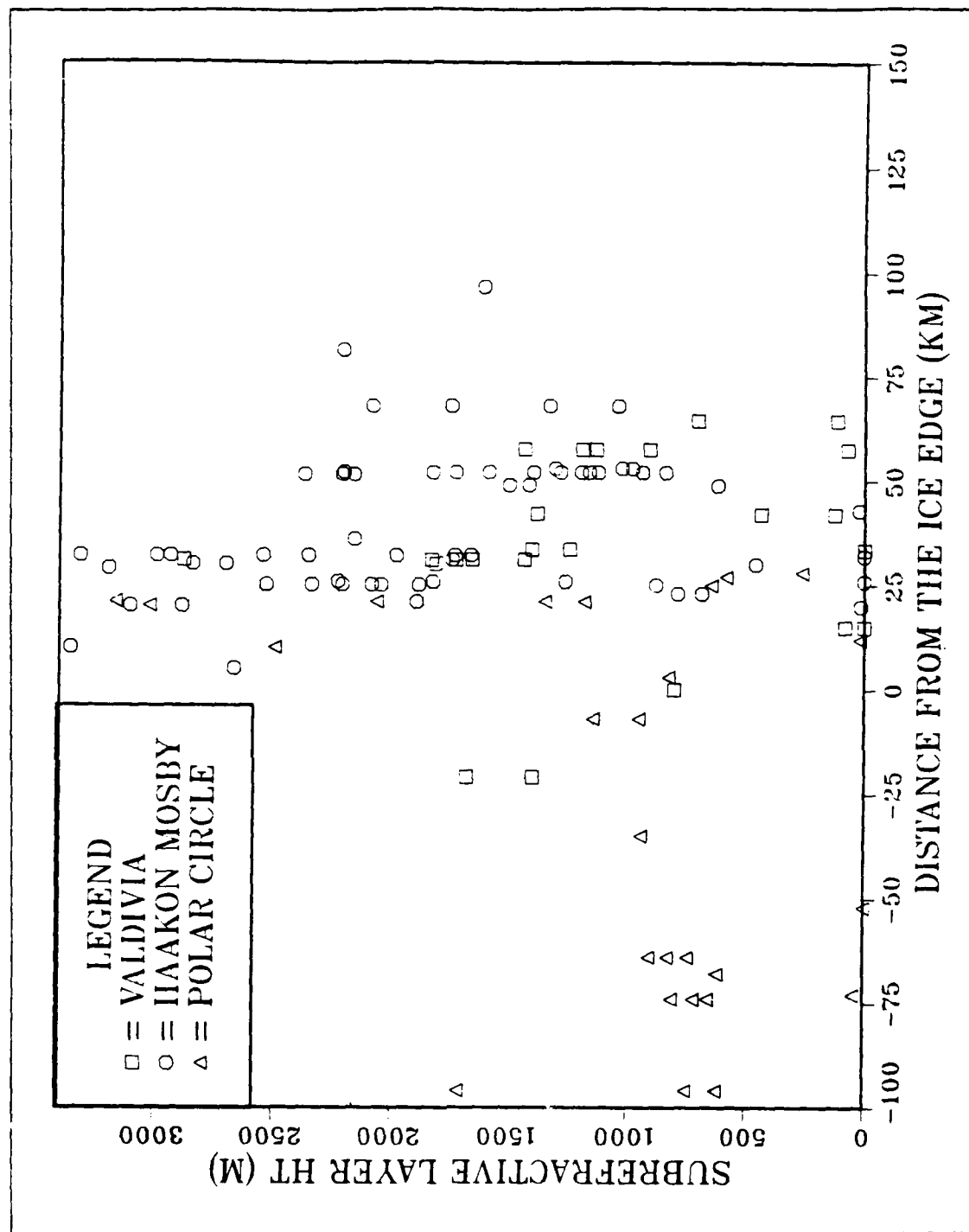Fig. 44.   Super-refractive layer height relative to distance from the ice edge.

Fig. 45.   Subrefractive layer height relative to distance from the ice edge .
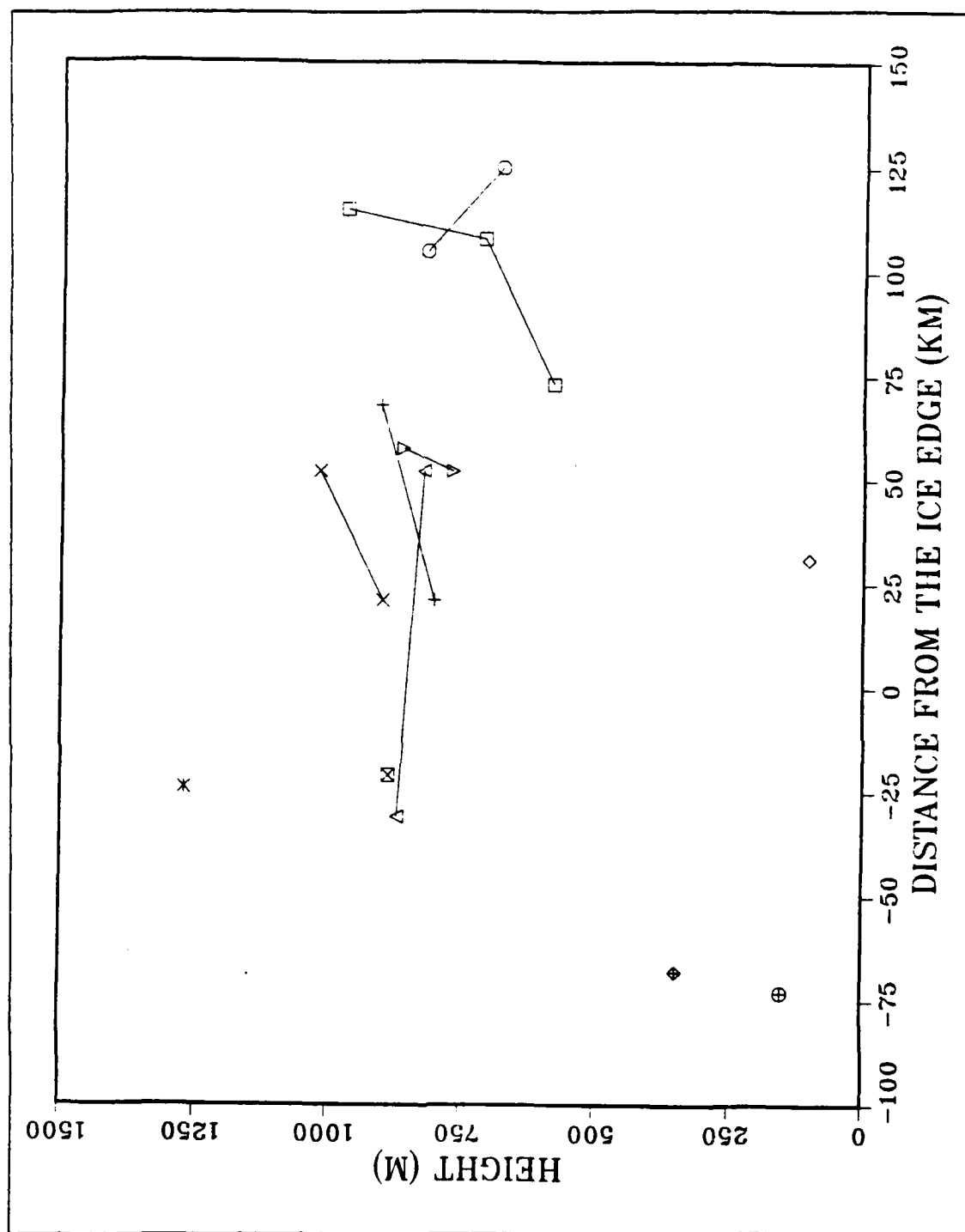
Fig. 46. Slope of duct heights recorded during the same launch episode relative to distance from the ice edge.
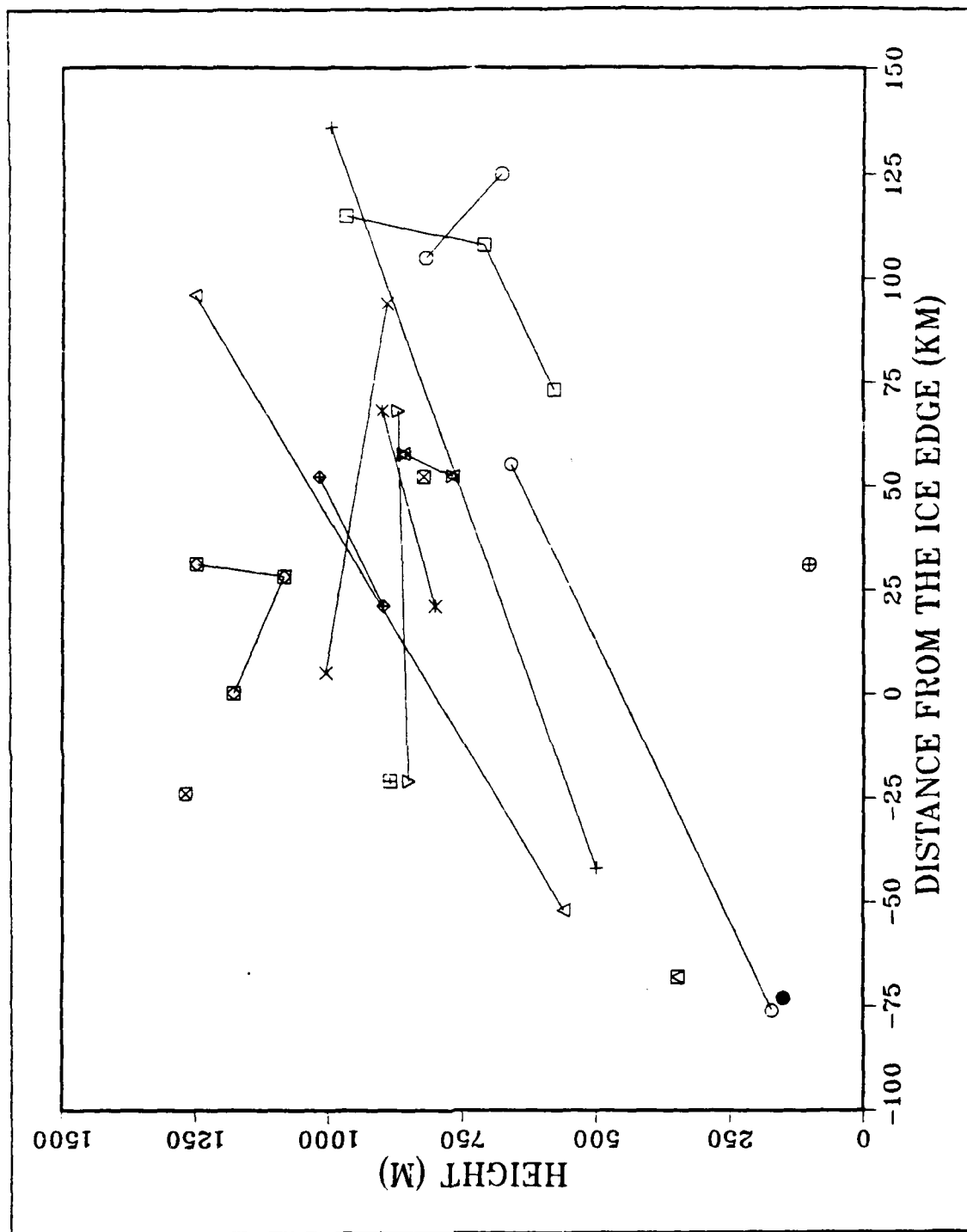
Fig. 47. Slope of duct and super-refractive layer heights during the same launch episode relative to distance from the ice edge.

possible explanations for the deviation of the heights over the MIZ. Mean and median values of the heights included all detections of ducting and super-refraction and not only those associated with the inversion over the well-mixed layer. Multiple ducts in the vertical were recorded five times during MIZEX-87. Multiple super-refractive layers were observed during 28 different launches. In these cases only the lowest of the layers was associated with the primary inversion. A recalculation of the mean values of height was done using only those refraction events that could be associated with the inversion layer of the MABL. The mean values for duct heights showed no significant change over the ice. Over the MIZ the mean height dropped from 982 m to 901 m. Over the water the mean dropped from 890 m to 772 m. This does not contribute to an explanation of the greater height values over the MIZ. A more probable explanation for the higher duct heights is that the rawinsonde launches within the MIZ region were conducted during times when the MABL was relatively deeper than what it was over the total MIZEX-87 period. Further investigation confirmed this suggestion. Of the seven ducts detected within the MIZ area, five of them were detected at times when the boundary layer inversion was relatively weak and the height of the mixed layer was higher than normal. The recalculation of the super-refractive layer mean heights resulted in a drop in the mean height over the MIZ from 1332 m to 916 m. Over the water the mean dropped slightly from 1192 m to 1117 m. The recalculated mean heights reflect the increase in the well-mixed layer heights observed by Guest and Davidson (1988).

Subrefractive layers were most closely correlated to areas just under cloud bases or under bands of higher moisture. Multiple levels of subrefraction were not observed over the ice. Conversely, over the MIZ and water there were 26 launch episodes that recorded multiple levels of subrefraction in the vertical. These layers ranged from the surface up to over 3000 m in height. Most of these episodes occurred in open water within 50 km of the ice edge.

The results of this study show that during the late winter/early spring the presence of ice has a definite effect not only on the height of the MABL but also on the level at which ducting, super-refraction and subrefraction are observed. Over the ice refraction anomalies were observed at relatively lower heights and were singular events. Over the MIZ and water the heights increased and greater incidences of multiple refractive layers were observed.

Willis (1987) performed a similar statistical analysis of EM ducting relative to the ice edge. A comparison of results indicates that ducts were observed much more frequently

in the summer during MIZEX-84. Willis reported that ducts were detected during 48.4% of the launches in the uncorrected data and 30% in the corrected data. This is compared to a detection rate of 21% during MIZEX-87. Although the frequency of ducting events differed substantially, the mean values of duct height were reasonably close to the uncorrected MIZEX-84 values. Willis reported an uncorrected over-ice mean height of 502 m and a height of 848 m over the water. These compare to the respective values of 632 m and 890 m observed during MIZEX-87. After the correction for dewpoint error was applied, the mean duct heights over the ice and water were lowered to 370 m and 560 m for the MIZEX-84 data. The correction applied to the dewpoint curves in the MIZEX-84 study caused the gradient of moisture near the inversion to be weaker. It also lowered the height at which the dewpoint began to decrease, to one that more closely matched the base of the inversion. Based on the method in which the correction was applied and on the results of the MIZEX-87 study, it is thought that the frequency of occurrence of ducting is more accurate in the case of the uncorrected data for MIZEX-84. Conversely, the average duct heights relative to the ice edge are best represented by the values determined from the corrected data.

The lower mean heights observed during MIZEX-84 could be due to the tendency towards stronger and more frequent ridging over the Fram Strait during the summer season caused by intensification of the Greenland High. This would result in a stronger subsidence rate aloft and a more depressed well-mixed layer height. The greater air/sea temperature differences observed during MIZEX-87 would also have increased the surface heat flux during the spring season. This would cause a relative increase in the TKE available for mixing in the boundary layer and a subsequent increase in the inversion base.

Average duct thicknesses were two to three times greater during MIZEX-84 than during MIZEX-87. A similar trend was observed in the average duct strengths. These differences would be expected due to the stronger inversions that develop during the summer. The inversion strength is weaker in the spring due to lower subsidence rates compared to the summer. This effect is partly offset by the greater surface heat flux expected during the spring season. The heat flux causes increased mixing in the boundary layer and increased entrainment of the air above the inversion. This not only raises the base but also increases the temperature jump across the inversion. The large-scale forcing, causing the rate of subsidence to vary, appears to have a much more significant effect on the strength and thickness of the ducts.

B. VARIABILITY OF THE REFRACTIVE STRUCTURE BETWEEN SHIPS

Of the 169 successful rawinsonde launches, 130 met the requirement for this portion of the spatial study of being launched within one hour of at least one other ship's rawinsonde. These rawinsondes were launched during 53 seperate launch episodes. The spatial variability between ships was examined for each type of EM refractivity. Table 4 gives a summary of the results.

1. Statistical Results

In 17 of the 53 launch episodes at least one duct was detected. Of these 17 episodes, one resulted in ducts being reported by all three ships. A duct was reported by two of the ships in five of the launch episodes. The remaining 11 launch episodes involved a duct being reported by only one ship. The specific circumstances surrounding several of these launches will be discussed in three case studies presented later. Of the 26 individual ducts detected, 66% were associated with the boundary layer capping inversion.

TABLE 4
PERCENTAGE OF DISTRIBUTION OF REFRACTIVE
LAYER MULTIPLICITY PER LAUNCH PERIOD

Type Layer	1 Ship	2 Ships	3 Ships
Trapping	65%	29%	6%
Super-refractive	41%	48%	11%
Subrefractive	71%	24%	5%

Super-refractive events were noted in 44 of the 53 launch episodes. All three ships reported super-refractive layers during five of the launch episodes. Two ships reported super-refractive layers during 21 of the episodes and only one ship reported a super-refractive layer during the remaining 18 episodes. 46% of the super-refractive layers detected were associated with the primary boundary layer inversion. In the case studies super-refractive layers detected on one ship are related to ducts detected on another ship during the same launch episode.

Subrefractive layers were noted during 38 of the 53 launch episodes. Of these, three ships reported concurrent subrefractive layers during only two of the episodes. In nine of the episodes subrefraction was reported by two of the ships. The remaining 27

76

episodes had only one ship detect a subrefractive layer. The large number of single ship episodes seems to suggest that subrefractive events may occur over smaller horizontal areas and may be caused by smaller-scale phenomena such as individual cloud layers or narrow bands of increased moisture levels.

2. Case Studies

A series of case studies was completed on various ducting episodes in order to more clearly understand the cause of the inhomogeneity observed in the refractive structure of the atmosphere during MIZEX-87.

a. Case One

Rawinsondes were launched from all three ships at approximately 1130 UTC 24 March. Six hours later the Valdivia and the Haakon Mosby launched again. Polar Circle did not launch at the 1730 UTC launch period. Fig. 48 shows the positions of the three ships at 1200 UTC and 1800 UTC with respect to each other and the ice edge. In this and the following figures showing ship's position, the Polar Circle is identified by a circle, the Haakon Mosby by a square and the Valdivia by a triangle. At both launches the Valdivia was about 350 km to the north of Haakon Mosby with the Polar Circle between.

At the 1130 UTC launch the Haakon Mosby and Polar Circle were less than 20 km apart and in the open water. The area was under the influence of the Greenland High and winds were off-ice. All three ships detected ducts during the first launch. Fig. 49 shows the potential temperature, dewpoint and specific humidity curves for the three rawinsondes. The associated M and N profiles for these rawinsondes are shown in Fig. 50. The thicker line represents the M-profile and the thin line the N-profile. The ducts were detected at 579 m on the Valdivia, 968 m on the Haakon Mosby and 710 m on the Polar Circle. The strange dewpoint profile on the Haakon Mosby could be in error. A duct located at the base of the temperature inversion would have a height of 830 m. Even with this correction there is still a significant difference in the duct heights at a range of less than 20 km.

At the 1730 UTC launch the temperature and dewpoint profiles in Fig. 51 indicate a weaker inversion that has been lifted by about 100 m over the past six hours at the Valdivia's position. This is reflected in the duct height as it increased to 678 m. This weakening was probably caused by a slight warming of the well-mixed layer and a reduction in subsidence aloft as the Valdivia approached the boundary layer front developing to the west. Conversely, the inversion detected on the Haakon Mosby has
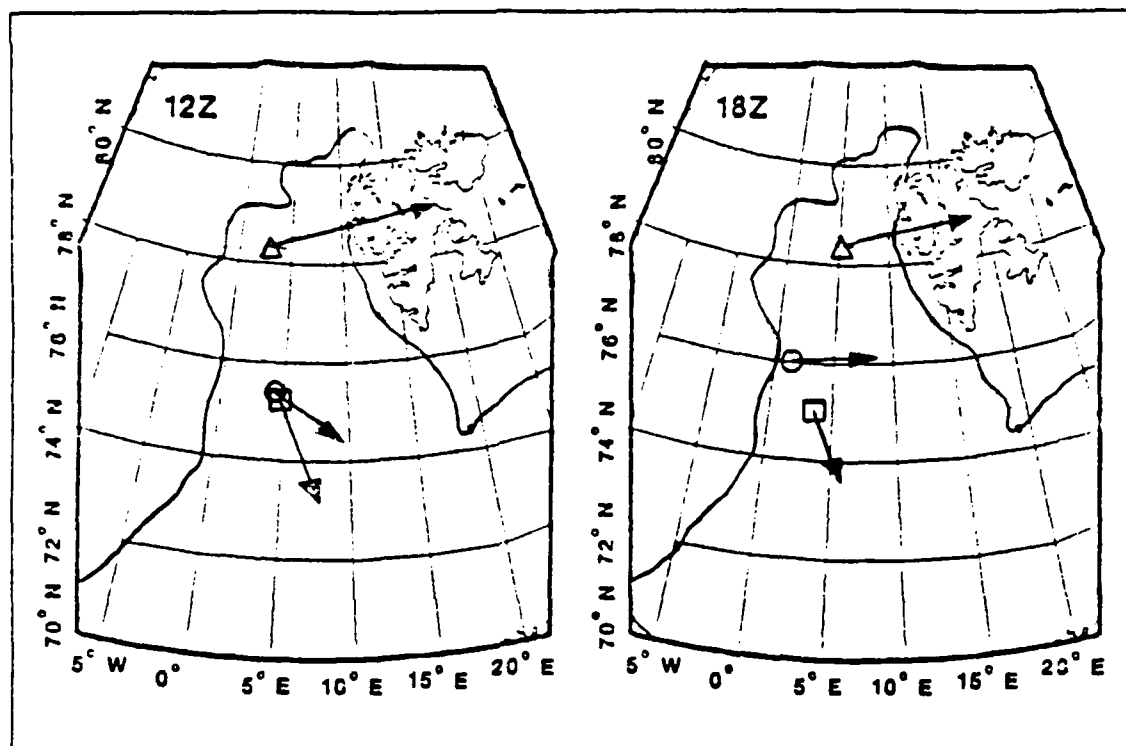
Fig. 48.   Ship positions at 1200 UTC and 1800 UTC 24 March 1987.

decreased in height and strengthened. The duct height decreased to 818 m and the duct thickness increased from 42 to 96 m. It is apparent that the Haakon Mosby is still under the influence of the high pressure system during the 1730 UTC launch.

In this case study the large scale features of a well-mixed layer and a capping inversion existed throughout the MIZEX area but there was considerable variability in the heights of the ducts detected by each ship.

b.   Case Two

In this situation a condition was observed in which the Polar Circle, positioned in the ice, recorded a duct at 1005 m. The Valdivia, stationed about 500 km to the southeast, recorded a super-refractive layer at 892 m. The Haakon Mosby was positioned midway between the other ships and showed no evidence of ducting or super-refraction. Fig. 52 shows the positions of the three ships at 1800 UTC 26 March as well as the potential temperature, dewpoint and specific humidity profiles for each ship within one hour of that time. The M and N profiles for this case are given in Fig. 53.

78

SPECIFIC HUMIDITY G/KG

SPECIFIC HUMIDITY G/KG

ALTITUDE M

2000

1000

0

POTENTIAL TEMPERATURE °C

24 MAR 1987 1112 GMT POLAR CIRCLE

LAT 75° 18'N LONG 4° 37'E

ALTITUDE M

2000

1000

0

POTENTIAL TEMPERATURE °C

24 MAR 1987 1129 GMT VALDIVIA

LAT 78° 23'N LONG 3° 9'E

SPECIFIC HUMIDITY G/KG

ALTITUDE M

2000

1000

0

POTENTIAL TEMPERATURE °C

24 MAR 1987 1145 GMT HAAKON MOSBY

LAT 75° 0'N LONG 21° 10' W

Fig. 49.   Rawinsonde profiles for launch episode of 1130 UTC 24 March 1987.

Fig. 50.   M and N profiles for launch episode of 1130 UTC 24 March 1987.

Fig. 51. Rawinsonde profiles and the associated M and N profiles for the launch episode of 1730 UTC 24 March 1987.

81

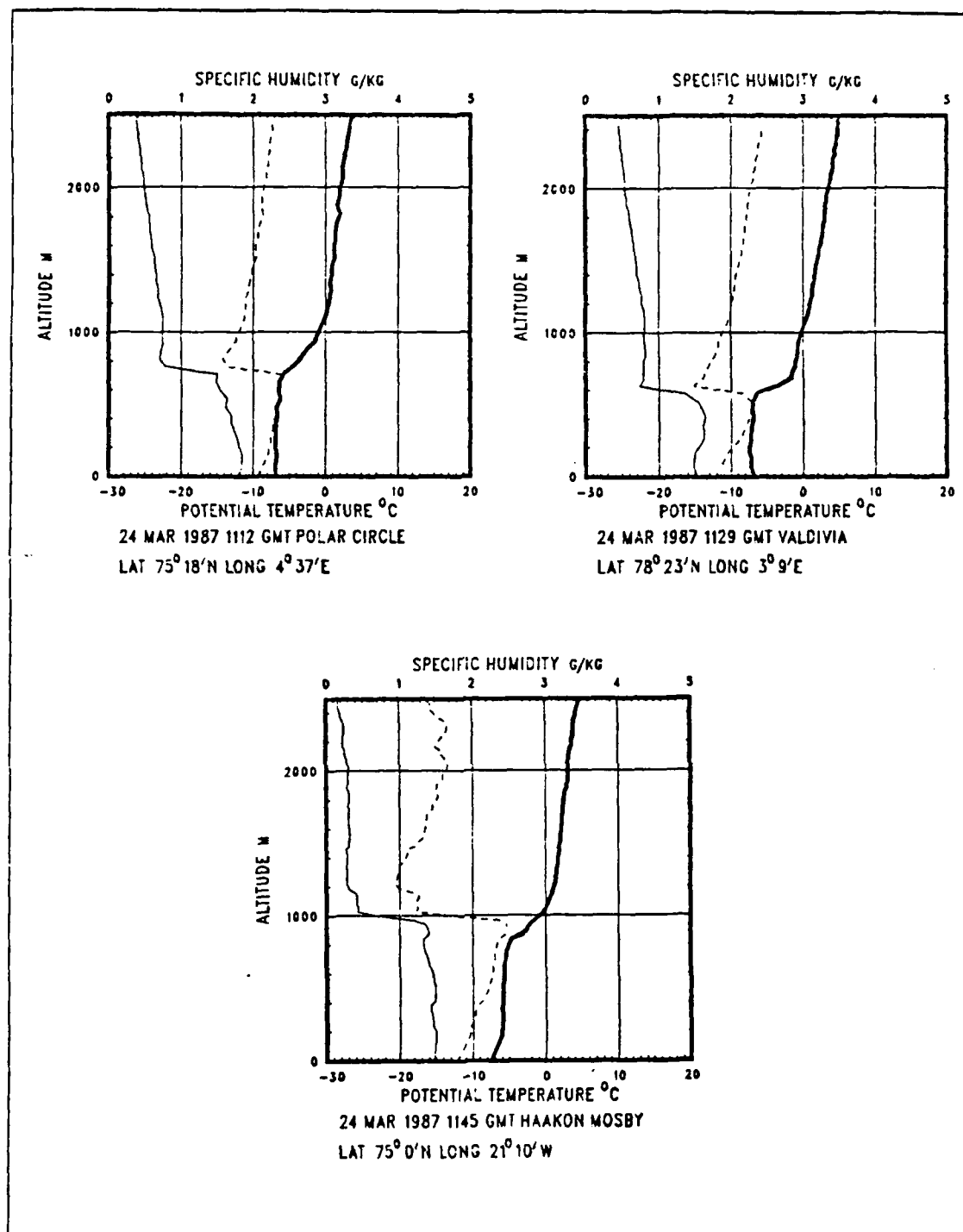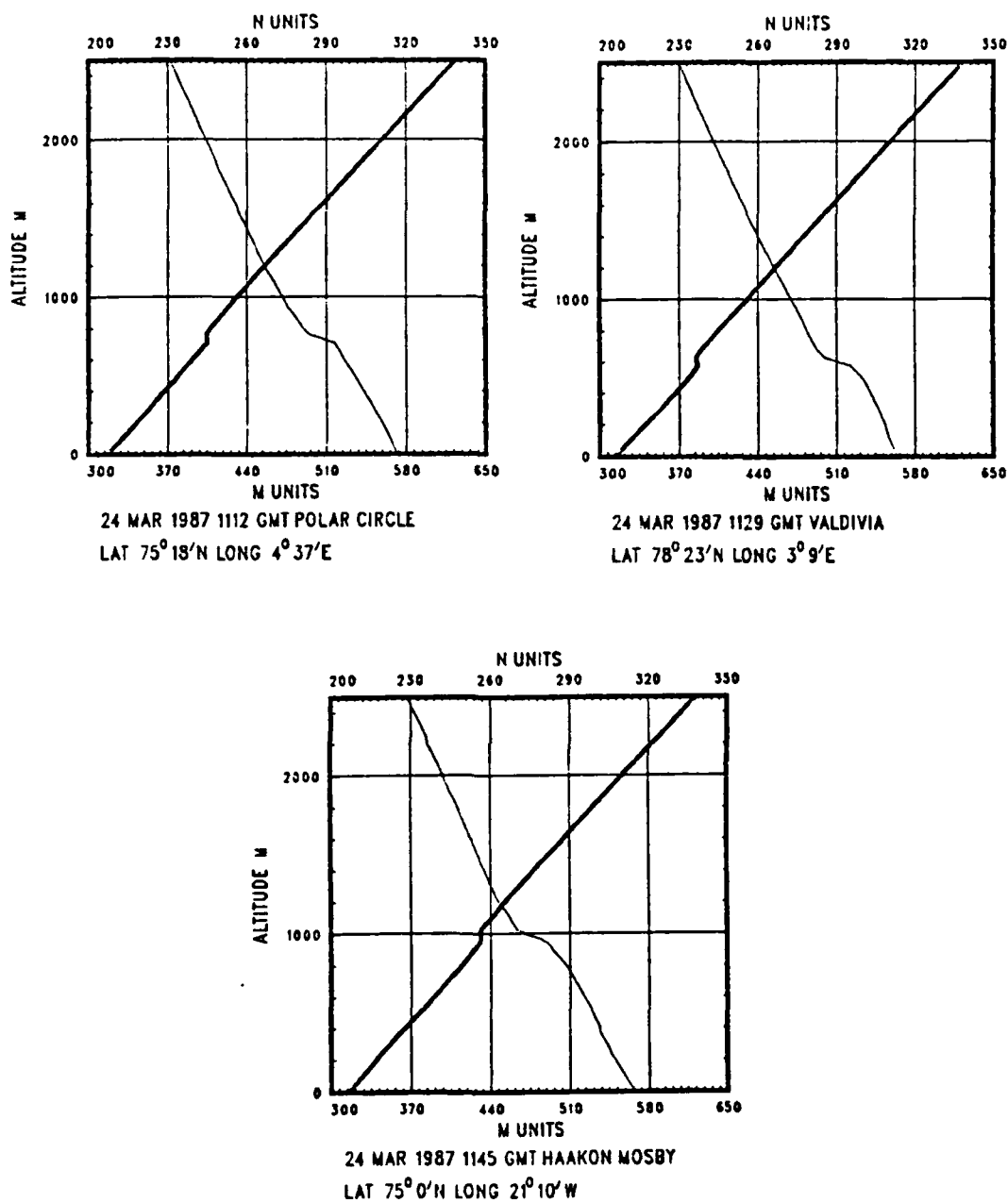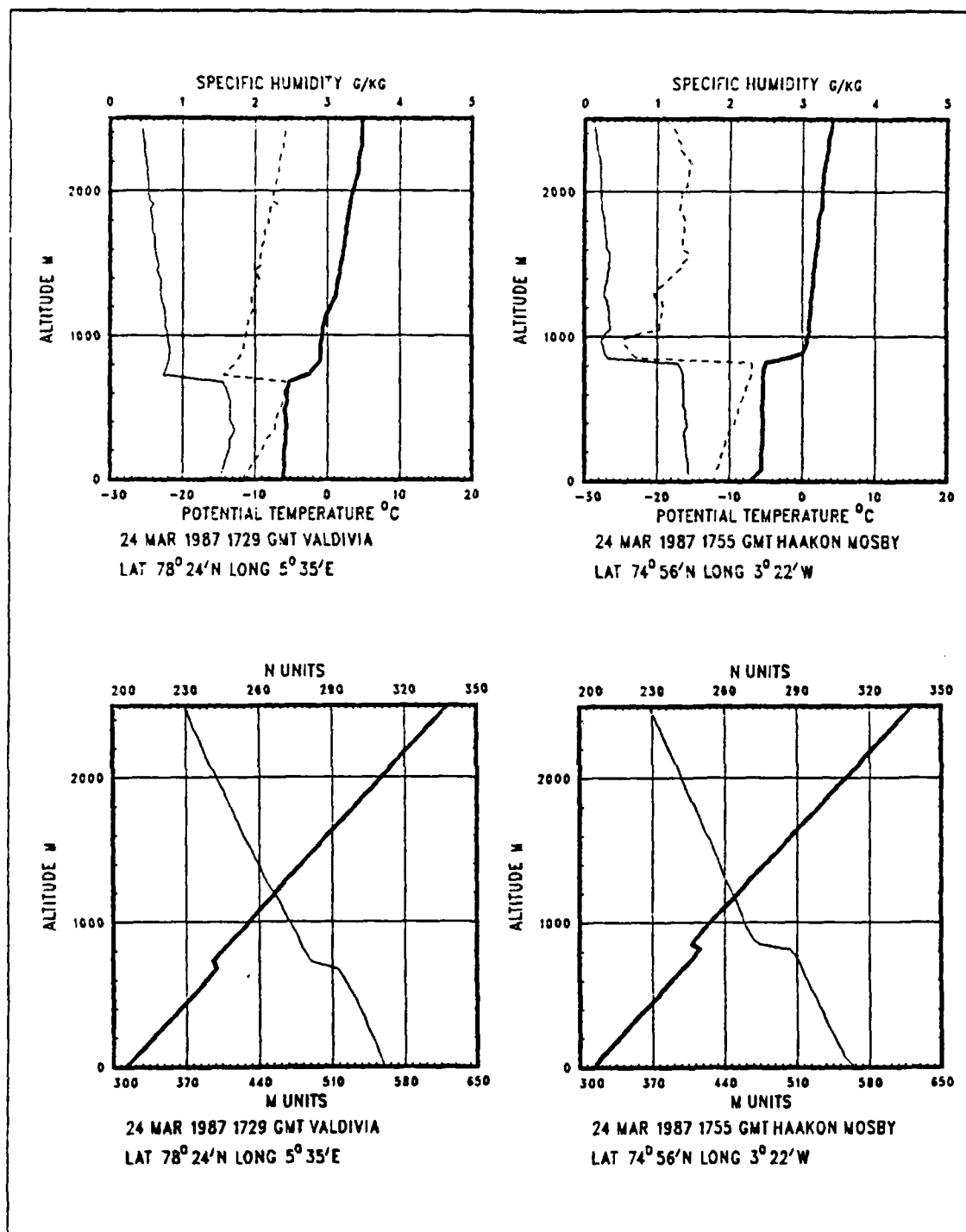A closer look at the synoptic picture during this launch episode explained the strange refractive structure observed during this case. The Haakon Mosby observed frontal passage of the boundary layer front at about 1600 UTC 26 March. The front effectively dissipated any inversion that had been present before and normalized the refractive structure. The Valdivia had experienced the frontal passage about 36 hours earlier and a redevelopment of the inversion is evident in Fig. 52 although it has not strengthened enough to permit ducting. The Polar Circle was still under the influence of the stable conditions aloft above the MABL. Observation of the launches just prior to and after the 1708 UTC launch by the Polar Circle revealed that the inversion base was lifting and the inversion was weakening in response to the approaching boundary layer front.

This case shows how a mesoscale meteorological phenomenon such as a boundary layer front can significantly alter the refractive structure of the atmosphere over a relatively short distance.

c. Case Three

This case examines four consecutive launch periods from 1130 UTC 1 April to 0530 UTC 2 April. Fig. 54 shows the relative positions of the ships during this period. The Valdivia was positioned over 400 km to the south of the other two ships. During this period the Valdivia was in an area under the influence of a passing synoptic-scale low and no incidents of ducting or super-refraction were detected. At the same time the Polar Circle, inside the ice edge, was always within 50-100 km of the Haakon Mosby, located just off the MIZ in the open water. Both of these ships were under the influence of high pressure.

During the 1130 UTC launch on 1 April, the Haakon Mosby detected a duct at 871 m. The Polar Circle, stationed 100 km to the west and in the ice, recorded a super-refractive layer at 851 m. At the 1730 UTC launch, the duct detected by the Haakon Mosby had descended to 822 m and the super-refractive layer observed six hours earlier by the Polar Circle had developed into a duct at 869 m. By the 2330 UTC launch time the ships had moved to within 60 km of each other. The Haakon Mosby detected a duct at 901 m and the Polar Circle observed a duct at 801 m. On the final launch at about 0530 UTC 2 April, the duct heights had increased on both vessels. Haakon Mosby detected a duct at 1017 m and the Polar Circle recorded a duct at 898 m. It appears that the inversion associated with the ducts has lifted at about the same rate between the third and fourth launch episodes.
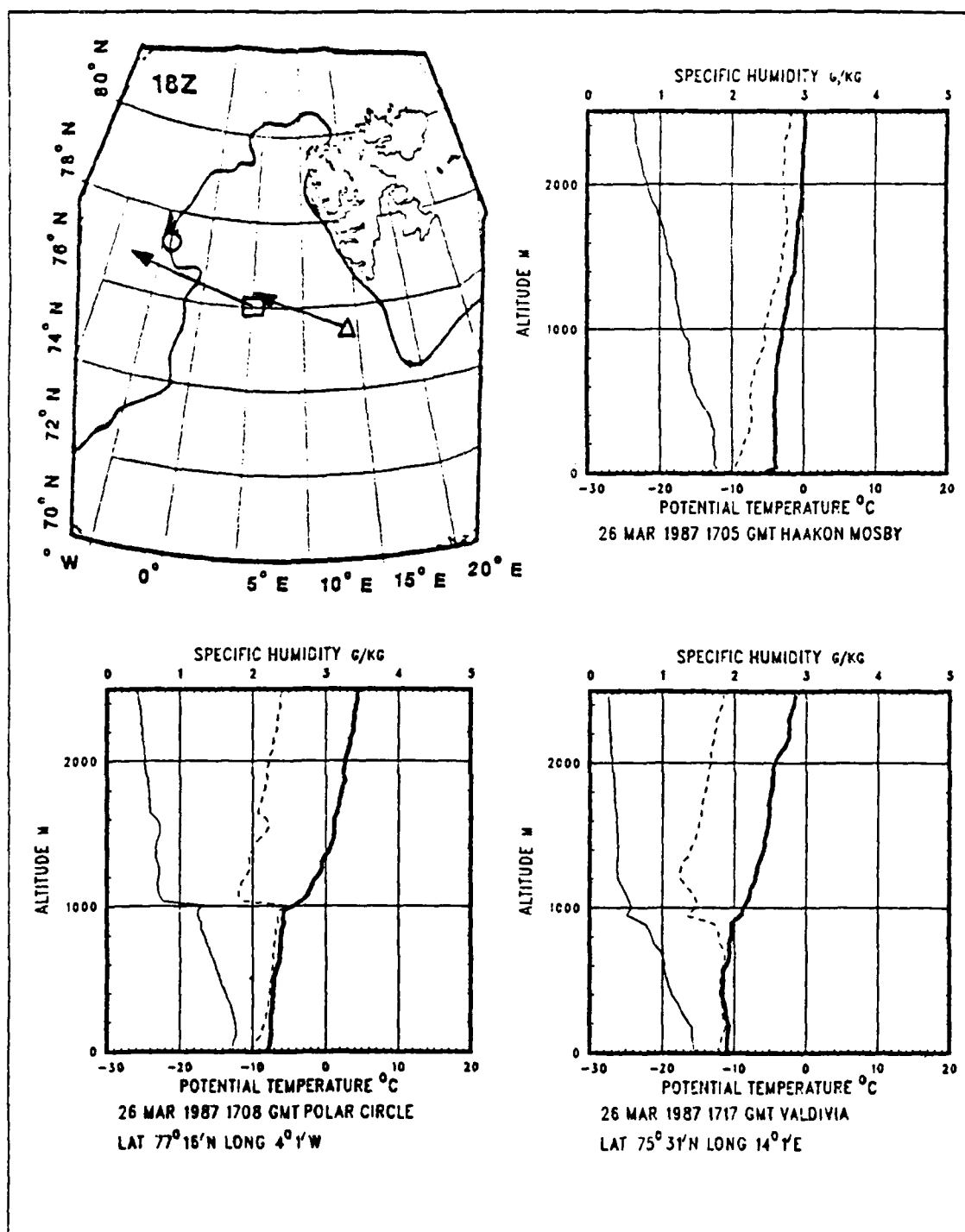
Fig. 52.   Ship positions at 1800 UT 26 March 1987 and rawinsonde profiles for the 1730 UT launch episode.
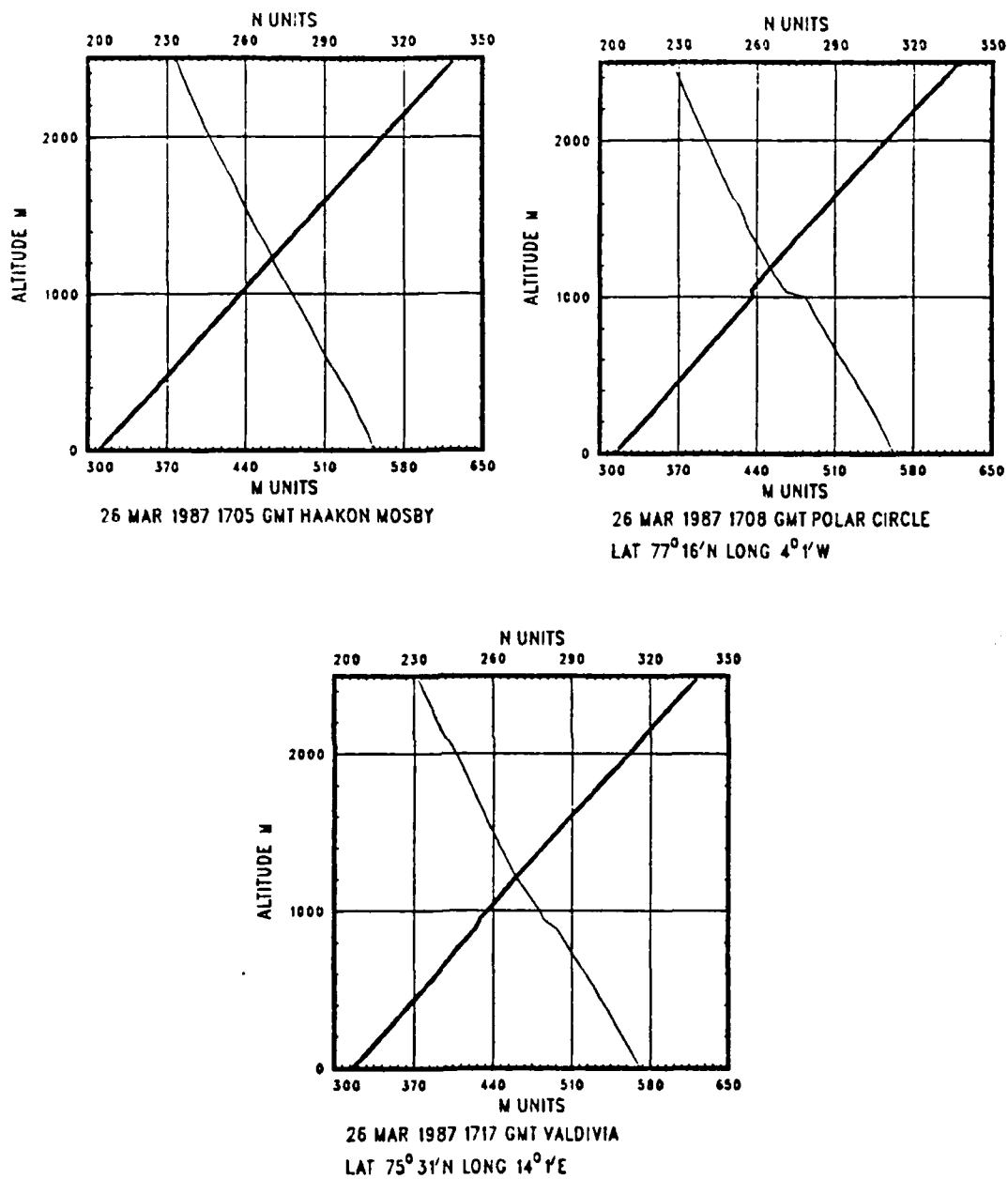
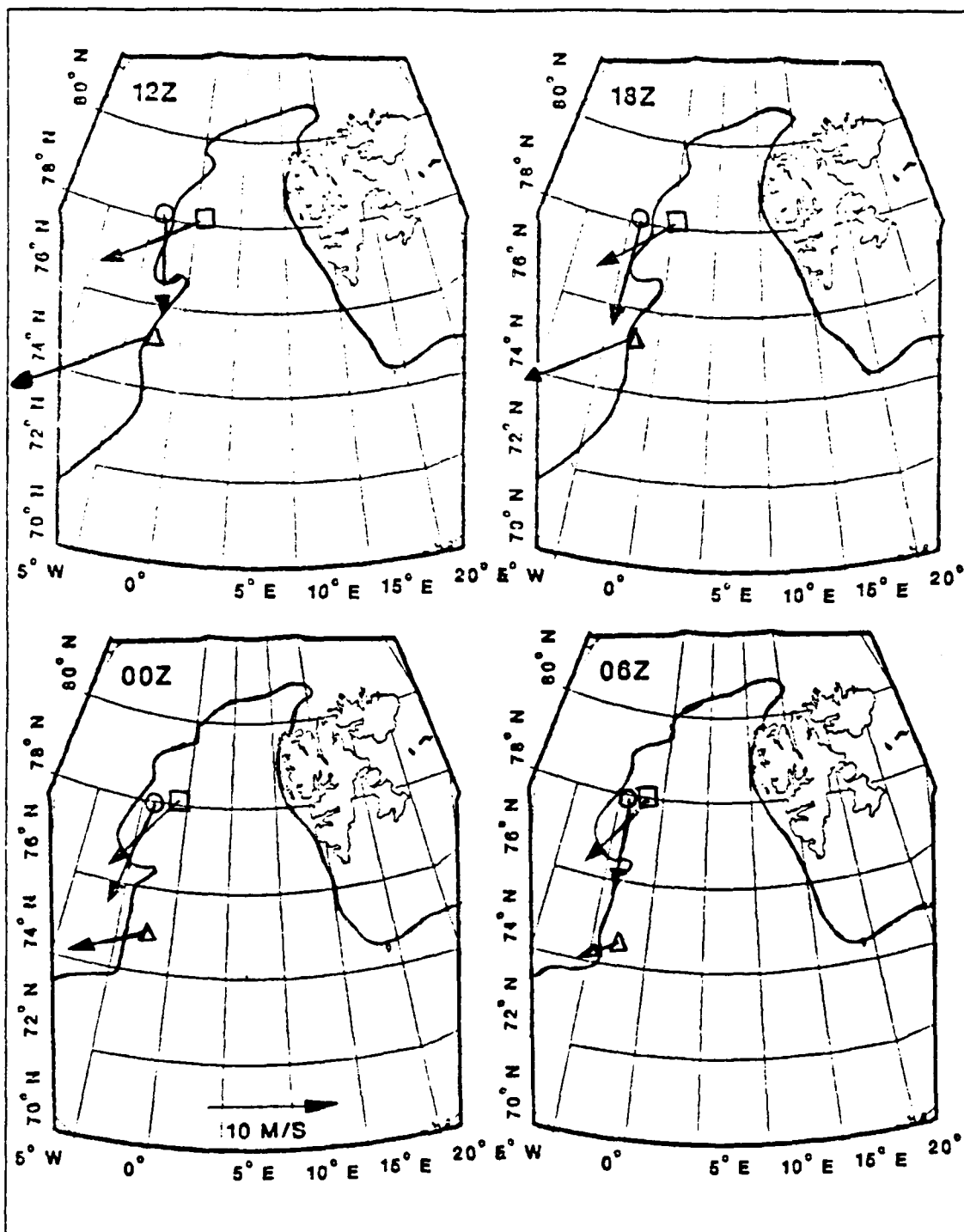Fig. 53.   M and N profiles for the 1730 UTC 26 March 1987 launch episode.

Fig. 54.   Ship positions from 1200 UT 1 April to 0600 UT 2 April 1987.

Figs. 55-58 show the rawinsonde profiles and their associated M and N profiles for the eight rawinsonde launches in which refractive events were observed. It can be seen in these figures that the duct heights increased as the inversion layer began to lift during the last two launch episodes. This was probably a result of the approaching front of the low pressure system to the south causing an increase in the instability in the boundary layer and a decrease in the subsidence aloft. The slope in the duct heights was positive going from ice to water during three of the four launches.

In this case it was observed that for ships relatively close to each other (less than 100 km) and under the influence of the same large-scale forcing, the vertical movement of the ducting layers was fairly consistent. The individual heights of the ducts were observed to vary from 50-100 m at each launch episode. Over the horizontal ranges in question this amount of variation appears to be quite small. The effect of these variations on EM wave propagation will be discussed shortly.

3. Comparison to MIZEX-84 Results

The refractive structure of the MABL examined by Willis (1987) using MIZEX-84 data also indicated a lack of horizontal homogeneity. Ducts were detected by at least two ships during the same launch episode only 20 of 61 times for the uncorrected data. This number dropped to only four after the dewpoint correction had been applied. Willis attributed some of the variations in duct height during individual episodes to the dewpoint saturation problem. However, the point was also made that inhomogeneity in the refractive structure seemed to be the norm rather the exception in the data.

C. EFFECTS OF HORIZONTAL INHOMOGENEITY IN THE REFRACTIVE STRUCTURE

Variability in the horizontal refractive structure is of significant importance to anyone interested in exploiting that structure for tactical purposes. It has been shown that the refractive structure around the MIZ varies greatly over range and is highly dependent on both the large-scale forcing of the atmosphere and the more isolated effects of the ice cover and the ice/ocean interface. IREPS is the only operational system currently used by the U.S. Navy to analyze the effects of the refractive structure on radar propagation. The input into IREPS is based on one sounding and the assumption is made that the atmosphere is horizontally homogeneous about 85% of the time (NOSC TD 659, 1981). Dotson (1987) demonstrated the necessity to obtain high resolution data to effectively identify small-scale refractive variations in the vertical. He also provided

Fig. 55.   Rawinsonde profiles and associated M and N profiles for 1130 UTC launch
episode on 1 April 1987.

SPECIFIC HUMIDITY G/KG

1 APR 1987 1655 GMT POLAR CIRCLE
LAT 78° 7'N LONG 3° 49'W

SPECIFIC HUMIDITY G/KG

1 APR 1987 1745 GMT HAAKON MOSBY
LAT 78° 10'N LONG 0° 30'W

N UNITS

1 APR 1987 1655 GMT POLAR CIRCLE
LAT 78° 7'N LONG 3° 49'W

N UNITS

1 APR 1987 1745 GMT HAAKON MOSBY
LAT 78° 10'N LONG 0° 30'W

Fig. 56.   Rawinsonde profiles and associated M and N profiles for 1730 UTC launch
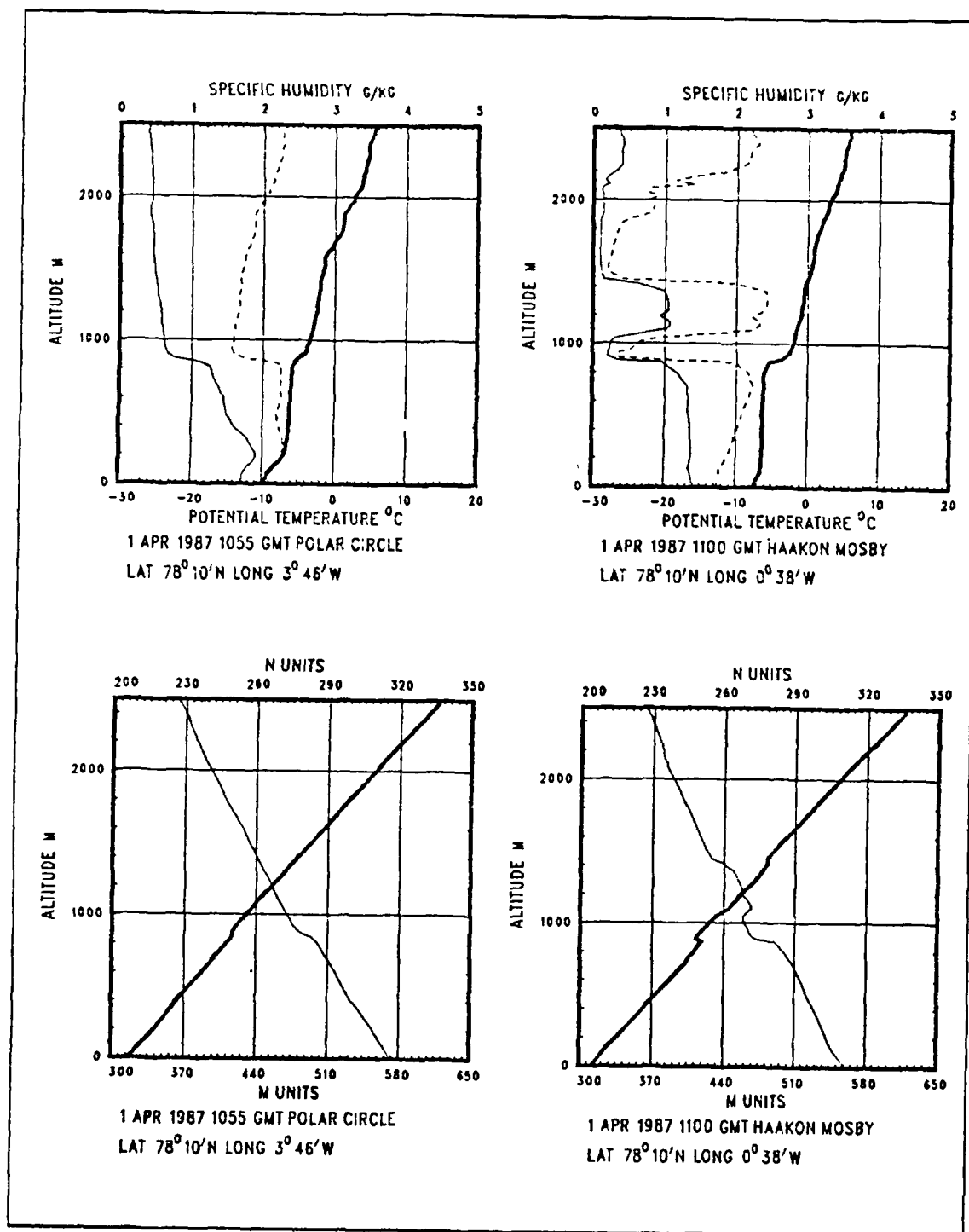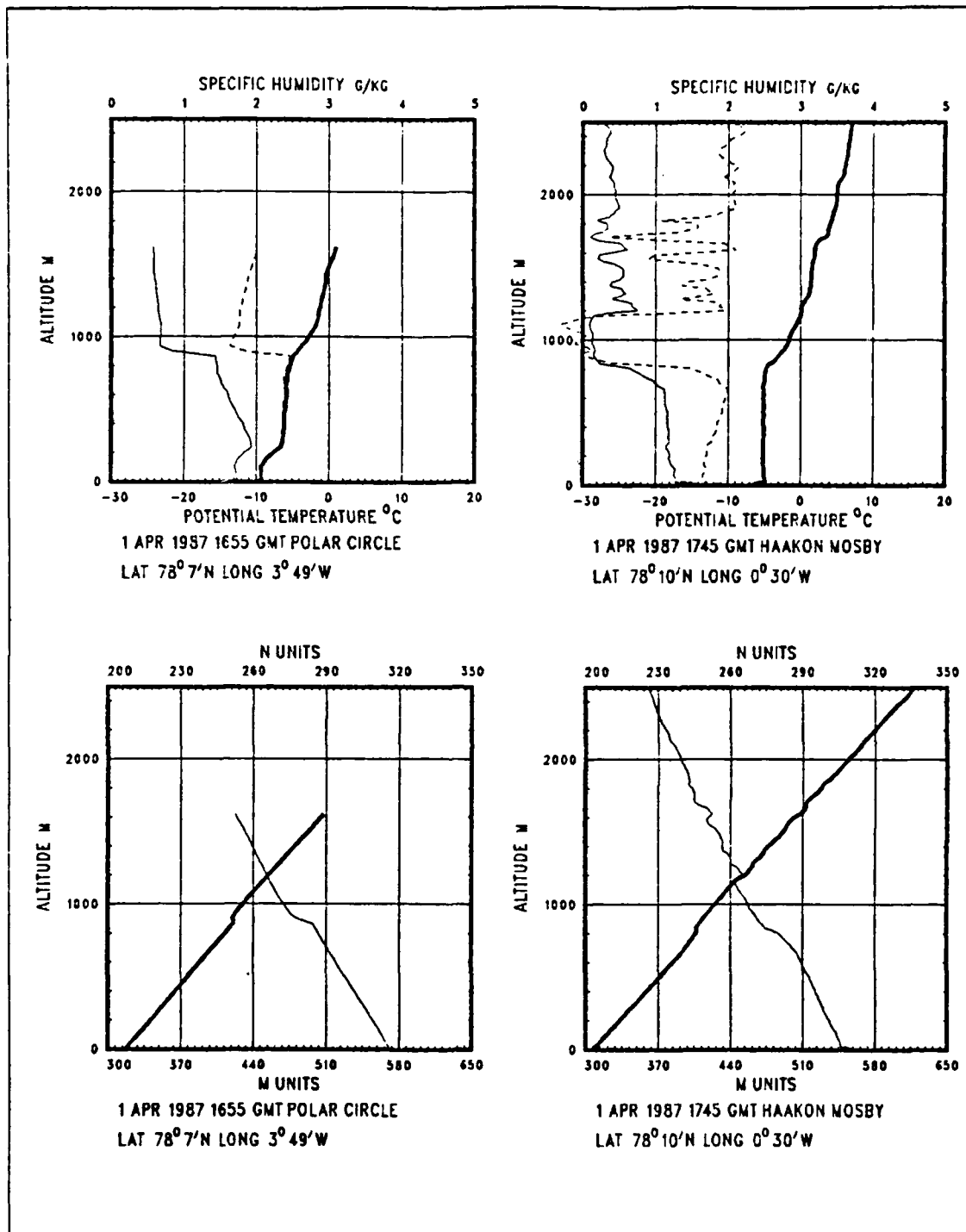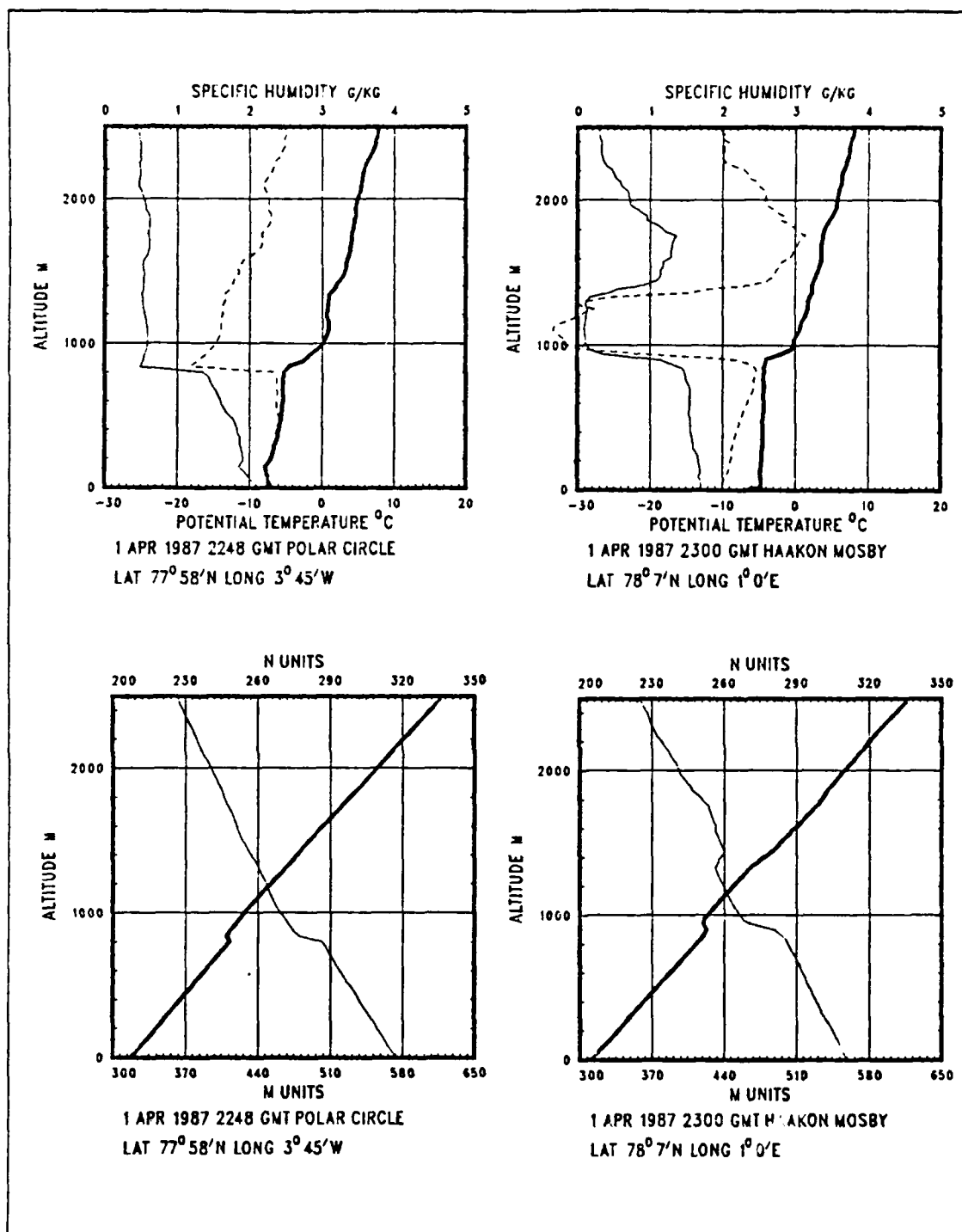episode on 1 April 1987.

88

Fig. 57. Rawinsonde profiles and associated M and N profiles for 2330 UTC launch episode on 1 April 1987.
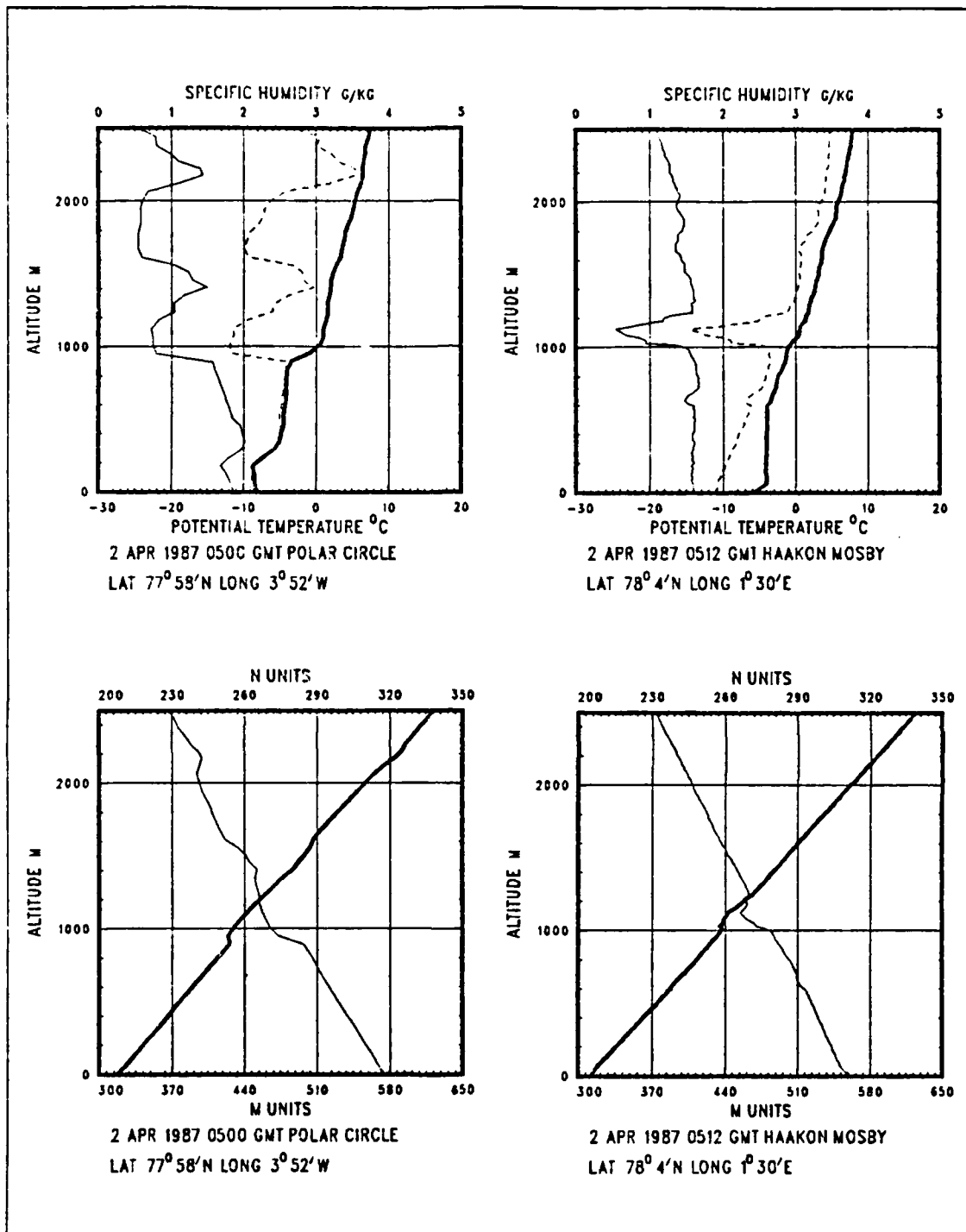
Fig. 58. Rawinsonde profiles and associated M and N profiles for 0530 UTC launch
episode on 2 April 1987.

evidence that horizontal inhomogeneity in the atmosphere is often more pronounced between two platforms than was previously assumed. This inhomogeneity must be taken into account when making predictions using IREPS which assumes a homogeneous refractive structure. A firm understanding of the forces driving the atmospheric conditions in between any two positions of interest is essential to the useful implementation of refractive effects prediction systems.

A range-dependent ray tracing program developed by Patterson (1987) was used to describe the effects of a varying refractive structure on the propagation paths of EM waves. Five different refractive structures were selected as input into the model. These included a horizontally homogeneous refractive structure, a refractive structure in which the trapping layer was allowed to slope upward with range, a refractive structure that began with a well defined trapping layer and changed to a normal refractive structure, a normal refractive structure that developed into a trapping layer and a trapping layer that abruptly changed into a normal refractive structure at a short range. Each of these refractive structures will be examined separately and compared to each other.

1. **Refractive Structure One**

A horizontally homogeneous refractive structure was used for the first study. The refractive structure was normal with the exception of one trapping layer based at 800 m. This height was chosen as it is approximately the average height of all the ducts observed during MIZEX-87. The thickness of the trapping layer was 50 m which was also close to the average thickness.

Fig. 59 shows the ray path for a transmitter positioned at the base of the trapping layer at 800 m. An increased concentration of EM wave energy is identified where the trace is shaded darker. The effect of the duct created by the trapping layer is evident as the wave energy is focused within the duct creating a dark narrow bundle of rays propagating straight out from the transmitter. Another effect of the trapping layer is to generate a radar shadow zone or radar hole just above the layer. This is a zone which is void or nearly void of EM wave energy due to the trapping layer's refracting the energy downward. Radar holes are of great tactical importance because a contact flying into such an area would become effectively invisible to the tracking system. It is noted in Fig. 59 that the radar hole begins to form at a range of about 40 km.

Two more runs were made with the homogeneous refractive structure but with the transmitter located above the trapping layer. The first of these depicted in Fig. 60 has the transmitter at an altitude of 900 m. Several changes are readily apparent in the

91

ray trace after the height change. The narrow beam of focused rays directed straight ahead is no longer present. With the transmitter above the trapping layer the wave fronts intersect the trapping layer at an angle of incidence that exceeds the critical angle necessary for the duct to trap the energy. The radar hole is more distinct and the hole begins to form at about 30 km. Additional runs demonstrated that the radar hole would form closer to the transmitter as the transmitter height was reduced to a level no less than the top of the trapping layer. As the transmitter was allowed to increase in height, the radar hole formed further away from the transmitter. Fig. 61 shows the radar hole forming at 75 km with the transmitter at a height of 1200 m. When the transmitter was raised to a height of 1600 m the lower rays of the beam pattern were trapped in the duct.

In the final run of this refractive structure, the transmitter was placed below the trapping layer at 700 m. Fig. 62 illustrates this situation. A radar hole did not form in this case. An area of increased energy is evident just above the trapping layer and slopes slightly upward.

2. Refractive Structure Two

This situation represents one in which a trapping layer, associated with the MABL capping inversion, is increasing in height as the range increases. The slope of the height increase was 100 m every 50 km. The trapping layer thickness was maintained at 50 m. This situation is similar to that observed during MIZEX-87 and represents the slope observed between observations over the ice and over the water. The initial refractivity profile in this series is identical to the one used in the previous homogeneous case with a trapping layer base of 800 m. The ray trace in this case is shown in Fig. 63 with a transmitter height of 800 m. The pattern is very similar to the one observed in Fig. 59. One difference is that the narrow beam of focused rays slopes upward as it follows the path of the duct created by the trapping layer. The lower boundary of the ray pattern was also altered by the slope of the duct and caused the lower rays to fail to reach and reflect off the surface. When the transmitter was placed at 900 m and at 700 m, the resulting ray traces showed virtually no difference in the ray patterns as compared to the homogeneous case. The ray patterns for a transmitter at 900 and 700 m for this case are shown in Figs. 64 and 65.

3. Refractive Structure Three

In this scenario the refractive structure was altered to simulate the presence of two dissimilar air masses in the region. A trapping layer at 800 m is followed 50 km down range by a 50 m thick trapping layer based at 900 m. The third refractivity profile
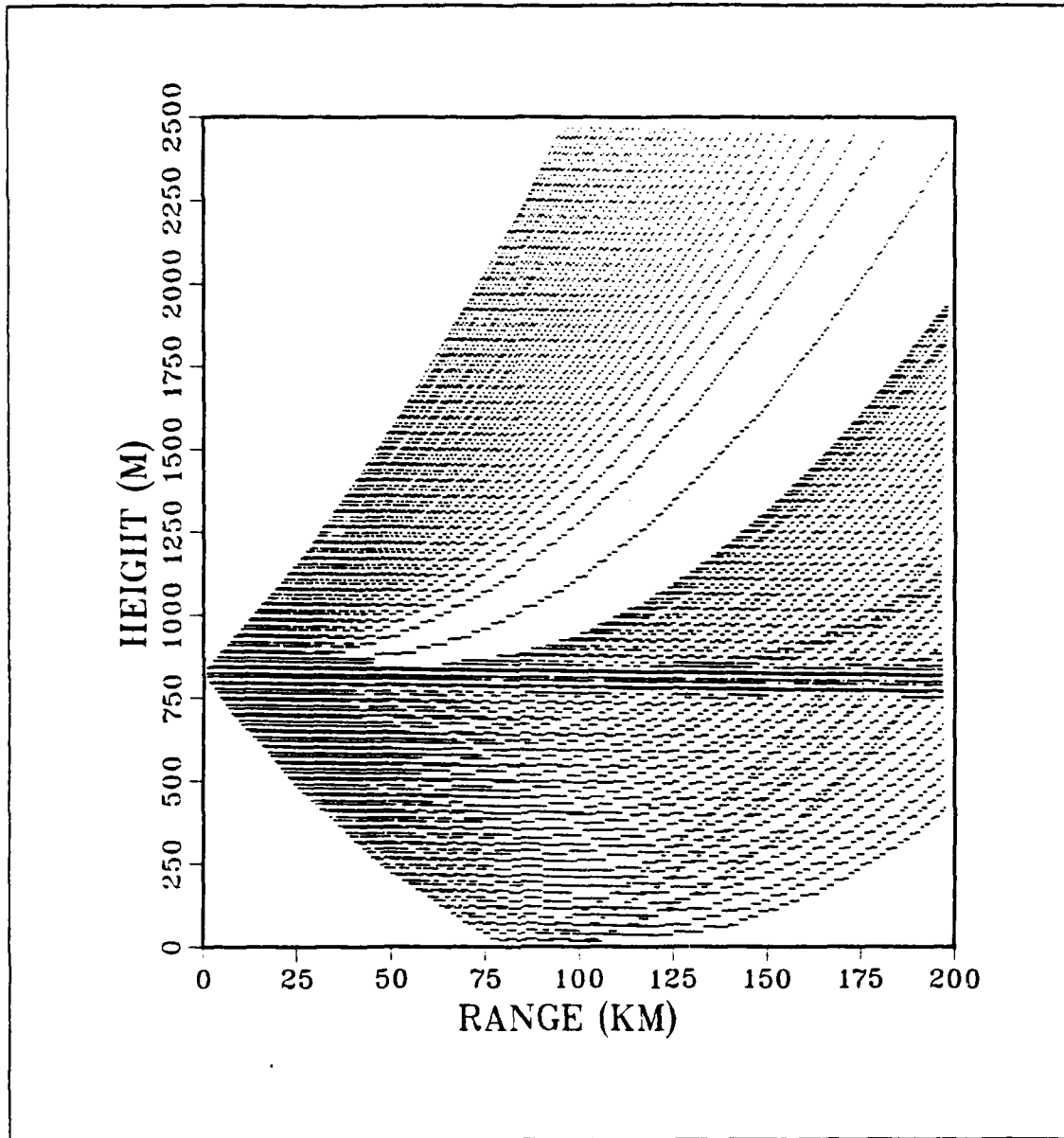
Fig. 59.   Ray trace for homogeneous refractive structure with trapping layer and transmitter at 800 m.

is a super-refractive profile with a base at 1000 m and a thickness of 100 m. The fourth profile is a normal refractivity proifile located 150 km down range from the original profile. The situation simulates that of a low pressure center slowly moving into an area previously dominated by high pressure where the trapping layers have formed. The low

Fig. 60. Ray trace for homogeneous refractive structure with trapping layer at 800 m and transmitter at 900 m.

pressure is simulated by the normal refractive structure observed during conditions of instability.

Fig. 66 shows the effect of this varying refractive structure when the transmitter is positioned within the duct. The narrow bundle of rays normally associated with the duct appeared to begin to spread out as it passed into the super-refractive layer and then

94
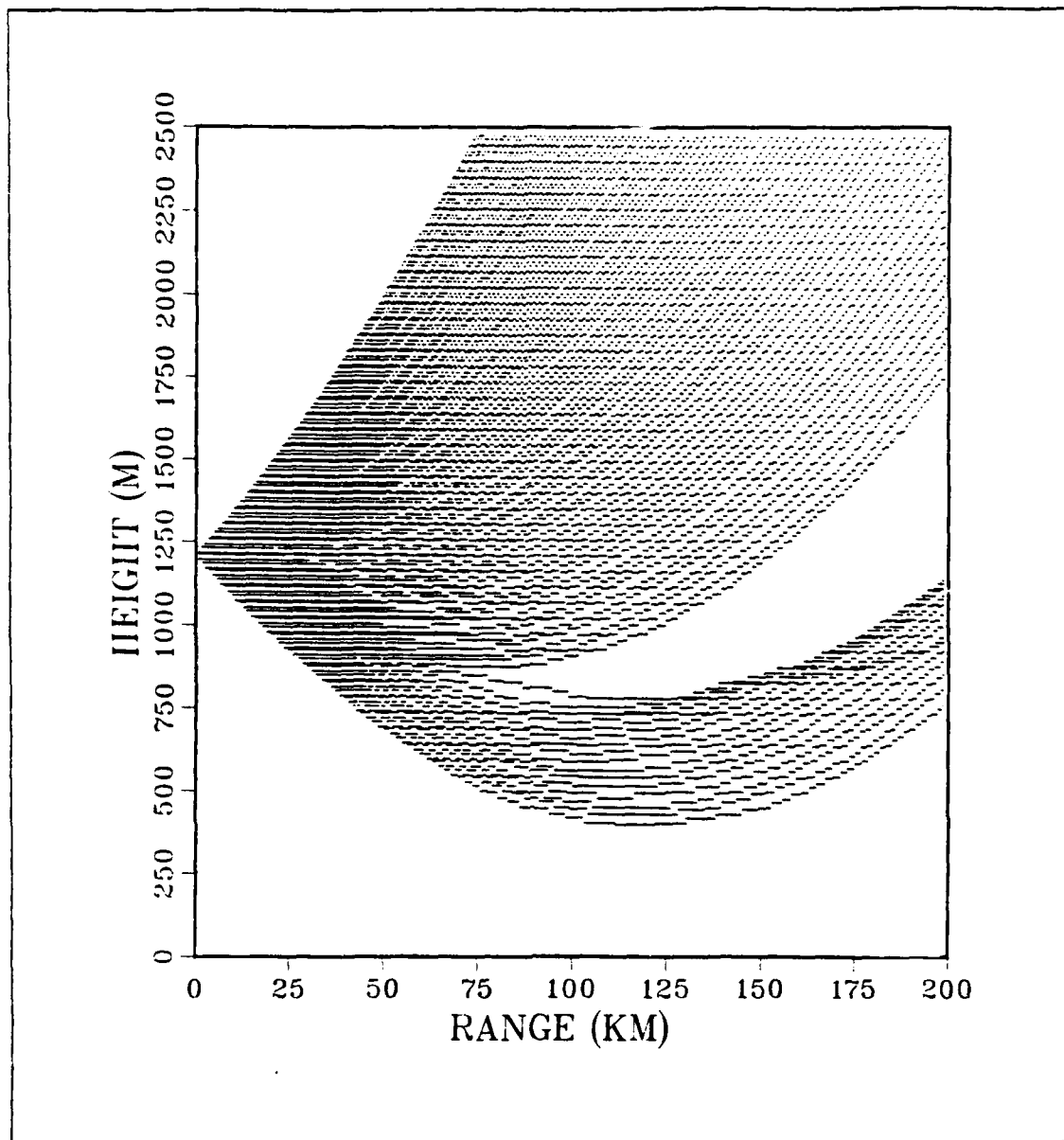
Fig. 61.   Ray trace for homogeneous refractive structure with trapping layer at 800
m and transmitter at 1200 m.

into the region of normal refractive conditions. The changing refractive structure caused
the initial ducting to begin to weaken with distance. This example helps to illustrate the
focusing effect that a trapping layer has. The ray bundle is still fairly distinct 100 km
after the trapping layer ceased to exist. A radar hole was also generated by this
refractive profile due to the initial trapping layer which existed out past 50 km. When
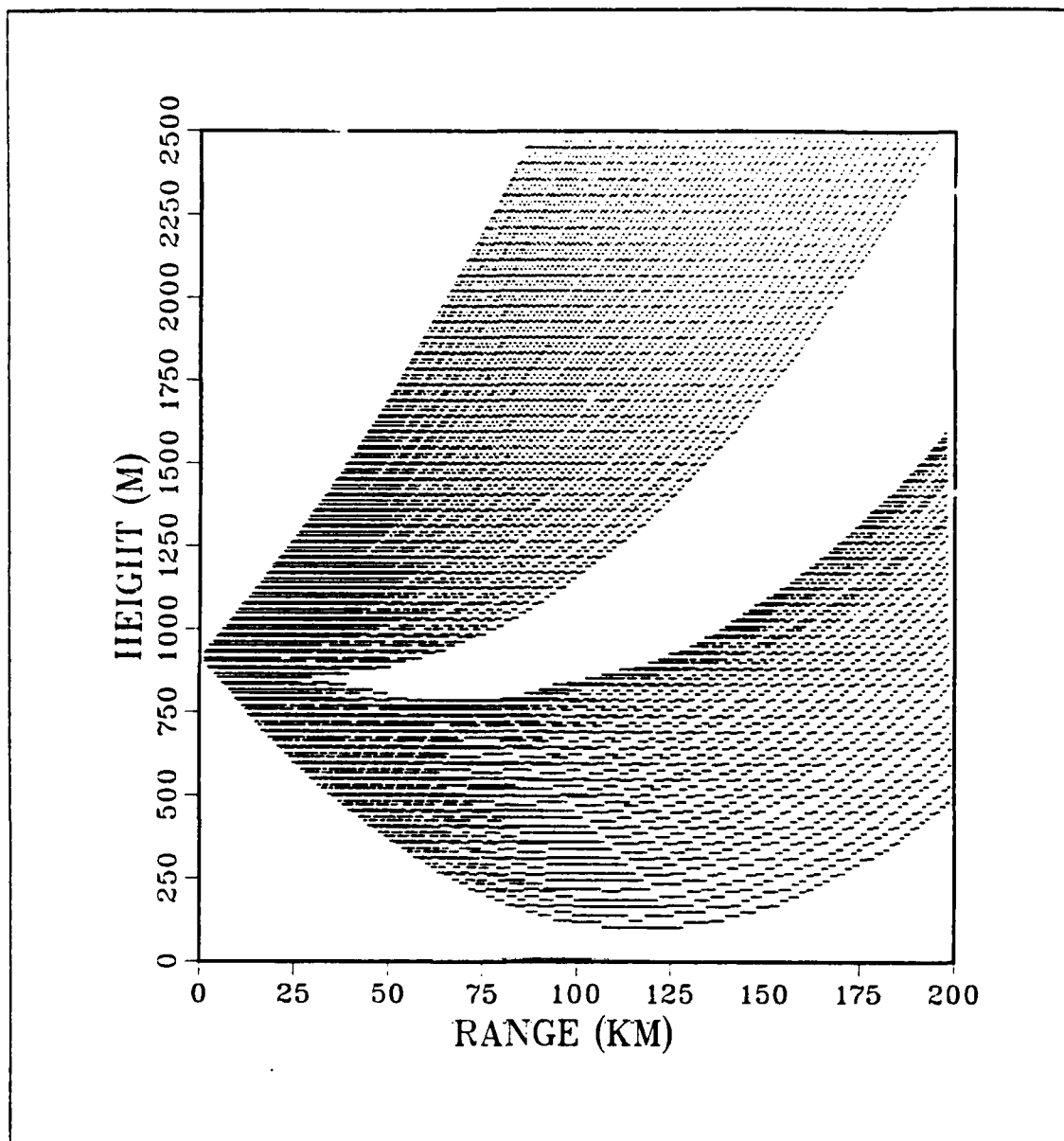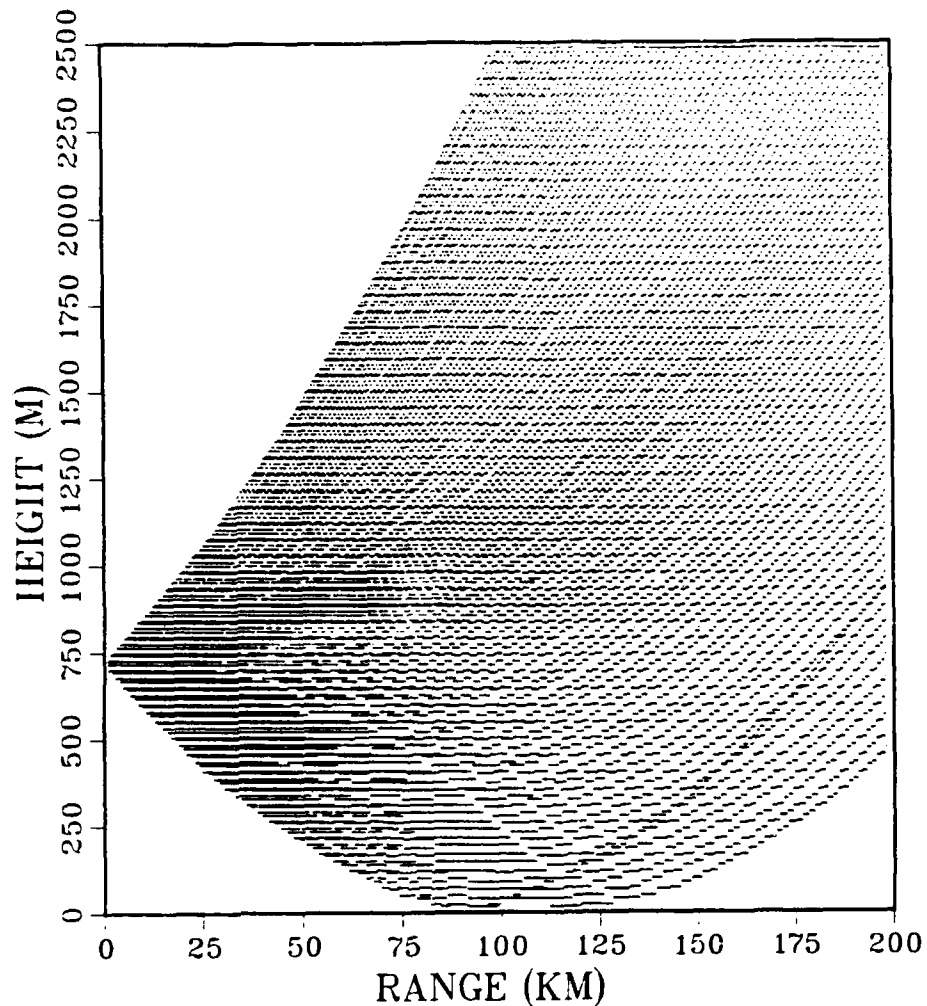
Fig. 62.   Ray trace for homogeneous refractive structure with trapping layer at 800 m and transmitter at 700 m.

the transmitter was placed at altitudes above and below the trapping layer the resulting ray patterns were once again almost identical to those shown in Figs. 60 and 62.

4.   Refractive Structure Four

This refractive structure was identical to that described in the previous section. In this case the transmitter was moved so that it would be within the normal refractive
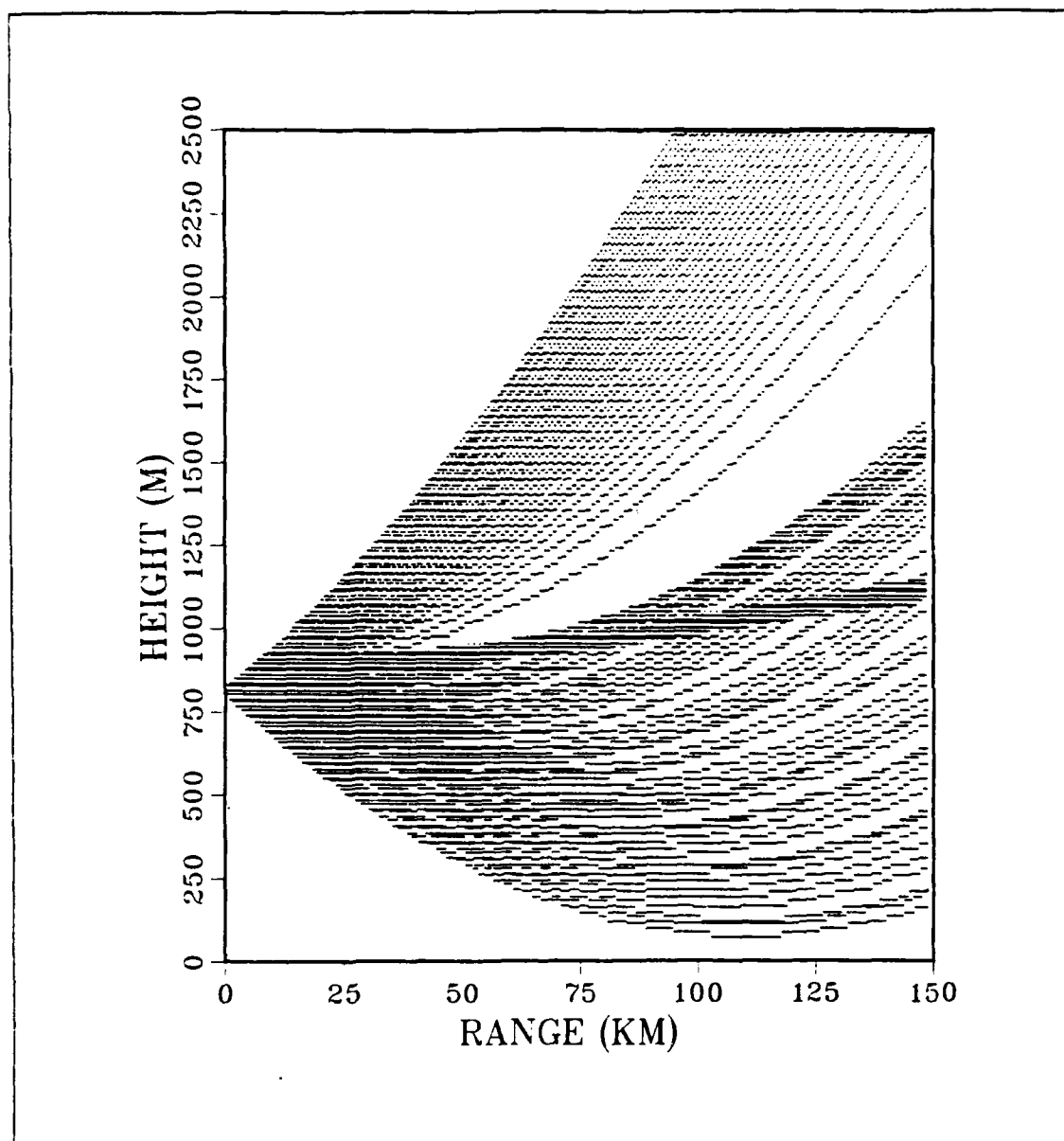
Fig. 63. Ray trace for upward sloping trapping layer with transmitter at 800 m.

layer and sending the beam out towards an area where trapping layers had formed. The initial height of the transmitter was placed again at 800 m. The ray pattern for this situation is illustrated in Fig. 67. The pattern is very smooth with no irregularities. The trapping layers do not appear to influence the pattern in any way. The 900 and 700 m runs produced the same type of ray trace.
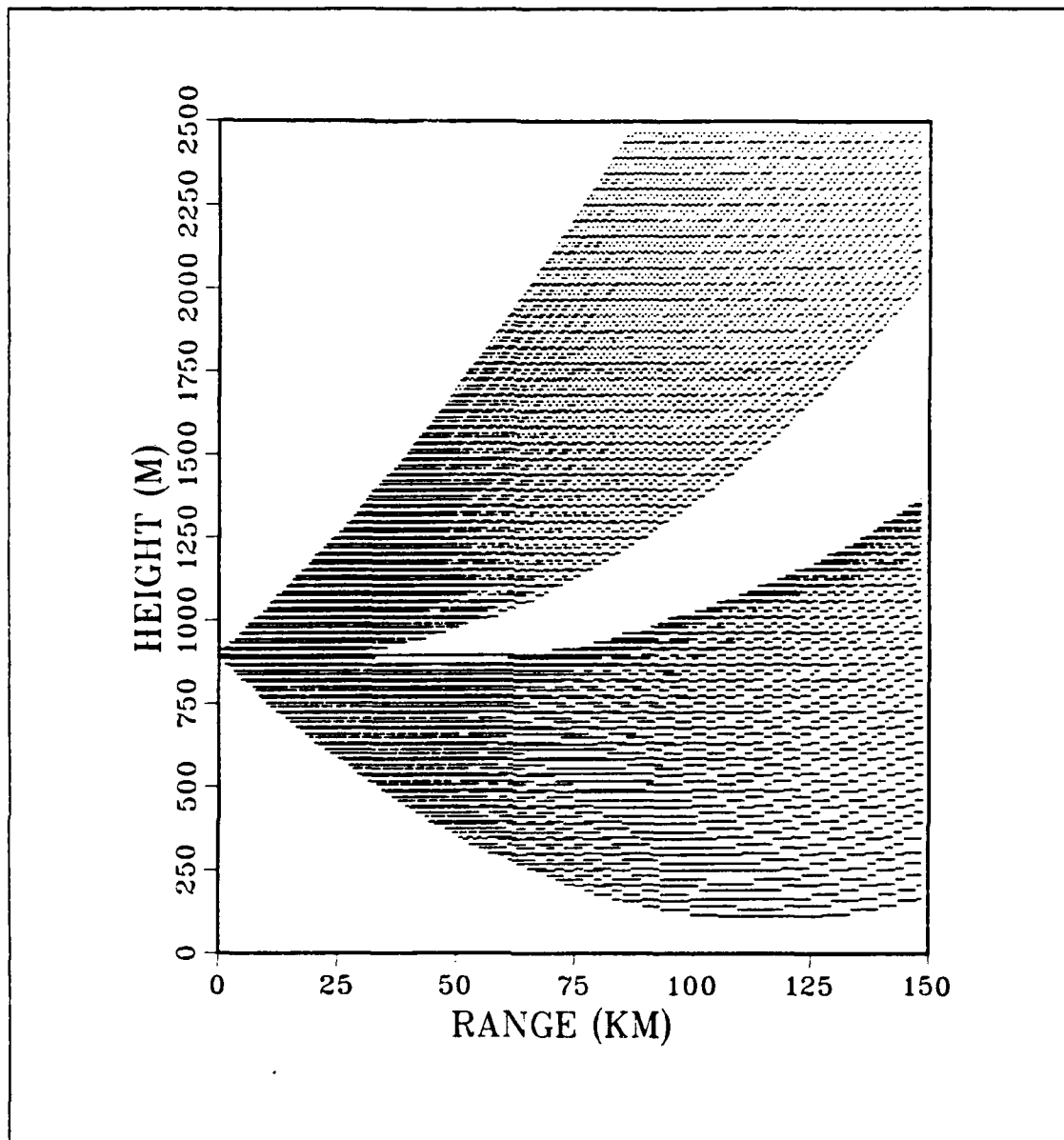
Fig. 64. Ray trace for upward sloping trapping layer with transmitter at 900 m.

Additional runs were made to see if the trapping layers down range would influence any of the rays if the transmitter height was increased substantially. The pattern shown in Fig. 68 with a transmitter height of 1500 m shows that the ray paths are significantly altered by the trapping layers resulting in a ray bundle focused downward as well as a large radar hole in the lower half of the pattern.
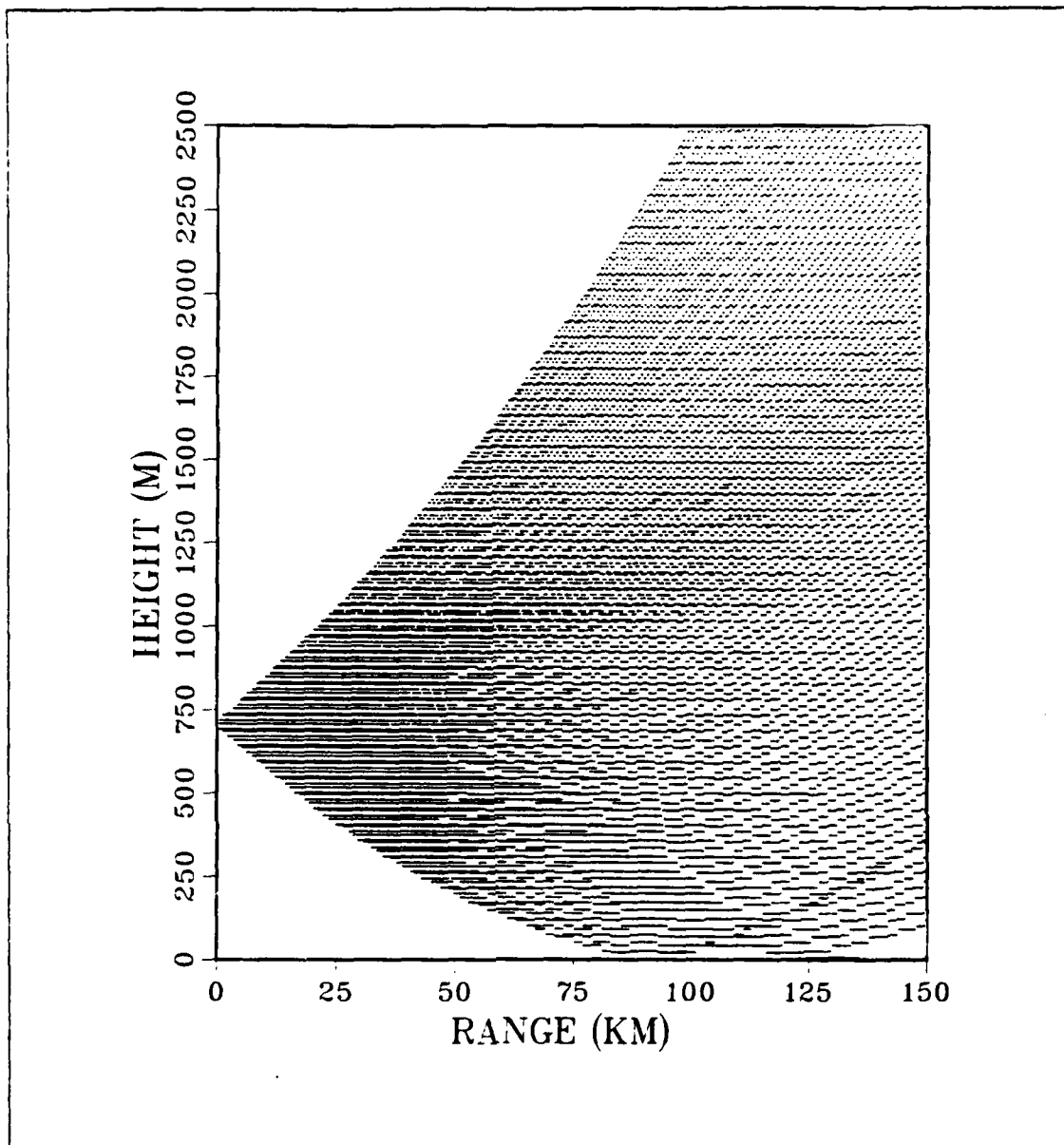
Fig. 65.   Ray trace for upward sloping trapping layer with transmitter at 700 m.

5.   Refractive Structure Five

In this final case a trapping layer at 800 m with a thickness of 50 m was followed by a normal refractive structure 20 km away. The relatively short separation distance was used to represent a rapidly moving frontal system moving into an area dominated by high pressure. This would result in a more abrupt change from a stable situation to that of of an unstable deeply mixed boundary layer. Fig. 69 shows the effect of this

99

Fig. 66.   Ray trace for refractive structure simulating two dissimilar air masses with transmitter at 800 m.

pattern with the transmitter located in the duct at 800 m. A single narrow bundle of rays is formed by the trapping layer. The bundle remains relatively intact but is refracted along with the rest of the rays along the ray path created by the normal refractive structure. One point of interest is that in this case the trapping layer did not extend far enough horizontally to project the ray bundle forward or to develop a radar hole.

100

Fig. 67.   Ray trace for refractive structure simulating two dissimilar air masses with transmitter at 800 m.

6.   Significant Observations

The refractive structure examined in this section helped to show how much of an effect trapping layers with a thickness of as little as 50 m can have on EM wave propagation. As the height of the transmitter was changed the ray paths were altered significantly, especially right around the trapping layer. The inhomogeneity of the

Fig. 68. Ray trace for refractive structure simulating two dissimilar air masses with transmitter at 1500 m.

atmosphere caused some variations in the structure of the ray patterns as the rays moved from one refractive condition to another. The level at which trapping layers were placed caused an appropriate variation in the slopes of the ray bundles associated with the layers. The last refractive structure helped to show that the distance over which a trapping layer exists is also essential in determining whether a radar hole will form. This is
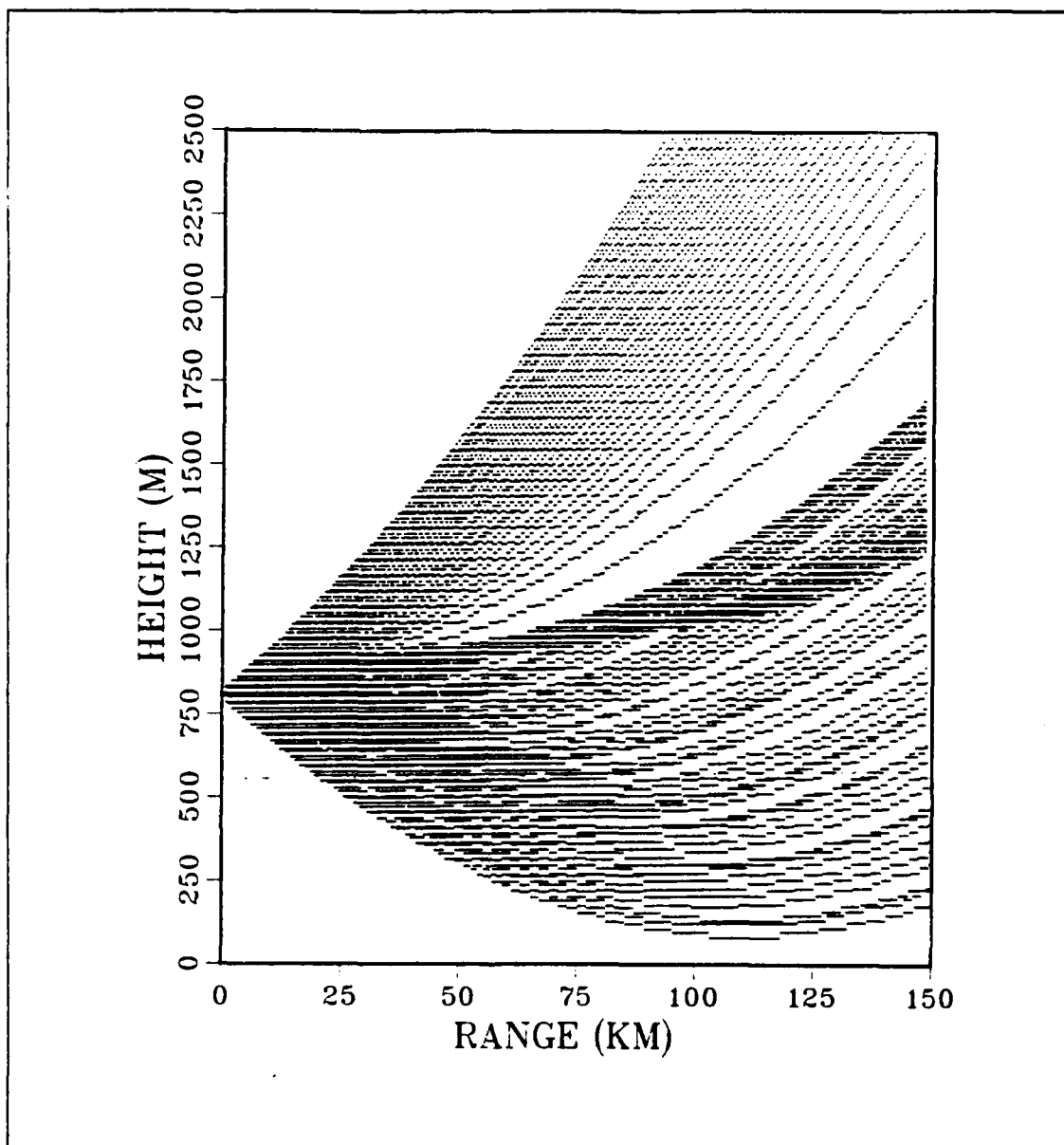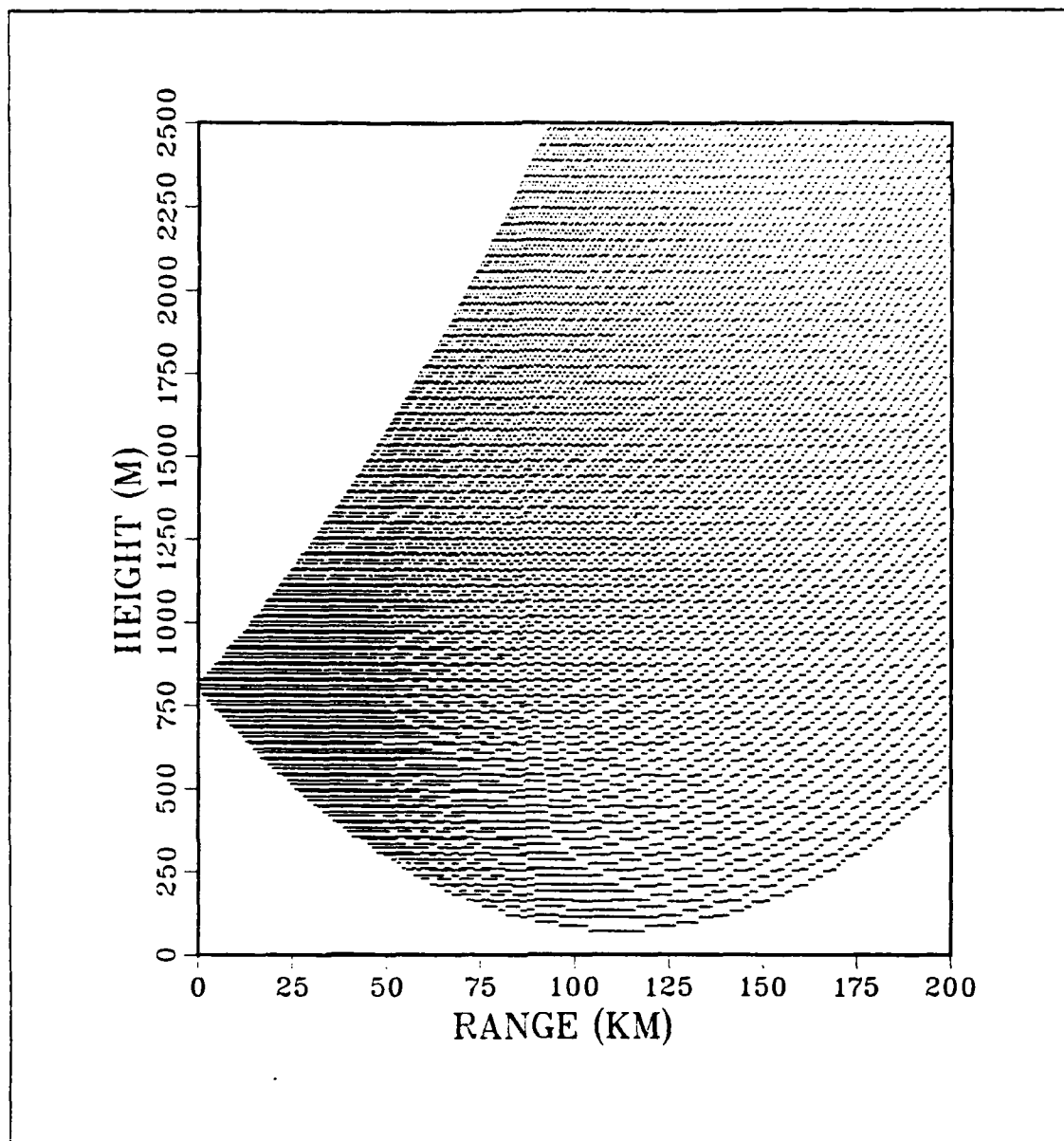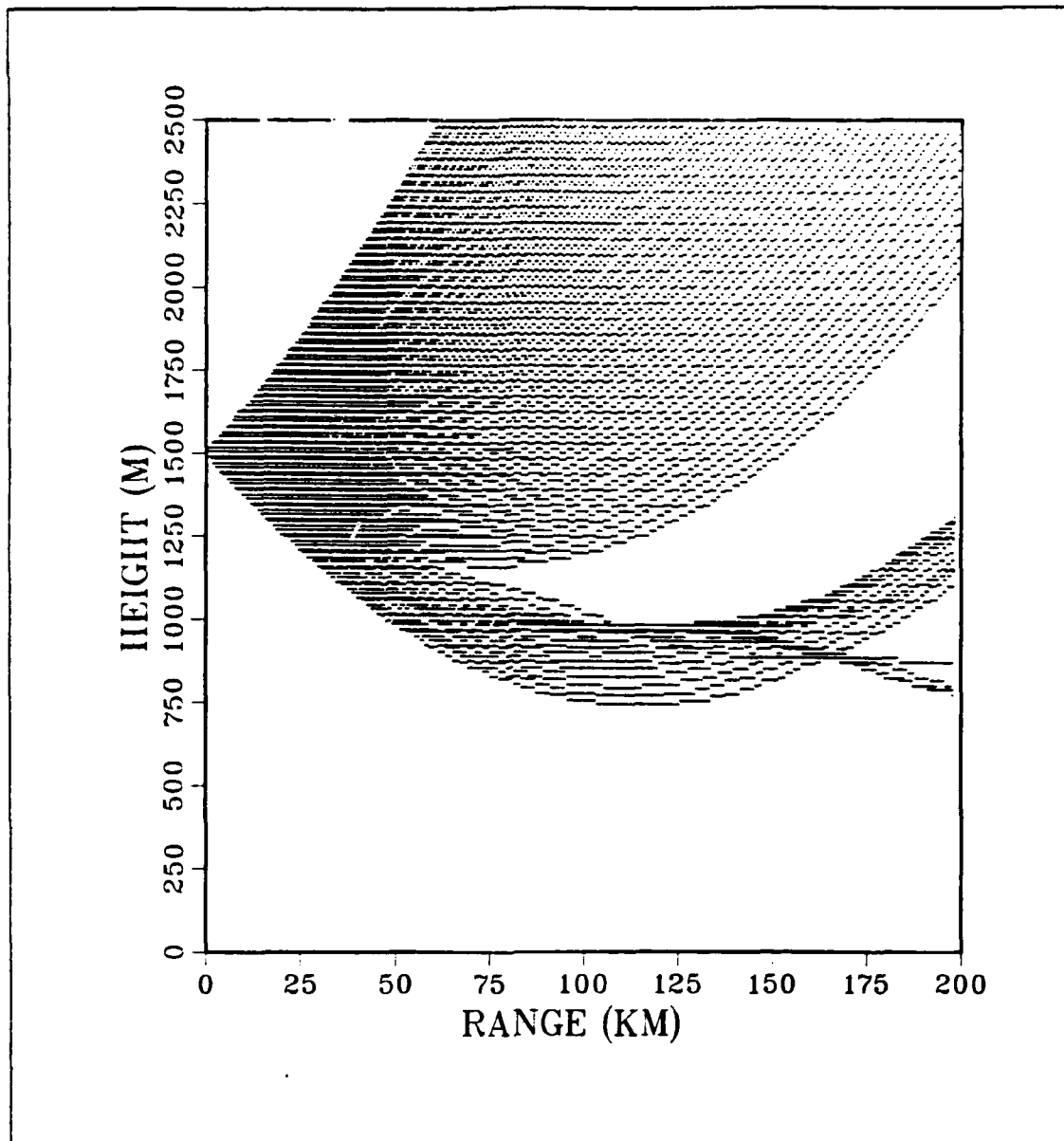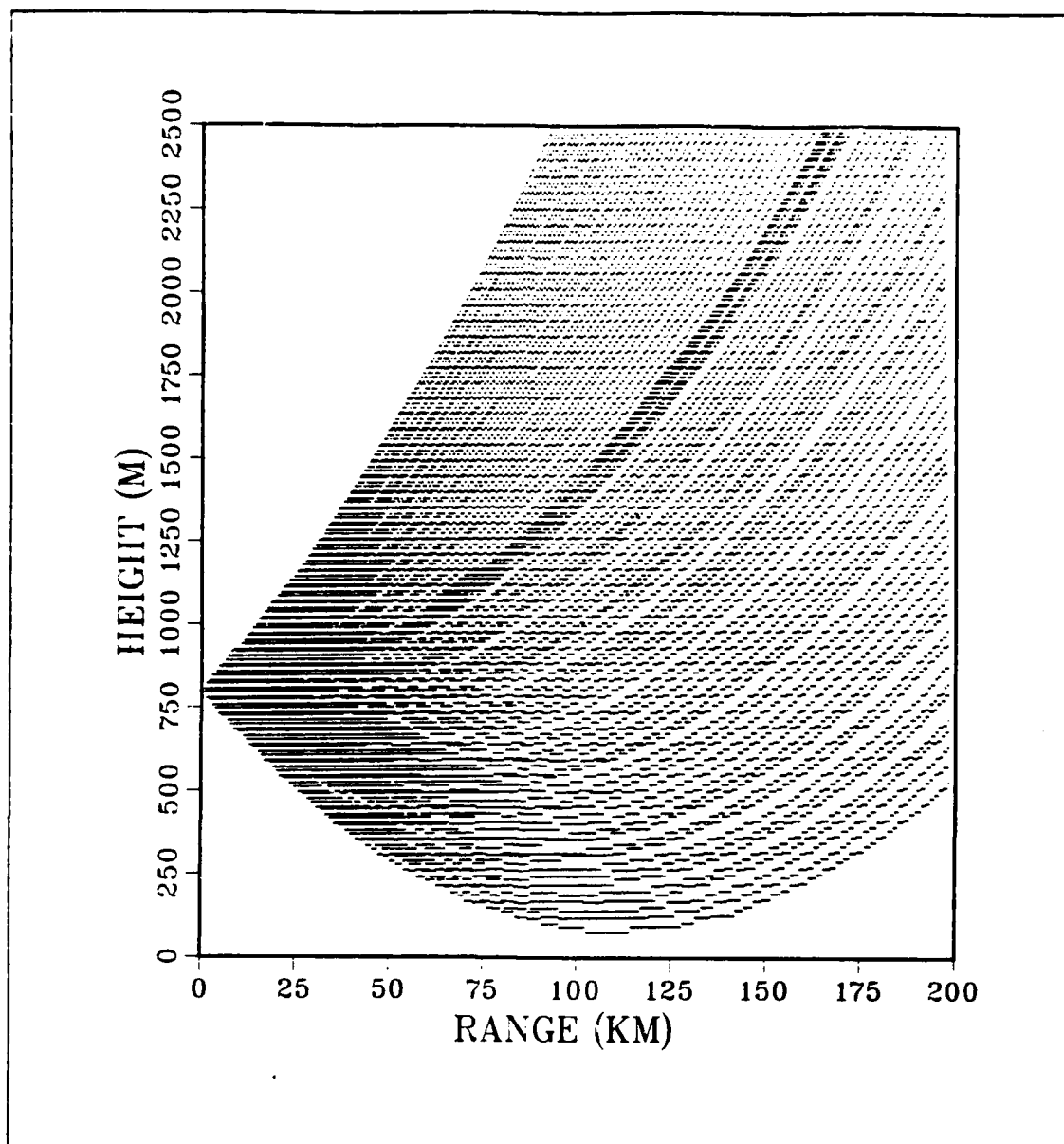
Fig. 69. Ray trace for refractive structure simulating two dissimilar air masses with transmitter at 800 m.

of added interest since the ranges over which EM ducting was observed during both MIZEX-84 and MIZEX-87 were thought to be quite short due to the many instances of only one ship detecting a duct.

VII. CONCLUSIONS

This thesis examined the temporal and spatial variability of the MABL around the Greenland Sea MIZ and its effect on EM refractivity. The data source for the thesis was composed of surface observations and upper-air data r. easured from three ships during MIZEX-87. The ships were positioned relative to the ce edge in order to observe the changes in atmospheric variables when moving from a surface covered by ice to a surface covered by water. The upper-air data were composed of a set of 169 rawinsonde profiles collected from 19 March - 11 April 1987.

A temporal study was done by looking at variations in the refractive structure during five different synoptic regimes. During periods the MIZEX area was under the influence of high pressure systems, the frequency of ducting and super-refraction was highest. During periods dominated by low pressure, the number of refractive events decreased considerably. When frontal passages were recorded the boundary layer deepened to greater than 2000 m and the refractive structure was normal with no ducting episodes recorded. The large-scale forcing brought on by different mesoscale and synoptic systems was determined to be the major element in determining the frequency of refractive events. This forcing also played a major role in determining the heights of the various refractive layers as well as their relative strengths and thicknesses.

A diurnal study showed that incidences of ducting and super-refraction occurred more often during the midday and early evening launch periods. An explanation for this observation was not obvious and is of sufficient interest to warrant further study.

A spatial study was also performed. Results indicated that refractive events such as ducting and super-refractive layers tended to slope upward in height relative to the ice edge when measured from over the ice to over the water. Greater heights over the MIZ were attributed to an increased occurrence of multiple vertical layers above the well-mixed layer for super-refractive layers. The possibility of statistical error due to insufficient data was brought up as a possible explanation for the higher duct heights. Incidences of ducting were generally caused by a well formed capping inversion above the well mixed layer. More than half of the incidences of super-refraction were also caused by the development of the inversion.

Another portion of the spatial study investigated the horizontal homogeneity of the refractive structure. Two or more ships observed ducts in only 35% of the cases when

104

ducts were detected. This shows that the lower atmosphere around the MIZ is relatively inhomogeneous when looking at that specific refractive structure. Understanding how the refractive structure varies with range is essential to the exploitation of the EM spectrum for tactical purposes.

A ray trace model was used to show variations in the paths of EM waves caused by horizontal inhomogeneity in the refractive structure. It was demonstrated that even a relatively thin trapping layer can greatly affect the normal ray path of a transmitting unit. The changes were most apparent when the transmitter was within a duct or when rays were intersecting the duct in such a way as to be trapped within it. The ray paths also varied when the refractive structure changed from one extreme to the other. The most important aspect was determined to be the position of the transmitter with respect to the duct. Since this is a variable often controlled by the operator, knowledge of the location of EM ducts and other anomalous refractive layers can increase ones tactical advantage by allowing the operator to place the transmitter at the best height for a given situation.

The refractivity studies showed that ducting normally occurred well above the surface. The ray trace model revealed that ducting around the MIZ can cause significant variations in the transmission path of an airborne detection or communications system. An absence of surface ducting was noted in the MIZEX-87 data. This was attributed to higher and weaker inversion layers. Ducting should not be considered a major concern for shipboard radar systems operating around the MIZ during the spring.

In comparing the early spring MIZEX-87 refractive structure to the summer case observed during MIZEX-84, it was noted that ducting occurred much less frequently during the spring. Duct heights were greater, duct thicknesses were less and duct strengths were weaker during MIZEX-87. This was attributed to a reduced level of subsidence in the spring as compared to the summer as well as an increased amount of mixing in the boundary layer caused by greater levels of heat flux. The strange dewpoint curves observed in many of the MIZEX-84 rawinsonde profiles were observed in only a small number of profiles in the MIZEX-87 data. This could be due to improvements in the design of the humidity sensor used in the rawinsondes. If the dewpoint phenomenon is not caused by instrument error it could be a seasonal phenomenon that occurs more frequently in the summer than in the spring. Additional research is necessary to solve this problem. Because the moisture in the atmosphere affects the refractive structure so

greatly, an understanding of this problem is essential to a complete understanding of the observed refractivity in the Arctic.

The surge of interest in the Arctic as a theatre for military operations as well as a region of economic potential requires the investment of increased time and resources for research in this region. Development of a larger data base for the study of the Arctic refractive structure is a necessary part of this research as our military forces seek to establish an increased presence in this region of the world.

LIST OF REFERENCES

Battan, L.J., 1973: *Radar Observation of the Atmosphere.* University of Chicago Press, 323 pp.

Buck, A.L., 1981: New equations for computing vapor pressure and enhancement factor. *J. Applied Meteorology,* **20,** 1527-1532.

Businger, J.A. and W.J. Shaw, 1984: The response of the marine boundary layer to mesoscale variations in sea-surface temperature. *Dyn. Atmos. and Oceans,* **8,** 267-281.

Dotson, M.E., 1987: An Evaluation of the Impact of Variable Temporal and Spatial Data Resolution upon IREPS, Master Thesis, Naval Postgraduate School, Monterey, California, 62 pp.

Dutton, J.A. and H.A. Panofsky, 1984: *Atmospheric Turbulence.* John Wiley and Sons Inc., New York, 397 pp.

Fairall, C.W., and R. Markson, 1987: Mesoscale variations in surface stress, heat fluxes, and drag coefficient in the marginal ice zone During the 1983 Marginal Ice Zone Experiment, *J. of Geophysical Research.,* **92,** 6921-6932.

Guest, P.S., and K.L. Davidson, 1988: *MIZEX 87 Meteorology Atlas ,* Naval Postgraduate School Report, NPS-63-88-004, Monterey, California, 137 pp.

Guest, P.S., K.L. Davidson, and C.A. Vaucher, 1988: Atmospheric boundary layer features observed in the spring marginal ice zone. *Preprints from Second AMS Conference on Polar Meteorology and Oceanography,* Madison, Wisconsin, 29-31 March. 1988, pp. 73-74.

Johnson, D.R., and J.D. Hawkins, 1987: The marginal ice zone experiment: 1987. *European Science Notes,* **41,** 567-570.

Johnson, G.L., D. Bradley and R.S. Winokur, 1984: United States Security Interests in the Arctic. *United States Arctic Interests in the 1980's and 1990's.* Springer-Verlag, New York, 369 pp.

Johannessen, O.M. and D.A. Horn, 1984: MIZEX 84: A brief overview. *MIZEX Bulletin.,* **V,** 1-5.

Kerr, D.E., 1951: *Propagation of Short Radio Waves.* McGraw-Hill, New York, 728 pp.

Lindsay, R.W., K.L. Davidson, M. Gube-Lenhardt, P.S. Guest, R. Picard, C. Wamser, 1986: *Synoptic weather events of MIZEX 84.,* unpublished manuscript, 46 pp.

MIZEX Bulletin VIII, 1986: *A science plan for a winter marginal ice zone experiment in the Fram Strait-Greenland Sea: 1987-1989,* **CRREL Special Report 86-9.**

National Science Foundation, 1987: *United States Arctic Research Plan.* Prepared by the Interagency Arctic Research Policy Committee, Washington DC, 334 pp.

Naval Ocean Systems Center, 1981: *IREPS Revision 2.2 User's Manual,* TD 659, San Diego, California, 135 pp.

Ohtake, T., K. Jayaweera and K.I. Sakurai, 1982: Observation of ice crystal formation in lower arctic atmosphere. *J. Atmos. Sci.,* **39**, 2898-2904.

Overland, J.E., 1985: Atmospheric boundary layer structure and drag coefficients over sea ice. *J. Atmos. Sci.,* **42**, 9029-9049.

Patterson, W.L., 1987: *A Raytrace Method for a Laterally Heterogeneous Environment,* Naval Ocean Systems Center report, TR 1180, San Diego, California, 64 pp.

Petterssen, S., W.C. Jacobs, and B.C. Haynes, 1956: *Meteorology of the Arctic.* Naval Operations for Polar Projects (OP-03A3), Washington DC, 207 pp.

Polmar, N., 1986: *Guide to the Soviet Navy.* Naval Institute Press, Annapolis, Maryland, 536 pp.

Richardson, E.L., 1984: *United States Arctic Interests in the 1980's and 1990's.* Springer-Verlag, New York, 369 pp.

Sater, J.E., A.G. Ronhovde, and L.C. Van Allen, 1971: *Arctic Environment and Resources.* The Arctic Institute of North America, Washington DC, 309 pp.

Schultz, R.R., 1987: Meteorological Features During the Marginal Ice Zone Experiment from 20 March to 10 April 1987, Master Thesis, Naval Postgraduate School, Monterey, California, 86 pp.

U.S. Department of Defense, 1987: *Soviet Military Power 1987,* Washington, DC, 159 pp.

Watkins, J.D., 1986: *The Maritime Strategy.* U.S. Naval Institute, 13 pp.

Willis, Z.S., 1987: The Spatial and Temporal Variability of the Arctic Atmospheric Boundary Layer and Its Effect on Electromagnetic (EM) Propagation, Master Thesis, Naval Postgraduate School, Monterey, California, 108 pp.

Wyngaard, J.C., 1973: On surface layer turbulence, *Workshop on Micrometeorology,* D.A. Haugen, Ed., Boston, Amer. Meteor. Soc., 101-148.

INITIAL DISTRIBUTION LIST

<div align="right">No. Copies</div>

1. Defense Technical Information Center   2
    Cameron Station
    Alexandria, VA 22304-6145

2. Library, Code 0142   2
    Naval Postgraduate School
    Monterey, CA 93943-5002

3. Chief of Naval Research   1
    800 N. Quincy Street
    Arlington, VA 22217-5000

4. Oceanographer of the Navy   1
    Naval Observatory
    34th and Massachusetts Avenue NW
    Washington, DC 20390-5000

5. Commander   1
    Naval Oceanography Command
    NSTL, MS 39522-5000

6. Commanding Officer   1
    Fleet Numerical Oceanography Center
    Monterey, CA 93943-5005

7. Chairman, Code 63Rd   1
    Department of Meteorology
    Naval Postgraduate School
    Monterey, CA 93943-5000

8. Chairman, Code 68Co   1
    Department of Oceanography
    Naval Postgraduate School
    Monterey, CA 93943-5000

9. Professor W.J. Shaw, 63Sr   3
    Naval Postgraduate School
    Monterey, CA 93943-5000

10. Professor K.L. Davidson, 63Ds   1
    Naval Postgraduate School
    Monterey, CA 93943-5000

11. LT Douglas J. Groters, USN   4
    1140 Tyler St.
    Annapolis, MD 21403

12. Commanding Officer   1
    Naval Environmental Prediction
    Research Facility
    Monterey, CA 93943-5006

13. Chairman, Oceanography Department   1
    U.S. Naval Academy
    Annapolis, MD 21402-5000

14. Scientific Liason Office   1
    Office of Naval Research
    Scripps Institution of Oceanography
    La Jolla, CA 92037-5000

15. Library Acquisitions   1
    National Center for Atmospheric Research
    P.O. Box 3000
    Boulder, CO 80307-5000

16. Jarold H. Groters   1
    1657 104th Ave.
    Zeeland, MI 49464

17. Defense Technical Information Center   1
    Cameron Station
    Alexandria, VA 22304-6145

18. Commanding Officer   1
    Naval Oceanographic Office
    NSTL Station
    Bay St. Louis, MS 39522

19. Commanding Officer   1
    Naval Ocean Research and Development Activity
    NSTL Station
    Bay St. Louis, MS 39522

20. Office of Naval Research (Code 420)   1
    Naval Ocean Research and Development Activity
    800 North Quincy Street
    Arlington, VA 22217

21. Commander   1
    Naval Ocean Systems Center
    San Diego, CA 92152

22. Commander   1
    Naval Sea Systems Command
    Washington D.C. 20362

23. LT Zdenka S. Willis
    Naval Polar Oceanography Center
    4301 Suitland Road
    Washington D.C. 20390-5180

1